AD_____

Award Number: W81XWH-04-1-0802

TITLE: Bioenergetic Approaches and Inflammation of MPTP Toxicity

PRINCIPAL INVESTIGATOR: M. Flint Beal, M.D.

CONTRACTING ORGANIZATION: Weill Medical College of Cornell University
New York, NY 10021

REPORT DATE: September 2007

TYPE OF REPORT: Annual

PREPARED FOR: U.S. Army Medical Research and Materiel Command
Fort Detrick, Maryland 21702-5012

REPORT DOCUMENTATION PAGE

Form Approved
OMB No. 0704-0188

1. REPORT DATE	**2. REPORT TYPE**	**3. DATES COVERED**
01-09-2007	Annual	1 Sep2006 – 31 Aug 2007

4. TITLE AND SUBTITLE

Bioenergetic Approaches and Inflammation of MPTP Toxicity

5a. CONTRACT NUMBER

5b. GRANT NUMBER
W81XWH-04-1-0802

5c. PROGRAM ELEMENT NUMBER

6. AUTHOR(S)

M. Flint Beal, M.D.

5d. PROJECT NUMBER

5e. TASK NUMBER

5f. WORK UNIT NUMBER

7. PERFORMING ORGANIZATION NAME(S) AND ADDRESS(ES)

Weill Medical College of Cornell University
New York, NY 10021

8. PERFORMING ORGANIZATION REPORT NUMBER

9. SPONSORING / MONITORING AGENCY NAME(S) AND ADDRESS(ES)
U.S. Army Medical Research and Materiel Command
Fort Detrick, Maryland 21702-5012

10. SPONSOR/MONITOR'S ACRONYM(S)

11. SPONSOR/MONITOR'S REPORT NUMBER(S)

12. DISTRIBUTION / AVAILABILITY STATEMENT
Approved for Public Release; Distribution Unlimited

13. SUPPLEMENTARY NOTES

14. ABSTRACT

NOT PROVIDED

15. SUBJECT TERMS
NOT PROVIDED

16. SECURITY CLASSIFICATION OF:				**18. NUMBER OF PAGES**	**19a. NAME OF RESPONSIBLE PERSON**
a. REPORT	**b. ABSTRACT**	**c. THIS PAGE**			USAMRMC
U	U	U	UU	42	**19b. TELEPHONE NUMBER** *(include area code)*

3. **TABLE OF CONTENTS**

4. INTRODUCTION

We are continuing to examine a number of neuroprotective agents in an MPTP model of PD. We are also continuing to utilize metabolomic profiling to identify novel biomarkers for PD and to investigate whether these occur in animal models of PD. We are continuing to develop and characterize a new animal model of PD by making a knock out of PINK1, a nuclear encoded kinase localized to mitochondria, and which causes autosomal recessive PD. We have completed a study of the effects of human dopaminergic stem cells in a 6-hydroxy dopamine model of PD.

Outline of Research Goals:

Task 1: To determine the ability of pharmacologic agents to prevent MPTP neurotoxicity.

1. Examine neuroprotective effects of phosphodiesterase IV inhibitor rolipram on MPTP.

2. Examine neuroprotective effects of mitochondrial targeted antioxidants (SS02 and SS31), which inhibit the MPT.

3. Examine neuroprotective effects of celastrol and promethazine on MPTP.

4. Examine a novel form of Coenzyme Q_{10} (CoQ_{10}) in the MPTP model of PD.

5. Examine the role of caspase 3 activation in activation of microglia and MPTP toxicity.

Task 2: To develop a new transgenic mouse model of PD by knocking out PINK1, a protein in which mutations cause autosomal recessive PD (months 1-48).

Task 3: To utilize metabolomic profiling to develop biomarkers for PD. We will utilize metabolomic profiling to study patients with PD and animal models of PD (months 1-48).

Task 4. To determine the efficacy of human dopaminergic stem cells in the 6-hydroxydopamine (6-OHDA) model of PD (months 6 -24).

5. BODY

Task 1: To determine the ability of pharmacologic agents to prevent MPTP neurotoxicity.

1. Examine neuroprotective effects of phosphodiesterase inhibitor rolipram on MPTP.

We have completed studies with the phosphodiesterase inhibitor rolipram. We saw protective effects with either 1.2 or 2.5 mg/kg. We also showed significant protective effects against dopamine depletion and loss of tyrosine hydroxylase neurons. These results have now been accepted for publication in *Experimental Neurology*.

2. Examine neuroprotective effects of mitochondrial targeted antioxidants (SS02 and SS31), which inhibit the MPT.

We have made substantial progress in these studies. We found that both of these compounds, which concentrate in mitochondria and have ROS scavenging properties are able to dose-dependently inhibit lipid peroxidation as measured by chemoluminescence. We also found that these compounds protect against MPP+ toxicity *in vitro*. We carried out studies against MPTP toxicity in mice. We found that both compounds were able to significantly protect against MPTP induced loss of dopamine, as well as loss of tyrosine hydroxylase neurons. The dopamine metabolites DOPAC and HVA showed similar effects. We are working on a manuscript describing these results, as well as other continuing studies.

3. Examine neuroprotective effects of celastrol and promethazine on MPTP.

We have completed studies of both of these compounds during our last report. We found marked neuroprotective effects of both compounds. The results were published in the *Journal of Neurochemistry* and in *Neurobiology of Disease* respectively.

4. Examine a novel form of coenzyme Q10 (CoQ10) in the MPTP model of PD.

We carried out a large number of studies, which showed that there were indeed significant protective effects. In particular, we were able to show that coenzyme Q administered in a chronic model of MPTP toxicity not only protected against loss of tyrosine hydroxylase neurons but it also protected against the development of alphasynuclein aggregates. This was a model in which MPTP was administered over one month by Alzet pump. These results we believe are particularly relevant to PD itself. We have prepared a manuscript, which is under review at the *Journal of Neurochemistry*.

5. Examine the role of caspase 3 activation in activation microglia and MPTP toxicity.

We continued our studies of matrix metalloprotease 3 (MMP3) and its role as a novel signaling proteinase from apoptotic neuronal cell death that activates microglia. We found that it is of importance in activating NADPH oxidase to generate superoxide and this play a direct role in dopamine cell death. We have recently completed initial studies, which have been published in *FASEB Journal*.

Task 2: To develop a new transgenic mouse model of PD by knocking out PINK1, a protein in which mutations can cause autosomal recessive PD (months 1-48).

We have generated the PINK1 knockout mice. Correctly targeted ES cells were used to inject and generate PINK1 knockout mouse founders. We are now continuing to expand the colony. We have found mild defects in motor behavior. We have also found impaired dopamine release using microdialysis. We have observed a number of different phosphorylated proteins on two-dimensional gels. Of particular interest, the protein OMI is phosphorylated by PINK1. This is of interest, since OMI is also implicated in PD. We intend to carry out studies examining these mice both histologically, as well as biochemically.

Task 3: To utilize metabolomic profiling to develop biomarkers for PD.

We are continuing out studies of metabolomic profiling. We have identified markers, which clearly separate unmedicated PD patients from controls. We then applied these markers to medicated PD patients who were able to obtain an equal separation. We examined a number of specific markers. These included uric acid, which was decreased in PD patients. We actually found increased levels of reduced glutathione, which is of interest, since this is activated by the Nrf2 transcriptional pathway, which is known to be activated in PD. Lastly, we found increased amount of 8-hydroxy-2-deoxyguanosine in the plasma. We are continuing studies of patients with LRRK2 mutations. It appears that they show unique metabolomic profiles. We will also obtain LRRK2 mutations. It appears that they show unique metabolomic profiles. We also obtained LRRK2 transgenic mice, which we also intend to study. These studies will take the next year to complete.

Task 4: To determine the efficacy of human dopaminergic stem cells in the 6-hydroxy dopamine (6-OHDA) model of PD.

With regard to this task, we have now completed it. We carried out the studies in collaboration with Dr Steve Goldman and Dr Neeta Roy. We carried out detailed histologic studies. The acquisition of highly-enriched dopaminergic populations is an important prerequisite to using HES-derived dopaminergic neurons for cell-based therapy. We utilized a new strategy improving the efficiency of dopaminergic neurogenesis from human ES cells. This involved co-culture with telomerase immortalized human mesencephalic astrocytes during induction of a dopaminergic phenotype using sonic hedgehog and FGF8. Using this means, we achieved a high efficiency enrichment of dopaminergic neurons. We then studied the ability of these to functionally replace and correct 6-OHDA lesioned adult rat brain. We found that there

was a significant substantial and long lasting restitution of motor function. We also measured for motor asymmetry and found that this was also corrected. There was efficient generation of TH positive neurons in all six animals studied. We also looked to see if the engrafted brains still showed evidence of mitosis amongst the engrafted population. We examined BDRU incorporation *in vivo*. This showed that approximately 6 ½ % of the neurons showed BDRU incorporation. Nevertheless, these are extremely promising results which set the stage for further studies before human transplantation. These studies were published last year in *Nature Medicine*.

6. KEY RESEARCH ACCOMPLISHMENTS

A. The finding that mitochondrial targeted antioxidants SS02 and SS31, which inhibit the MPT are neuroprotective against MPTP toxicity in mice, as well as MPP+ toxicity in cell culture.

B. The finding that a reduced novel form of CoQ10 is effective in the MPTP model of PD. We also showed that CoQ was effective in a chronic model of MPTP toxicity. We furthermore found that MPTP toxicity was significantly attenuated in MMP3 deficient mice, which lack the MMP3 activation in microglia. This was accompanied by a decrease in superoxide generation, which was mediated by NADPH oxidase.

C. We have developed a knockout model of PINK1. We are continuing to study these mice to enable a full characterization.

D. We have continued metabolomic profiling and now have shown that we can separate unmedicated PD patients from controls as well as medicated PD patients from controls. This work is in the process of being prepared for publication. We also showed that a number of specific metabolites were altered including 8-dydroxy-2-deoxyguanosine and reduced uric acid.

E. We developed a novel technique for increasing the induction of dopaminergic phenotype in human ES derived dopaminergic neurons. We demonstrated and published that this was effective in reversing a motor deficit in rats lesioned with 6-hydroxy-dopamine.

7. REPORTABLE OUTCOMES

Cleren C, Calingasan NY, Chen J, Beal MF. Celastrol protects against MPTP- and 3-nitropropionic acid-induced neurotoxicity. J Neurochem 2005:94:995-1004

Abeliovich A, Beal MF. Parkinsonism genes: culprits and clues. J Neurochem 2006:99:1062-1072

Lin MT and Beal MF. Mitochondrial dysfunction and oxidative stress in neurodegenerative diseases. Nature 2006;443:787-795

Roy NS, Cleren C, Singh SK, Yang L, Beal MF, Goldman SA. Functional engraftment of human ES cell-derived dopaminergic neurons enriched by coculture with telomerase-immortalized midbrain astrocytes. Nat Med 2006; 12:1259-1268

8. CONCLUSIONS

We have made considerable progress in our research goals. We have characterized a number of agents, which show protection against MPTP toxicity. We have developed a new transgenic mouse model of PD by knocking out PINK1. We are continuing metabolomic profiling studies of PD patients and we have found that we can identify unique biomarkers in patients with LRRK2 mutations. We have completed studies of transplantation of human ES cell derived dopaminergic neurons into a 6-hydroxy-dopamine model of PD and have shown successful restitution of behavioral abnormalities.

9. REFERENCES

None

10: APPENDICES

Cleren C, Calingasan NY, Chen J, Beal MF. Celastrol protects against MPTP- and 3-nitropropionic acid-induced neurotoxicity. J Neurochem 2005;94:995-1004

Journal of Neurochemistry, 2005, 94, 995–1004 doi:10.1111/j.1471-4159.2005.03253.x

Celastrol protects against MPTP- and 3-nitropropionic acid-induced neurotoxicity

Carine Cleren, Noel Y. Calingasan, Junya Chen and M. Flint Beal

Department of Neurology and Neuroscience, Weill Medical College of Cornell University, New York-Presbyterian Hospital, New York, New York, USA

Abstract

Oxidative stress and inflammation are implicated in neurodegenerative diseases including Parkinson's disease (PD) and Huntington's disease (HD). Celastrol is a potent anti-inflammatory and antioxidant compound extracted from a perennial creeping plant belonging to the *Celastraceae* family. Celastrol is known to prevent the production of proinflammatory cytokines, inducible nitric oxide synthase and lipid peroxidation. Mice were treated with celastrol before and after injections of MPTP, a dopaminergic neurotoxin, which produces a model of PD. A 48% loss of dopaminergic neurons induced by MPTP in the substantia nigra pars compacta was significantly attenuated by celastrol treatment. Moreover, celastrol treatment significantly reduced the depletion in dopamine concentration induced by MPTP. Similarly, celastrol significantly decreased the striatal lesion volume induced by 3-nitropropionic acid, a neurotoxin used to model HD in rats. Celastrol induced heat shock protein 70 within dopaminergic neurons and decreased tumor necrosis factor-α and nuclear factor κ B immunostainings as well as astrogliosis. Celastrol is therefore a promising neuroprotective agent for the treatment of PD and HD.

Keywords: celastrol, gliosis, heat shock protein 70, Huntington, inflammation, Parkinson.

J. Neurochem. (2005) 94, 995–1004.

Parkinson's disease (PD) is a progressive neurodegenerative disorder which most commonly manifests between the fifth and seventh decade with bradykinesia, tremor and postural rigidity. At disease onset, a large proportion of dopaminergic neurons in the substantia nigra pars compacta (SNpc) have degenerated, resulting in a depletion of dopamine (DA) in the striatum (Hornykiewicz 1966). The causes of PD remain unknown but substantial evidence suggests an etiology involving both genetic and environmental factors (Greenamyre and Hastings 2004; Moore *et al.* 2004).

Huntington's disease (HD) is an inherited autosomal dominant neurodegenerative disorder which is characterized by choreiform abnormal movements, cognitive deficits and psychiatric manifestations and is associated with preferential degeneration of medium spiny GABAergic neurons located in the striatum (Harper 1991). Whereas the genetic defect responsible for HD is clearly identified as an expansion of a polyglutamine sequence within the huntingtin protein (The Huntington's Disease Collaborative Research Group 1993), many of the pathological mechanisms linking the mutant protein to the neurodegeneration remain highly speculative. The pathogenesis of PD and HD appears to involve oxidative stress, mitochondrial dysfunction, microglial activation and production of proinflammatory cytokines (Blum *et al.* 2001; Deckel 2001; Orr *et al.* 2002; Beal 2003; Beal and Ferrante 2004).

Administration of the succinate dehydrogenase inhibitor 3-nitropropionic acid (3-NP) produces, in rodents and primates, the principal features of HD (Brouillet *et al.* 1998; Blum *et al.* 2002). There is degeneration of striatal medium-sized spiny GABAergic neurons (Beal *et al.* 1993), abnormal movements and cognitive deficits (Brouillet *et al.* 1999; El Massioui *et al.* 2001). Administration of MPTP, in primates and rodents, reproduces the characteristic degeneration of nigrostriatal dopaminergic neurons with a decrease in striatal DA (Heikkila *et al.* 1984; Ramsay and Singer

Received December 22, 2004; revised manuscript received April 5, 2005; accepted April 7, 2005.

Address correspondence and reprint requests to Dr M. Flint Beal, Department of Neurology and Neuroscience, Weill Medical College of Cornell University, 525 East 68th Street, Room F-610, New York, NY, USA. E-mail: fbeal@med.cornell.edu

Abbreviations used: DA, dopamine; DMSO, dimethylsulfoxide; HD, Huntington's disease; HSP, heat shock protein; IκBα, inhibitor alpha; NFκB, nuclear factor κ B; 3-NP, 3-nitropropionic acid; OSA, octanesulfonic acid; PBS, phosphate-buffered saline; PD, Parkinson's disease; SNpc, substantia nigra pars compacta; TH, tyrosine hydroxylase; TNF-α, tumor necrosis factor-α.

1986). Both toxins lead to mitochondrial dysfunction, production of oxidative stress, release of proinflammatory cytokines and gliosis (Brouillet *et al.* 1999; Blum *et al.* 2001).

Celastrol, a triterpene, is a potent anti-inflammatory and antioxidant that is extracted from the root bark of an ivy-like vine, *Tripterygium wilfordii Hook*, which belongs to the family of *Celastraceae*. In China, this plant has a long history of use in traditional medicine for treating fever and joint pain. Studies have shown that celastrol suppresses microglial activation, pro-inflammatory cytokine production and the formation of inducible nitric oxide (Allison *et al.* 2001). Celastrol has been shown to strongly inhibit lipid peroxidation induced by ADP and Fe^{2+} (Sassa *et al.* 1990). In rat liver mitochondrial membranes, its IC_{50} was 7 μM and it was 15 times more effective than the most commonly used antiperoxidative agent, alpha-tocopherol (Sassa *et al.* 1990). The dienonephenol moiety of celastrol inhibits the peroxidation of outer and inner mitochondrial membranes by direct radical scavenging, while the anionic carboxyl group prevents the attack of oxygen radicals on the inner membrane by increasing its negative surface charge (Sassa *et al.* 1994). Celastrol is of great interest as it is a compound which could be easily placed into human clinical trials due to its lack of toxicity. We investigated the neuroprotective effects of celastrol in rodent models of PD and HD.

Materials and methods

Materials

All reagents were purchased from Sigma (St Louis, MO, USA) except celastrol which was purchased from Microsource (Gaylordsville, CT, USA) and dissolved in a mixture of dimethylsulfoxide (DMSO) and cremophore (10%/90%). Despite the fact that this mixture was always used as a solvent, we only refer to 'DMSO' in order to make the figures and text more concise. 3-NP was dissolved in distilled water and the pH was adjusted to 7.4. MPTP was dissolved in phosphate-buffered saline (PBS). 2,3,5-triphenyl tetrazolium chloride was diluted (2%) in distilled water.

Animals and procedures

The experiments were carried out on mice and rats in accordance with the NIH Guide for the Care and Use of Laboratory Animals. All procedures were approved by the local Animal Care and Use Committee. Mice (four per cage) and rats (two per cage) were maintained in a temperature/humidity-controlled environment under a 12-h light/dark cycle with free access to food and water. Male Swiss Webster mice (8–12 mice per group, 12 weeks old) were injected with celastrol (3 mg/kg, i.p.) or 'DMSO'(10% DMSO/90% cremophore; 10 mL/kg) 12 h before and 12 h after receiving the first MPTP injection (15 mg/kg, i.p. each 2 h × 4 doses) or PBS injections (10 mL/kg). Therefore, each celastrol/MPTP-treated mouse received two celastrol injections (3 mg/kg, i.p.) 24 h apart and four MPTP injections (15 mg/kg, i.p.) 2 h apart. The last MPTP injection was performed 6 h after the first injection. Mice were killed 7 days later by cervical dislocation. Male Lewis rats (12 weeks old) were anesthetized with isoflurane before being subcutaneously implanted with osmotic minipumps (2ML1 Alzet pump) containing 3-NP. Rats were continuously infused with 3-NP for 5 days at a daily dose of 54 mg/kg (Ouary *et al.* 2000). Beginning 24 h after the surgery, rats were injected twice a day with celastrol (3 mg/kg/dose, i.p.) until killing. Rats were killed 5 days after the surgery.

HPLC measurement of dopamine and metabolites

For measurement of DA and its metabolites, dissected striata were immediately frozen on dry ice and stored at −80°C. Tissues were sonicated and centrifuged in chilled 0.1 M perchloric acid (about 100 μL/mg tissue). The supernatant fluids were taken for measurements of levels of DA and its metabolites 3,4-dihydroxyphenylacetic acid and homovanillic acid by HPLC, as modified from our previously described method (Beal *et al.* 1990). Briefly, 10 μL supernatant fluid was isocratically eluted through an 80 × 4.6-mm C18 column (ESA, Inc., Chelmsford, MA, USA) with a mobile phase containing 75 mM of NaH_2PO_4, 1.5 mM octanesulfonic acid (OSA), 5% acetonitrile (pH 3) and detected by a two-channel Coulochem II electrochemical detector (ESA, Inc.). The flow rate was 1 mL/min. Concentrations of DA and its metabolites are expressed as nanograms per milligram of protein. The protein concentrations of tissue homogenates were measured with the protein analyse protocol (Bio-Rad Laboratories, Hercules, CA, USA) and HTS7000+ plate reader (Perkin Elmer, Norwalk, CT, USA).

Measurement of inducible heat shock protein 70 levels by ELISA

Dissected mouse substantia nigras as well as rat striata were immediately frozen on dry ice and stored at −80°C. The expression of heat shock protein (HSP)70 was measured using a StressXpress HSP70 ELISA kit (Stressgen Biotechnologies, Victoria, BC, Canada) according to the manufacturer's instructions with some modifications, i.e. the frozen tissue was placed in a 1-mL Dounce homogenizer with 250 μL (substantia nigra) or 500 μL (striata) of extraction reagent and homogenized manually with 15 strokes of the pestle. Samples were not diluted and were incubated for 3 h.

Histological and stereological analyses

Fresh brains were fixed by immersion in 4% paraformaldehyde overnight at 4°C. Before sectioning, the tissues were placed in 30% glucose overnight at 4°C for cryoprotection. Serial coronal sections (50 μm thick) were cut through the substantia nigra (mice) or the striatum (rats) using a cryostat. In the mice, two sets consisting of eight sections each, 100 μm apart, were prepared. One set of sections was used for Nissl staining and the other was processed for tyrosine hydroxylase (TH) immunohistochemistry using the avidin-biotin peroxidase technique (Vectastain ABC kit; Vector Laboratories, Burlingame, CA, USA). A rabbit anti-TH affinity-purified antibody (1 : 3000; Chemicon, Temecula, CA, USA) was used. The numbers of Nissl-stained or TH-immunoreactive cells in the SNpc were counted using the optical fractionator (West *et al.* 1991). Analysis was performed using a system consisting of an Eclipse E600 microscope (Nikon, Melville, NY, USA) equipped with a computer-controlled LEP BioPoint motorized stage, DEI-750 video camera, Dimension 4300 computer (Dell, Round Rock, TX, USA)

and the Stereo Investigator (v. 4.35) software program (Microbrightfield, Burlington, VT, USA). Tissue sections were examined using a Plan Apo 100× objective lens (Nikon) with a 1.4 numerical aperture. The size of the x–y sampling grid was 140 μm. The counting frame thickness was 14 μm and the counting frame area was 4900 μm^2. The coefficient of error and coefficient of variation were also determined. A separate set of sections was used for immunohistochemistry using antibodies detailed in Table 1.

Double label immunofluorescence was employed to demonstrate colocalization of TH and HSP70. For the quantification in the SNpc of HSP70 immunoreactivity in nuclear and cytoplasmic compartments, three sections per mouse (100 μm apart) were analysed (n = 5 mice per group). The numbers of neurons per section with predominant staining in either the nuclei or perikarya were determined. Data are expressed as a percentage of neurons with intense nuclear staining. The numbers of tumor necrosis factor-α (TNF-α)-immunoreactive cells in the substantia nigra of mice were estimated stereologically using the optical fractionator technique as described for the TH-positive cell counts. Only intensely stained cells were counted.

For 3-NP lesion volume analysis, brains were sectioned at 2-mm intervals. Slices were immediately placed in 2% 2,3,5-triphenyl tetrazolium chloride in the dark for 30 min and then stored, protected from light, in 4% paraformaldehyde. Lesions, noted by pale staining, were evaluated on the surface of each section using a Microcomputer Image Device (Imaging Research Inc., St. Catherine, ON, Canada). Lesion volumes were calculated by multiplying the lesion area by the slice thickness. We previously showed that these measurements exhibit no significant differences from those obtained with Nissl staining (Schulz *et al.* 1995).

Statistical analysis

All data were computed in a database (Instat® software; GraphPad Software Inc., San Diego, CA, USA) and expressed as mean ± SEM. Differences between groups and interaction between treatments were assessed by Student's t-test (unpaired) or by a one-way ANOVA followed, when appropriate, by a Student–Newman Keuls post-hoc test. A probability level of 5% ($p < 0.05$) was considered significant.

Results

Celastrol attenuated dopaminergic neuron loss induced by MPTP in the substantia nigra pars compacta

Dimethylsulfoxide-treated mice that received MPTP (15 mg/kg, i.p. q 2 h × 4 doses) sustained a 48% ($p < 0.001$) loss of Nissl-immunopositive neurons and a 48% ($p < 0.01$) loss of TH-immunopositive dopaminergic neurons within the SNpc compared with DMSO/PBS-treated mice (Fig. 1 and Table 2). Celastrol alone (3 mg/kg, i.p. q 12 h × 2 doses) did not have any effect on the number of Nissl-immunopositive neurons or on the number of TH-immunopositive neurons. However, celastrol treatment significantly diminished the MPTP-induced loss of SNpc neurons. Indeed, celastrol protected against the loss of Nissl- ($p < 0.001$) and TH- ($p < 0.01$) immunopositive neurons. This protection was strong as the number of Nissl- and TH-immunopositive neurons was not significantly different between the DMSO/PBS and celastrol/MPTP groups.

Celastrol reduced MPTP-induced depletion of striatal dopamine levels

Celastrol alone had no effect on striatal DA levels (Fig. 2). MPTP administration induced a 37% depletion of striatal DA level compared with DMSO/PBS-treated mice ($p < 0.001$). Celastrol significantly protected against the MPTP-induced depletion of striatal DA ($p < 0.05$). The striatal DA levels of celastrol/MPTP-treated mice were not significantly different from those of celastrol/PBS-treated mice. MPTP treatment also induced a significant decrease in striatal 3,4-dihydroxyphenylacetic acid (−34%, $p < 0.001$) and homovanillic acid (−29%, $p < 0.001$). Celastrol treatment prevented the MPTP-induced 3,4-dihydroxyphenylacetic acid depletion ($p < 0.05$).

Celastrol reduction of MPTP neurotoxicity is accompanied by increased heat shock protein 70 expression in the substantia nigra pars compacta

Heat-shock chaperones such as HSP70 have been shown to confer protection in a *Drosophila* model of PD (Auluck *et al.* 2002). We therefore examined whether the protection observed could result, at least in part, from an increase in the inducible form of HSP70 by celastrol. At 1 week after two injections of celastrol (3 mg/kg, q 24 h × 2 doses), HSP70 immunostaining was strongly increased in the SNpc of celastrol/PBS-treated mice. As revealed by immunocytochemistry, the solvent 'DMSO' (10%/90%) used to dissolve celastrol also enhanced HSP70 immunostaining in the SNpc. However, the inducible form of HSP70 was almost totally

Table 1 List of antibodies used

	Antibody	Company	Dilution
HSP70	Rabbit anti-HSP70 (HSP72) polyclonal	Stressgen Biotechnologies, Victoria, BC, Canada	1 : 2000
TNF-α	Rabbit anti-TNF-αpolyclonal	Calbiochem-Novabiochem Corporation, San Diego, CA, USA	1 : 100
NFκB	Affinity-purified rabbit anti-NFκB p65 polyclonal	Santa Cruz Biotechnology, Inc., Santa Cruz, CA, USA	1 : 500
CD40L	Goat anti-CD40L rabbit polyclonal	Santa Cruz Biotechnology, Inc.	1 : 1000
TH	Anti-TH	Chemicon, Temecula, CA, USA	1 : 4000

HSP, heat shock protein; NFκB, nuclear factor κ B; TH, tyrosine hydroxylase; TNF-α, tumor necrosis factor-α.

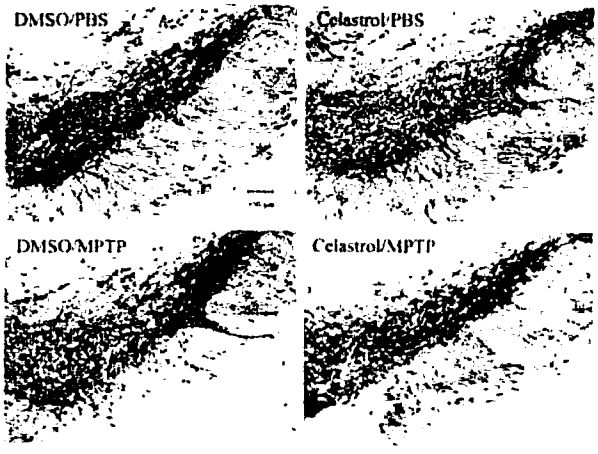

Fig. 1 Effect of celastrol treatment on MPTP-induced loss of dopamine neurons in mice. Photomicrographs of tyrosine hydroxylase-immunostained sections through the substantia nigra pars compacta showing MPTP-induced loss of dopaminergic neurons and the neuroprotective effect afforded by celastrol. DMSO, dimethylsulfoxide; PBS, phosphate-buffered saline.

absent in DMSO/MPTP-treated mice 1 week after the treatment. In contrast to DMSO/MPTP-treated mice that only weakly express HSP70 at 1 week, celastrol/MPTP-treated mice showed increased HSP70 immunolabeling (Fig. 3a).

The observation that celastrol induced an increase in HSP70, obtained by immunohistochemistry, was confirmed by biochemistry. Measurement of inducible HSP70 by ELISA showed that 7 days after only two celastrol injections (3 mg/kg, q 24 h), the level of the inducible form of HSP70 was significantly increased in the substantia nigra ($p < 0.05$). The two injections of DMSO did not significantly increase HSP70 compared with control (Fig. 3b).

Table 2 Stereological counts of tyrosine hydroxylase- (TH) and Nissl-positive neurons (optical fractionator) in the substantia nigra pars compacta for each group

	Nissl (mean ± SEM)	TH (mean ± SEM)
DMSO/PBS	11 188 ± 408	9604 ± 419
Celastrol/PBS	11 071 ± 596	9483 ± 683
DMSO/MPTP	5760 ± 697	4975 ± 1119
compared with DMSO/PBS	$p < 0.001$	$p < 0.01$
Celastrol/MPTP	9658 ± 609	8575 ± 331
compared with DMSO/PBS	$p < 0.001$	$p < 0.001$

Celastrol prevented the loss of Nissl- ($p < 0.001$) and TH- ($p < 0.01$) positive neurons induced by MPTP. DMSO, dimethylsulfoxide; PBS, phosphate-buffered saline.

Celastrol induced nuclear translocation of cytoplasmic heat shock protein 70

Double label immunofluorescence showed colocalization of HSP70 with TH, indicating that increased nigral HSP70 expression occurred within dopaminergic neurons. HSP70 was observable in the cytoplasm as well as in the nucleus of dopaminergic neurons (Fig. 3c). Quantification of HSP70 in both compartments showed that, in the SNpc of DMSO/MPTP-treated mice, 27% of HSP70 was in the nucleus while 73% remained in the cytoplasm. However, in celastrol/MPTP-treated mice, 47% of HSP70 was in the nucleus, indicating that celastrol induced a translocation of inducible HSP70 from the cytoplasm to the nucleus ($p < 0.001$ compared with DMSO/PBS-treated mice) (Fig. 3d). The nuclear translocation of inducible HSP70 is necessary for the generation of newly expressed HSP70 (Barrett *et al.* 2004).

Celastrol attenuated MPTP neurotoxicity by attenuating inflammation

In view of the known potent anti-inflammatory activity of celastrol, its effects on the production of TNF-α and nuclear factor κ B (NFκB) were investigated. Treatment with DMSO plus MPTP induced increased immunostaining for the inflammatory cytokine TNF-α in the SNpc (Fig. 4a). Intensely stained cells for TNF-α were counted stereologically in the substantia nigra (Fig. 4b). There were no intensely stained cells in control groups. The number of TNF-α-immunoreactive cells was significantly lower ($p < 0.05$) in the celastrol/MPTP- than in the DMSO/MPTP-treated mice. During the inflammatory process, TNF-α production activates the transcription factor NFκB, inducing release of inflammatory cytokines (Ghosh and Karin 2002). In our experiment, DMSO/MPTP treatment increased NFκB immunoreactivity in the SNpc (Fig. 4a). Celastrol treatment reduced MPTP-induced immunoreactivity of NFκB, confirming that celastrol both directly and indirectly inhibits activation of different mediators of the inflammatory pathway.

Celastrol reduced striatal lesion volumes induced by 3-nitropropionic acid in rats

Chronic delivery of 3-NP in rats via osmotic minipumps (54 mg/kg/day, s.c.) induced striatal lesions with a volume of approximately 12 mm^3 (Fig. 5). Celastrol treatment (3 mg/kg, i.p. q 12 h × 8 doses) significantly reduced 3-NP-induced neurodegeneration. Indeed, in celastrol/3-NP-treated rats, the lesion volume was nearly absent (0.17 mm^3) and reduced by 98% ($p < 0.05$) compared with DMSO/3-NP-treated rats.

Celastrol induced heat shock protein 70 in the striata of 3-nitropropionic acid-treated rats

Heat-shock chaperones such as HSP70 have been shown to confer protection in models of HD (Dedeoglu *et al.* 2002) and polyglutamine-mediated neurodegeneration (Warrick *et al.* 1999). Therefore, we checked whether the strong

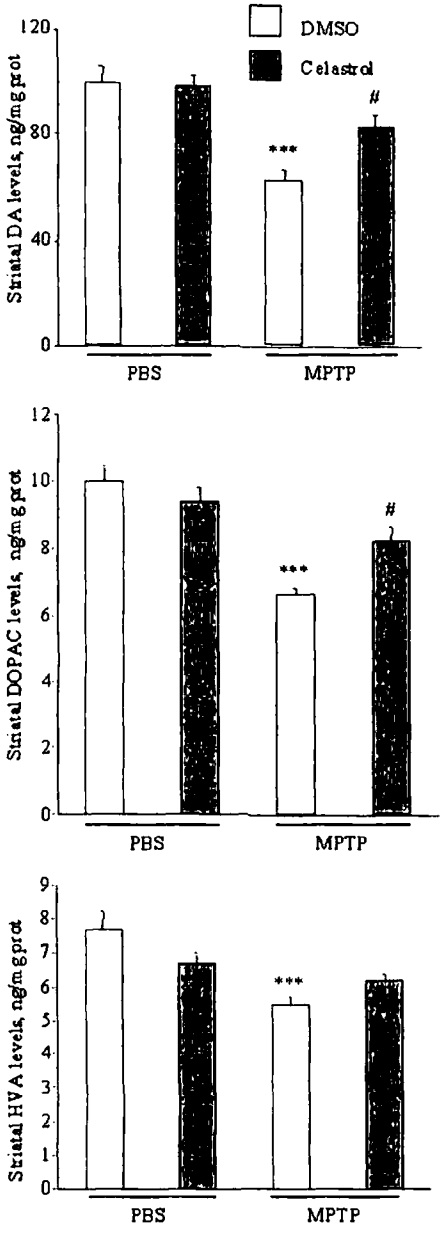

Fig. 2 Effects of celastrol and MPTP treatments on striatal levels of dopamine (DA), 3,4-dihydroxyphenylacetic acid (DOPAC) and homovanillic acid (HVA). Celastrol treatment significantly attenuated the DA and DOPAC depletions induced by MPTP. ***$p < 0.001$ compared with dimethylsulfoxide (DMSO)/phosphate-buffered saline (PBS)-treated mice; #$p < 0.05$ compared with DMSO/MPTP-treated mice.

protection afforded by celastrol treatment resulted from HSP70 induction. The inducible form of HSP70 was weakly present in DMSO/3-NP-treated rats as assessed by immunohistochemistry (Fig. 6a). The localization of HSP70 expression in the striata of celastrol/3-NP-treated rats was similar to that observed at the site of neurodegeneration in 3-NP-treated rats. Celastrol treatment in 3-NP-treated rats enhanced HSP70 expression by 19% ($p < 0.05$) as assessed by ELISA (Fig. 6b).

Celastrol reduces 3-nitropropionic acid-induced astrogliosis in rats

Celastrol stongly reduced 3-NP-induced neurotoxicity, probably by inducing HSP70. The results obtained with the 3-NP model are in accordance with those obtained in the MPTP model. As 3-NP is known to induce astrogliosis (Beal *et al.* 1993), we decided to examine the effects of celastrol on astrogliosis. CD40L, an inflammatory factor characteristic of astroglial cells, showed a marked staining of astrocytes in the striata of DMSO/3-NP-treated rats (Fig. 7). Celastrol treatment strongly reduced 3-NP-induced astrogliosis.

Discussion

Celastrol protected dopaminergic neurons against the neurotoxic effects of MPTP. It prevented both the degeneration of nigrostriatal dopaminergic neurons and the loss of striatal DA induced by MPTP. Celastrol also strongly reduced the volume of striatal lesions induced by a chronic 3-NP treatment.

Heat shock protein 70, the major inducible heat shock chaperone, is induced in response to oxidative stress and neuronal injury. HSP70 plays a protective role by preventing protein misfolding and aggregation as well as oxidative injury and apoptosis (Yenari 2002). In *Drosophila* models, HSP70 has been shown to confer protection against alpha-synuclein toxicity Auluck *et al.* 2002) and polyglutamine-mediated neurodegeneration (Warrick *et al.* 1999; Bonini 2002). We found that mice overexpressing HSP70 were less sensitive to 3-NP toxicity (Dedeoglu *et al.* 2002). Moreover, a recently published study reported that HSP70 gene transfer to DA neurons, by injection of a recombinant adeno-associated virus in mice, protects against MPTP-induced neurotoxicity (Dong *et al.* 2005)

Celastrol activates heat shock transcription factor 1. It shares kinetic features with heat shock, including rapid induction within minutes and a similar magnitude of induction (Westerheide *et al.* 2004). The EC_{50} value was 3 μM. Celastrol induced heat shock transcription factor 1 DNA binding, hyperphosphorylation of heat shock transcription factor 1 and expression of chaperone genes. The HSP70 protein and mRNA levels were similar to those which occurred with 42°C heat shock in both HeLa and neuroblastoma cells. Celastrol protected cells from subsequent lethal heat stress and decreased apoptotic cell death. Induction of HSPs is known to intervene at multiple points in the apoptotic pathway, including inhibition of c-Jun N-terminal kinase activation and prevention of cytochrome *c* release and caspase activation (Green and Kroemer 2004).

Celastrol therefore has a number of mechanisms by which it may exert neuroprotective effects, including anti-inflamma-

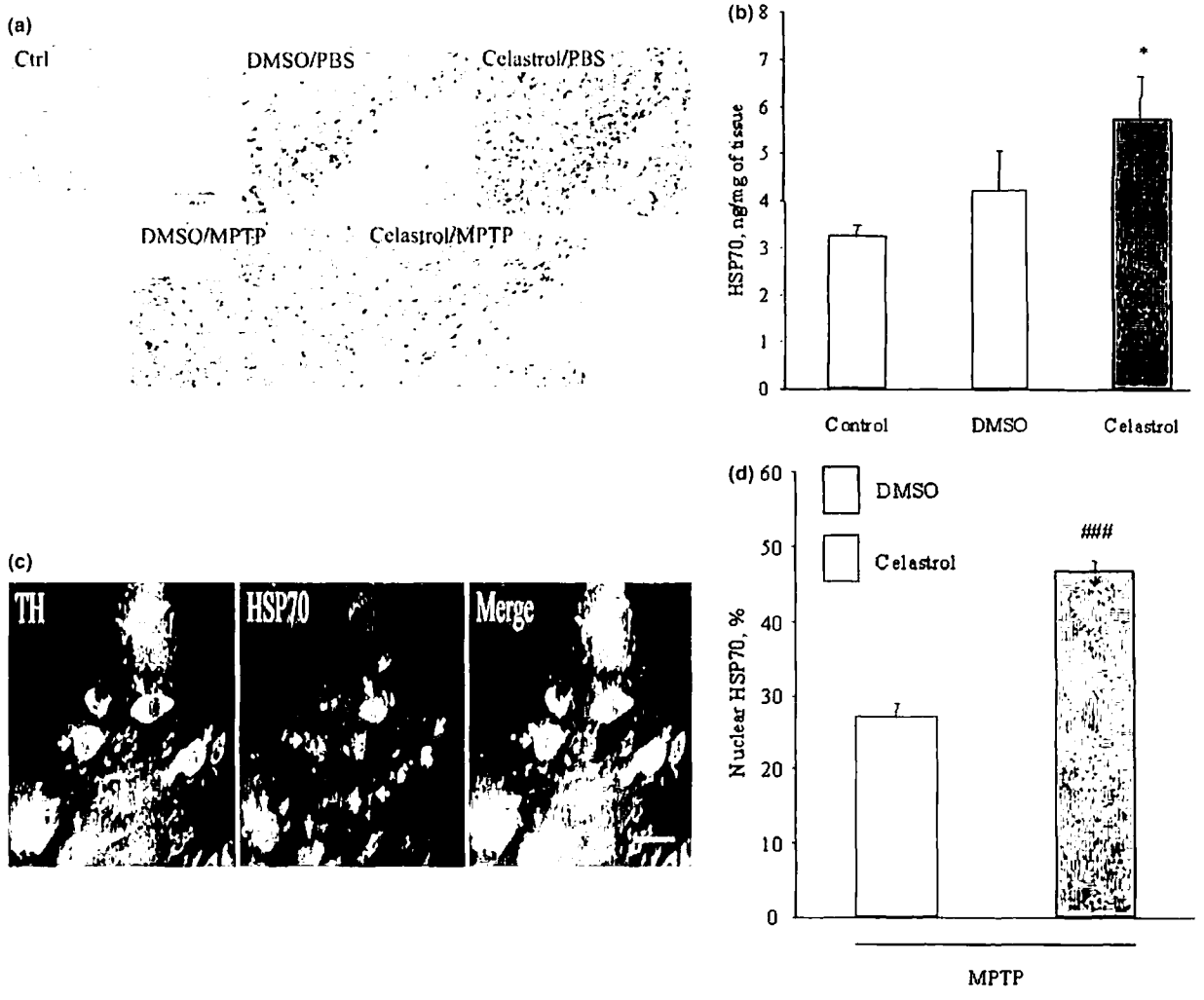

Fig. 3 Celastrol induced an increase of heat shock protein (HSP)70 immunoreactivity and protein level in the substantia nigra as well as HSP70 nuclear translocation. (a) Inducible HSP70 immunoreactivity in the substantia nigra pars compacta (SNpc) of control (Ctrl) or MPTP-lesioned mice treated with dimethylsulfoxide (DMSO) or celastrol. Upper panel, DMSO or celastrol-induced enhancement of HSP70 immunoreactivity in phosphate-buffered saline (PBS)-treated mice. Lower panel, celastrol-induced enhancement of HSP70 immunoreactivity in MPTP-treated mice. (b) Effect of celastrol treatment on HSP70 levels in the substantia nigra. Two injections of celastrol increased HSP70 levels at 7 days. $^{*}p < 0.05$ compared with control mice. (c) Colocalization of tyrosine hydroxylase (TH) (left panel) and HSP70 (middle panel) in the cytoplasm of dopaminergic neurons (arrows). The merge shows the presence of HSP70 immunoreactivity in the nucleus of TH-positive neurons. Scale bar for the right panel, 25 μm. (d) Quantification of HSP70 immunoreactivity in the SNpc of MPTP-treated mice. The numbers of neurons with predominant staining in either the nuclei or perikarya per section were determined. Data are expressed as a percentage of neurons with intense nuclear staining. Celastrol treatment induced the nuclear translocation of HSP70 in MPTP-treated mice. $^{###}p < 0.001$ compared with DMSO/MPTP-treated mice.

tory and antioxidative effects and its ability to up-regulate HSPs. Indeed, some anti-inflammatory compounds are able to activate the DNA-binding activity of the heat shock transcription factor 1 and, in consequence, HSP70 expression (Morimoto and Santoro 1998). Therefore, we examined the effect of celastrol on HSP70 expression 1 week after only two injections of celastrol in mice. We observed an increase of HSP70 levels, measured by both ELISA and HSP70 immunostaining, in the SNpc. We also observed an enhancement of HSP70 immunoreactivity 1 day after MPTP treatment (result not shown) which was reduced after 1 week. MPTP treatment (20 mg/kg, q 12 h × 4 doses) in mice was reported to result in a transient up-regulation of HSP70 expression in the substantia nigra from 4 h to 2 days after the first MPTP injection, which was no longer observable at 4 days after the treatment (Kuhn *et al.* 2003). Our results are consistent with a

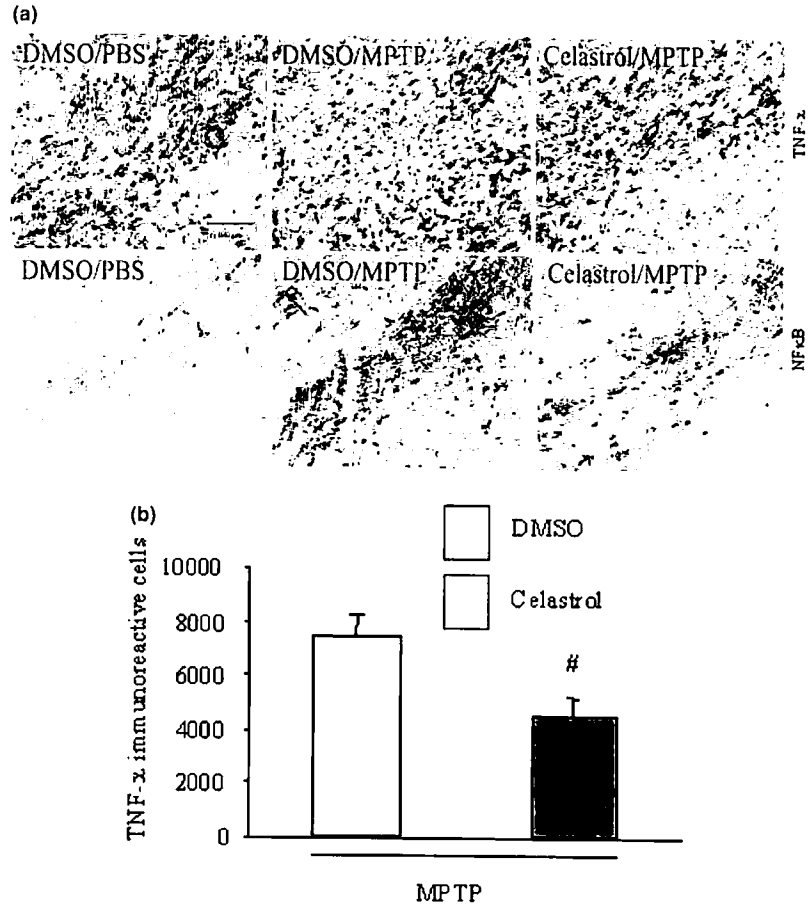

Fig. 4 Tumor necrosis factor-α (TNF-α) and nuclear factor κ B (NFκB) immunoreactivity in the substantia nigra pars compacta of control or MPTP-lesioned mice treated with dimethylsulfoxide (DMSO) or celastrol. (a) Celastrol attenuated the MPTP-induced increases in TNF-α and NFκB immunoreactivity in dopaminergic neurons. (b) Number of TNF-α-immunoreactive cells in the substantia nigra. The number of TNF-α-immunoreactive cells was significantly lower in the celastrol/MPTP-treated mice than in the DMSO/MPTP-treated mice. #$p < 0.05$ compared with DMSO/MPTP-treated mice. PBS, phosphate-buffered saline.

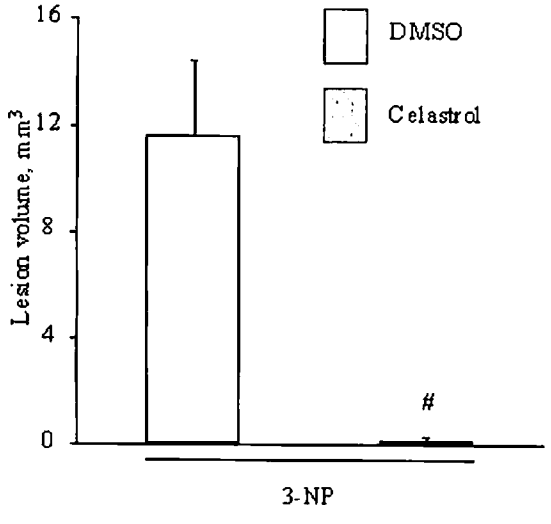

Fig. 5 Effect of celastrol treatment on 3-nitropropionic acid (3-NP)-induced striatal lesions in rats. Celastrol strongly reduced the lesion resulting from the 3-NP treatment. #$p < 0.05$ compared with dimethylsulfoxide (DMSO)/3-NP-treated rats.

recent study showing that celastrol (3 μM) induces HSP70 protein and mRNA levels in HeLa and neuroblastoma cells (Westerheide *et al.* 2004).

In our study, celastrol enhanced HSP70 expression in MPTP-treated mice. HSP70 may protect by regulating matrix metalloproteinases (Lee *et al.* 2004). In the brain, HSP70, by an as yet unknown mechanism, can increase Bcl-2 expression which, in turn, blocks cytochrome *c* release and subsequent effector caspase activation (Creagh *et al.* 2000; Gabai *et al.* 2002; Yenari 2002). We observed more nuclear HSP70 in celastrol/MPTP- than in DMSO/MPTP-treated mice. This difference presumably resulted from the known cytoplasm to nucleus translocation of inducible HSP70, necessary for the generation of newly expressed HSP70 (Barrett *et al.* 2004).

In their review, Malhotra and Wong (2002) reported that HSP70 prevents the activation of NFκB by stabilizing the Nuclear factor Kappa B inhibitor-alpha (NFκB–IκBα) complex. The induction of the heat shock response before a proinflammatory signal inhibits NFκB activation and NFκB-dependent proinflammatory gene expression. Schmidt and

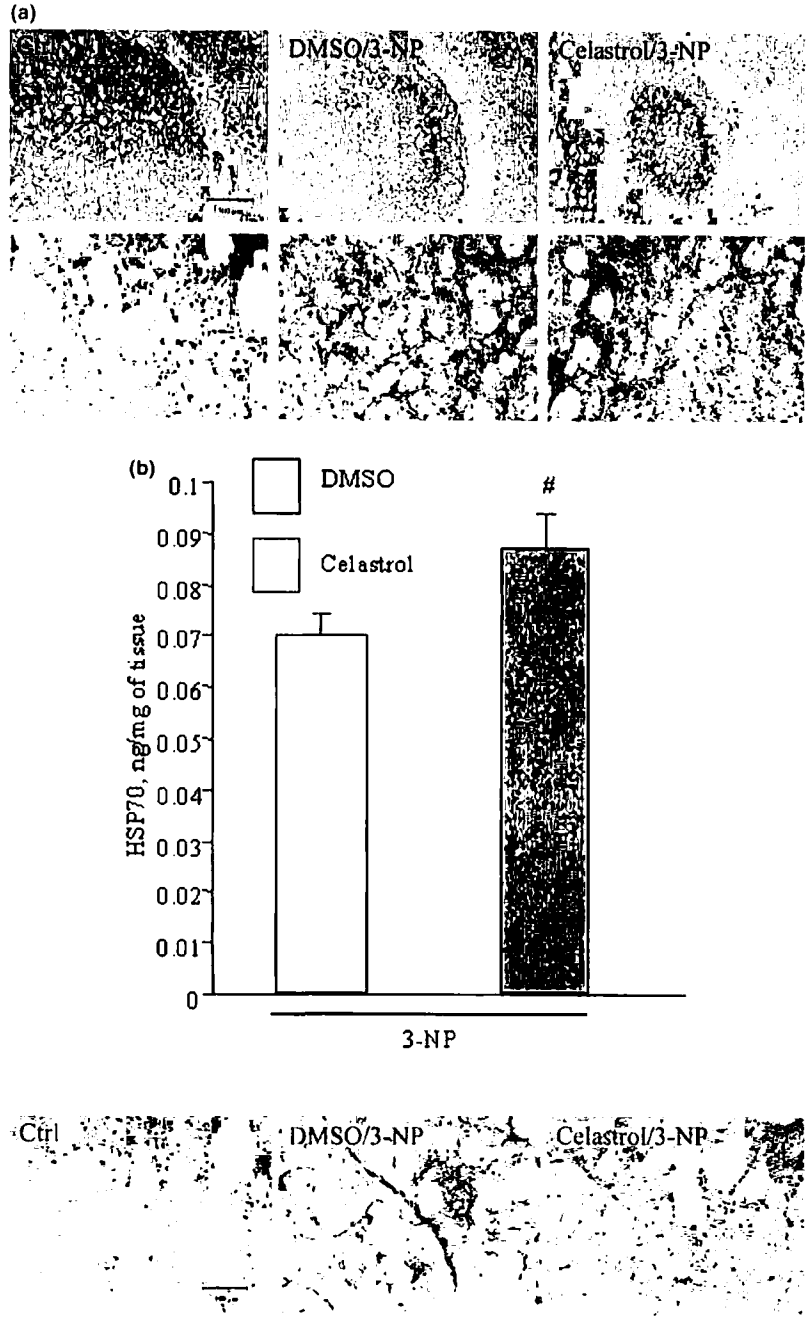

Fig. 6 Celastrol induces heat shock protein (HSP)70 in the striatum of 3-nitropropionic acid (3-NP)-lesioned rat. (a) Upper panel, HSP70 staining was absent in control (Ctrl), moderate in the striatum of dimethylsulfoxide (DMSO)/3-NP-treated mice and most intense in celastrol/3-NP-treated mice. HSP70 labeling occurred in neurons and neuropil within the focal region vulnerable to 3-NP neurotoxicity. Lower panel, higher magnification (4×). (b) Celastrol treatment increased HSP70 expression in the striata of 3-NP-treated rats. #$p < 0.05$ compared with DMSO/3-NP-treated rats.

Fig. 7 CD40L immunoreactivity in the striatum of 3-nitropropionic acid (3-NP)-lesioned rat. CD40L-immunoreactive astrocytes proliferate in dimethylsulfoxide (DMSO)/3-NP-treated rat and are attenuated by celastrol treatment. Ctrl, control.

Abdulla (1988) reported that there is a correlation between the extent of interleukin-1β reduction and the level of HSP induction by chemical inducers in THP-1 cells. Therefore, we investigated the effects of celastrol on inflammation. MPTP treatment induces a peak of inflammation at 7 days after its injection (Ciesielska *et al.* 2003). TNF-α is produced primarily by macrophages and plays a major role in the pathogenesis of inflammation. In our study, MPTP induced a marked increase in TNF-α immunostaining in the SNpc 7 days after MPTP administration. Celastrol treatment of MPTP-injected mice significantly reduced the MPTP-induced increase of TNF-α. Binding of TNF-α to its membrane receptor TNF-R1 activates multiple downstream signaling events including activation of caspases and NFκB-mediated transcription. One consequence is an up-regulation of the transcription factor NFκB (Ghosh and Karin 2002). To investigate whether celastrol modified TNF-α activity, we stained the SNpc for NFκB. At 7 days after the treatment,

MPTP induced an increase in NFκB immunoreactivity. Celastrol reduced the increase in NFκB staining in MPTP-treated mice. The dopaminergic neuroprotection observed in celastrol/MPTP-treated mice may therefore result, in part, from the HSP70-induced anti-inflammatory properties of celastrol, which induces a down-regulation of the transcription factor NFκB. This may prevent NFκB-induced release of cytokines, including interleukin-1 and -6.

In our experiments we observed that celastrol exerted a strong neuroprotective effect in another model of neurodegeneration. Celastrol almost completely prevented 3-NP-induced striatal lesions. As observed in the MPTP model, it is probable that celastrol protected against 3-NP toxicity by inducing HSP70. Indeed, HSP70 was induced by celastrol treatment within the upper lateral region of the striatum which is more vulnerable to 3-NP neurotoxicity. The 3-NP model has features in common with the MPTP model, such as inflammation and astrogliosis (Brouillet *et al.* 1999). TNF-α released from macrophages binds to astrocytes, activating them and leading to astrogliosis (Ridet *et al.* 1997). Many functions have been attributed to astroglia, including ion homeostasis, uptake of neurotransmitters and contribution to the immune system (Takuma *et al.* 2004). Astroglia also play a role in the preservation of the host tissue integrity after injury (Dervan *et al.* 2003). We examined the effects of celastrol on 3-NP-induced astrogliosis. As expected, the striata of rats treated with 3-NP showed numerous reactive astrocytes. Celastrol treatment strongly reduced 3-NP-induced astrogliosis in rats.

Conclusions

Celastrol treatment in MPTP-treated mice was sufficient to attenuate the loss of DA and dopaminergic neurons. Celastrol also strongly reduced 3-NP-induced striatal lesions. The neuroprotective effect of celastrol may be multifactorial. Celastrol treatment induced an increase of inducible HSP70 in the substantia nigra of MPTP-treated mice, 7 days after injections, and in the striata of 3-NP-treated rats. Celastrol treatment also resulted in a strong nuclear translocation of HSP70 necessary for the generation of newly expressed HSP70. Induced HSP70 may prevent TNF-α and NFκB activation, inhibiting the release of proinflammatory cytokines and astrogliosis. We observed that celastrol treatment reduced induced inflammation and astrogliosis. HSP70 may also reduce apoptosis. Our results suggest that celastrol could play a therapeutic role in preventing and/or delaying the onset and progression of PD and HD.

Acknowledgements

The work was supported by grants from National Institute of Neurological Disorders and Stroke, the Department of Defense, Michael J. Fox Foundation and Parkinson's Disease Foundation.

References

Allison A. C., Cacabelos R., Lombardi V. R., Alvarez X. A. and Vigo C. (2001) Celastrol, a potent antioxidant and anti-inflammatory drug, as a possible treatment for Alzheimer's disease. *Prog. Neuropsychopharmacol. Biol. Psychiat.* **25**, 1341–1357.

Auluck P. K., Chan H. Y., Trojanowski J. Q., Lee V. M. and Bonini N. M. (2002) Chaperone suppression of alpha-synuclein toxicity in a Drosophila model for Parkinson's disease. *Science* **295**, 865–868.

Barrett M. J., Alones V., Wang K. X., Phan L. and Swerdlow R. H. (2004) Mitochondria-derived oxidative stress induces a heat shock protein response. *J. Neurosci. Res.* **78**, 420–429.

Beal M. F. (2003) Mitochondria, oxidative damage, and inflammation in Parkinson's disease. *Ann. NY Acad. Sci.* **991**, 120–131.

Beal M. F. and Ferrante R. J. (2004) Experimental therapeutics in transgenic mouse models of Huntington's disease. *Nat. Rev. Neurosci.* **5**, 373–384.

Beal M. F., Kowall N. W., Swartz K. J. and Ferrante R. J. (1990) Homocysteic acid lesions in rat striatum spare somatostatin-neuropeptide Y (NADPH-diaphorase) neurons. *Neurosci. Lett.* **108**, 36–42.

Beal M. F., Brouillet E., Jenkins B. G., Ferrante R. J., Kowall N. W., Miller J. M., Storey E., Srivastava R., Rosen B. R. and Hyman B. T. (1993) Neurochemical and histologic characterization of striatal excitotoxic lesions produced by the mitochondrial toxin 3-nitropropionic acid. *J. Neurosci.* **13**, 4181–4192.

Blum D., Torch S., Lambeng N., Nissou M., Benabid A. L., Sadoul R. and Verna J. M. (2001) Molecular pathways involved in the neurotoxicity of 6-OHDA, dopamine and MPTP: contribution to the apoptotic theory in Parkinson's disease. *Prog. Neurobiol.* **65**, 135–172.

Blum D., Galas M. C., Gall D., Cuvelier L. and Schiffmann S. N. (2002) Striatal and cortical neurochemical changes induced by chronic metabolic compromise in the 3-nitropropionic model of Huntington's disease. *Neurobiol. Dis.* **10**, 410–426.

Bonini N. M. (2002) Chaperoning brain degeneration. *Proc. Natl Acad. Sci. USA* **99**, S16 407–S16 411.

Brouillet E., Guyot M. C., Mittoux V., Altairac S., Conde F., Palfi S. and Hantraye P. (1998) Partial inhibition of brain succinate dehydrogenase by 3-nitropropionic acid is sufficient to initiate striatal degeneration in rat. *J. Neurochem.* **70**, 794–805.

Brouillet E., Conde F., Beal M. F. and Hantraye P. (1999) Replicating Huntington's disease phenotype in experimental animals. *Prog. Neurobiol.* **59**, 427–468.

Ciesielska A., Joniec I., Przybylkowski A., Gromadzka G., Kurkowska-Jastrzebska I., Czlonkowska A. and Czlonkowski A. (2003) Dynamics of expression of the mRNA for cytokines and inducible nitric synthase in a murine model of the Parkinson's disease. *Acta Neurobiol. Exp.* **63**, 117–126.

Creagh E. M., Carmody R. J. and Cotter T. G. (2000) Heat shock protein 70 inhibits caspase-dependent and -independent apoptosis in Jurkat T cells. *Exp. Cell Res.* **257**, 58–66.

Deckel A. W. (2001) Nitric oxide and nitric oxide synthase in Huntington's disease. *J. Neurosci. Res.* **64**, 99–107.

Dedeoglu A., Ferrante R. J., Andreassen O. A., Dillmann W. H. and Beal M. F. (2002) Mice overexpressing 70-kDa heat shock protein show increased resistance to malonate and 3-nitropropionic acid. *Exp. Neurol.* **176**, 262–265.

Dervan A. G., Totterdell S., Lau Y. S. and Meredith G. E. (2003) Altered striatal neuronal morphology is associated with astrogliosis in a chronic mouse model of Parkinson's disease. *Ann. NY Acad. Sci.* **991**, 291–294.

Dong Z., Wolfer D. P., Lipp H. P. and Bueler H. (2005) Hsp70 gene transfer by adeno-associated virus inhibits MPTP-induced nigro-

striatal degeneration in the mouse model of Parkinson disease. *Mol. Ther.* 11, 80–88.

El Massioui N., Ouary S., Cheruel F., Hantraye P. and Brouillet E. (2001) Perseverative behavior underlying attentional set-shifting deficits in rats chronically treated with the neurotoxin 3-nitropropionic acid. *Exp. Neurol.* 172, 172–181.

Gabai V. L., Mabuchi K., Mosser D. D. and Sherman M. Y. (2002) Hsp72 and stress kinase c-jun N-terminal kinase regulate the bid-dependent pathway in tumor necrosis factor-induced apoptosis. *Mol. Cell Biol.* 22, 3415–3424.

Ghosh S. and Karin M. (2002) Missing pieces in the NF-kappaB puzzle. *Cell* 109, S81–S96.

Green D. R. and Kroemer G. (2004) The pathophysiology of mitochondrial cell death. *Science* 305, 626–629.

Greenamyre J. T. and Hastings T. G. (2004) Biomedicine. Parkinson's — divergent causes, convergent mechanisms. *Science* 304, 1120–1122.

Harper P. S. (ed.) (1991) *Huntington's Disease*. Saunders, London.

Heikkila R. E., Cabbat F. S., Manzino L. and Duvoisin R. C. (1984) Effects of 1-methyl-4-phenyl-1,2,5,6-tetrahydropyridine on neostriatal dopamine in mice. *Neuropharmacology* 23, 711–713.

Hornykiewicz O. (1966) Dopamine (3-hydroxytyramine) and brain function. *Pharmacol. Rev.* 18, 925–964.

Kuhn K., Wellen J., Link N., Maskri L., Lubbert H. and Stichel C. C. (2003) The mouse MPTP model: gene expression changes in dopaminergic neurons. *Eur. J. Neurosci.* 17, 1–12.

Lee J. E., Kim Y. J., Kim J. Y., Lee W. T., Yenari M. A. and Giffard R. G. (2004) The 70 kDa heat shock protein suppresses matrix metalloproteinases in astrocytes. *Neuroreport* 15, 499–502.

Malhotra V. and Wong H. R. (2002) Interactions between the heat shock response and the nuclear factor-kappaB signaling pathway. *Crit. Care Med.* 30, S89–S95.

Moore D. J., West A. B., Dawson V. L. and Dawson T. M. (2004) Molecular pathophysiology of Parkinson's disease. *Annu. Rev. Neurosci.* (Epub ahead of print).

Morimoto R. I. and Santoro M. G. (1998) Stress-inducible responses and heat shock proteins: new pharmacologic targets for cytoprotection. *Nat. Biotechnol.* 16, 833–838.

Orr C. F., Rowe D. B. and Halliday G. M. (2002) An inflammatory review of Parkinson's disease. *Prog. Neurobiol.* 68, 325–340.

Ouary S., Bizat N., Altairac S., Menetrat H., Mittoux V., Conde F., Hantraye P. and Brouillet E. (2000) Major strain differences in response to chronic systemic administration of the mitochondrial toxin 3-nitropropionic acid in rats: implications for neuroprotection studies. *Neuroscience* 97, 521–530.

Ramsay R. R. and Singer T. P. (1986) Energy-dependent uptake of N-methyl-4-phenylpyridinium, the neurotoxic metabolite of 1-methyl-4-phenyl-1,2,3,6-tetrahydropyridine, by mitochondria. *J. Biol. Chem.* 261, 7585–7587.

Ridet J. L., Malhotra S. K., Privat A. and Gage F. H. (1997) Reactive astrocytes: cellular and molecular cues to biological function. *Trends Neurosci.* 20, 570–577.

Sassa H., Takaishi Y. and Terada H. (1990) The triterpene celastrol as a very potent inhibitor of lipid peroxidation in mitochondria. *Biochem. Biophys. Res. Commun.* 172, 890–897.

Sassa H., Kogure K., Takaishi Y. and Terada H. (1994) Structural basis of potent antiperoxidation activity of the triterpene celastrol in mitochondria: effect of negative membrane surface charge on lipid peroxidation. *Free Radic. Biol. Med.* 17, 201–207.

Schmidt J. A. and Abdulla E. (1988) Down-regulation of IL-1 beta biosynthesis by inducers of the heat-shock response. *J. Immunol.* 14, 2027–2034.

Schulz J. B., Henshaw D. R., Matthews R. T. and Beal M. F. (1995) Coenzyme Q10 and nicotinamide and a free radical spin trap protect against MPTP neurotoxicity. *Exp. Neurol.* 132, 279–283.

Takuma K., Baba A. and Matsuda T. (2004) Astrocyte apoptosis: implications for neuroprotection. *Prog. Neurobiol.* 72, 111–127.

The Huntington's Disease Collaborative Research Group (1993) A novel gene containing a trinucleotide repeat that is expanded and unstable on Huntington's disease chromosomes. *Cell* 72, 971–983.

Warrick J. M., Chan H. Y., Gray-Board G. L., Chai Y., Paulson H. L. and Bonini N. M. (1999) Suppression of polyglutamine-mediated neurodegeneration in Drosophila by the molecular chaperone HSP70. *Nat. Genet.* 4, 425–428.

West M. J., Slomianka L. and Gundersen H. J. (1991) Unbiased stereological estimation of the total number of neurons in the subdivisions of the rat hippocampus using the optical fractionator. *Anat. Rec.* 231, 482–497.

Westerheide S. D., Bosman J. D., Mbadugha B. N., Kawahara T. L., Matsumoto G., Kim S., Gu W., Devlin J. P., Silverman R. B. and Morimoto R. I. (2004) Celastrols as inducers of the heat shock response and cytoprotection. *J. Biol. Chem.* [Epub ahead of print].

Yenari M. A. (2002) Heat shock proteins and neuroprotection. *Adv. Exp. Med. Biol.* 513, 281–299.

nature medicine

ARTICLES

Functional engraftment of human ES cell–derived dopaminergic neurons enriched by coculture with telomerase-immortalized midbrain astrocytes

Neeta S Roy[1], Carine Cleren[1], Shashi K Singh[1], Lichuan Yang[1], M Flint Beal[1] & Steven A Goldman[1,2]

To direct human embryonic stem (HES) cells to a dopaminergic neuronal fate, we cocultured HES cells that were exposed to both sonic hedgehog and fibroblast growth factor 8 with telomerase-immortalized human fetal midbrain astrocytes. These astrocytes substantially potentiated dopaminergic neurogenesis by both WA09 and WA01 HES cells, biasing them to the A9 nigrostriatal phenotype. When transplanted into the neostriata of 6-hydroxydopamine–lesioned parkinsonian rats, the dopaminergic implants yielded a significant, substantial and long-lasting restitution of motor function. However, although rich in donor-derived tyrosine hydroxylase–expressing neurons, the grafts exhibited expanding cores of undifferentiated mitotic neuroepithelial cells, which can be tumorigenic. These results show the utility of recreating the cellular environment of the developing human midbrain while driving dopaminergic neurogenesis from HES cells, and they demonstrate the potential of the resultant cells to mediate substantial functional recovery in a model of Parkinson disease. Yet these data also mandate caution in the clinical application of HES cell–derived grafts, given their potential for phenotypic instability and undifferentiated expansion.

HES cells can generate all major somatic cell lineages[1–3], including glia and neurons[4,5]. Among the latter, a variety of neuronal phenotypes have been induced in HES-cell cultures; importantly, the instructions for generating specific lineages appear generally conserved between mouse and human ES cells. Midbrain dopaminergic neurons have been selectively induced from both mouse and human ES cells, under the dual influence of sonic hedgehog (SHH) and fibroblast growth factor (FGF)-8 (refs. 6–9). However, SHH + FGF8–induced cultures produce many other neuronal phenotypes, and they have generally not achieved the high levels of dopaminergic enrichment required for therapeutic engraftment. Coculture with stromal feeder cells and striatal astrocytes has thus been used to accentuate dopaminergic neuronal production *in vitro*[7,10,11]. Yet despite strong evidence for the existence of mesencephalic glial signals for dopaminergic neuronal differentiation and survival[12,13], no studies have yet attempted to mimic developmental dopaminergic induction from ES cells with mesencephalic glia. Absent such astrocyte-potentiated dopaminergic differentiation, the most enriched dopaminergic preparations thus far reported have comprised less then half of the total cell pool, as defined by the fraction of tyrosine hydroxylase–expressing (TH^+) neurons among all cells.

The acquisition of more highly enriched dopaminergic populations is an important prerequisite to using HES cell–derived dopaminergic neurons for cell-based therapy, as non-dopaminergic neuronal derivatives may yield unpredictable or deleterious neurological side-effects, and incompletely differentiated HES cells are potentially tumorigenic upon implantation[14]. We describe here a new strategy for improving the efficiency of dopaminergic neurogenesis from HES-cell cultures, using coculture with telomerase-immortalized human fetal mesencephalic astrocytes during SHH + FGF8–mediated neuronal induction. By this means, we achieved the high-efficiency enrichment of dopaminergic neurons, in numbers and phenotypic uniformity compatible with therapeutic implantation. We then tested the hypothesis that these highly enriched dopaminergic preparations would provide significant functional benefit when transplanted into an experimental model of Parkinson disease, the 6-hydroxydopamine (6-OHDA)-lesioned rat. We found that when engrafted into the striata of 6-OHDA–lesioned rats, these cells indeed mediated the significant and substantial restitution of motor function in the lesioned recipients, relative to untreated lesioned rats. However, we also noted that the grafts exhibited phenotypic instability, with a central diminution in dopaminergic neurons, and—even more troubling—persistent proliferation of undifferentiated cells in the transplant cores.

RESULTS

SHH + FGF8-exposed HES cells yield dopaminergic neurons

We cultured HES cells from the H1 and H9 cell lines as anchored ES cells, before FGF2-dependent neuralization to stage 2, under feeder-free culture conditions. TH^+ neurons were generated in the presence of N-terminal SHH and FGF8, using minor modifications (see Methods) of described protocols[6,7] (Fig. 1a). At stage 3, in ITSF

[1]Departments of Neurology & Neuroscience, Weill Medical College of Cornell University, New York, New York 10021, USA. [2]Departments of Neurology, Neurosurgery and Pediatrics, University of Rochester Medical Center, Rochester, New York 14642, USA. Correspondence should be addressed to N.S.R. (ner2004@med.cornell.edu) or S.A.G. (steven_goldman@urmc.rochester.edu)

Received 24 August; accepted 15 September; published online 22 October 2006; doi:10.1038/nm1495

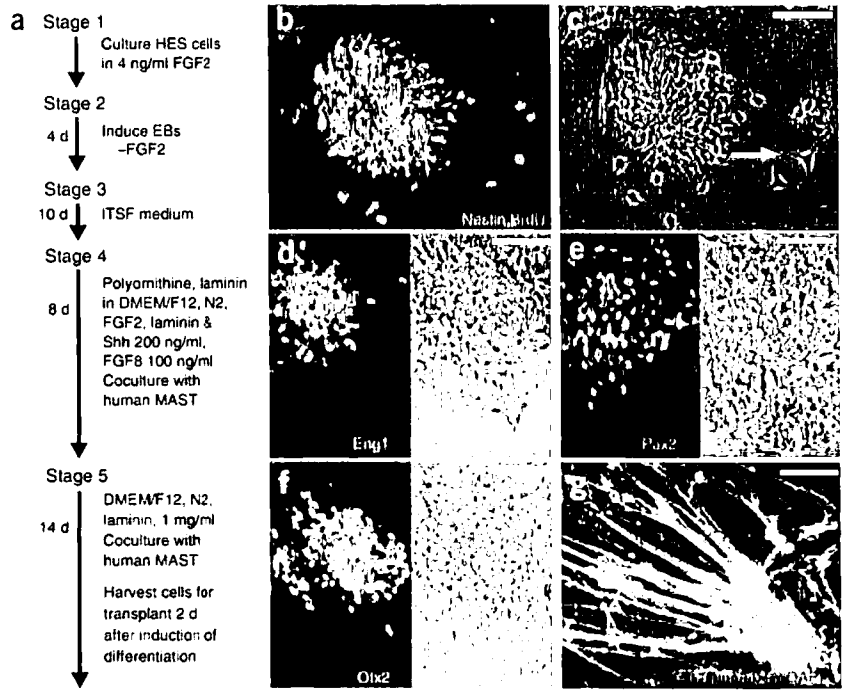

Figure 1 Dopaminergic neurons can be generated from HES cells. (a) Outline of the serial induction and differentiation of dopaminergic neurons from HES cells. Initially undifferentiated human embryonic stem cells are used as a substrate for neuralization, followed by dopaminergic induction. (b,c) Formation of rosettes at stage 3. These rosettes, b, primarily expressed nestin (red) and were highly mitotic, as indicated by BrdU incorporation (green). Some spontaneous differentiation to neurons could be seen at the edge of the rosettes, c. (d–f) Induction of dopaminergic progenitors at stage 4, as indicated by the presence of engrailed1 (Engl, d), Pax2 (e) and Otx2 (f). (g) At stage 5, TH-immunoreactive (red) βIII-tubulin$^+$ neurons (green) were observed (seen here 7 d after initiation of stage 5). Scale bars: b–f, 80 μm; g, 40 μm.

medium, small rosettes comprised of dividing nestin$^+$ cells formed (Fig. 1b), many of which exhibited spontaneous neuronal differentiation (Fig. 1c). When treated with FGF2 + FGF8 + SHH in stage 4, the cells then expressed transcription factors typical of midbrain dopaminergic progenitors, including Pax2, Otx2 and engrailed1 (Engl) (Fig. 1d–f). Subsequent FGF2 + FGF8 + SHH withdrawal and inclusion of BDNF + GDNF + 0.5% FBS in stage 5 resulted in the differentiation of these cells as TH$^+$ neurons (Fig. 1g). In H9 cultures exposed to FGF2 with FGF8 + SHH in stage 4, 25.2 ± 5.6% (mean ± s.e.m.) of βIII-tubulin$^+$ neurons expressed TH, compared with 11.8 ± 4.0% in controls supplemented with FGF2 alone (n = 3 experiments, each in triplicate). A similar pattern was seen in H1 cultures, in which 18.4 ± 11.8% of the βIII-tubulin$^+$ cells exposed to FGF2 + FGF8 + SHH during stage 4 expressed TH in stage 5, compared with 10.7 ± 2.4% in controls exposed to FGF2 only (300 cells scored per experiment, random fields; n = 3) (Supplementary Fig. 1 online).

hTERT transduction yields a line of human midbrain astrocytes

We next asked if dopaminergic neurogenesis by HES cells might be further potentiated by inducing the dopaminergic phenotype while concurrently recreating some of the cellular environment of the developing ventral midbrain. We therefore sought to coculture neuralized HES cells with human astrocytes derived from the developing ventral midbrain. To this end, we first established a stable line of human mesencephalic astrocytes. The ventral midbrain of a 21-week-gestational-age human fetus was dissected and dissociated, then infected with a retrovirus encoding hTERT, under CMV promoter control, placed upstream of a puromycin selection cassette under IRES control in pBABE (ref. 15). A stable line was obtained by puromycin selection and characterized antigenically after three passages 1 month apart, spanning approximately 21–24 population doublings. These cells expressed astrocytic GFAP (Fig. 2a,b) and did not express either early oligodendrocytic (A2B5, O4) or neuronal (βIII-tubulin) markers (data not shown). They were passaged to 35 population doublings before use; we have now maintained these cells for over 2 years in continuous culture as a stable line that we have designated human midbrain astrocyte–hTERT (hMAST-TERT) cells. In addition to hMAST-TERT cells, we also generated a line of hTERT-immortalized astrocytes from the rostrolateral neocortical plate of a 22-week fetus, similarly designated as human forebrain astrocyte–hTERT (hFAST-TERT) cells.

Midbrain glia potentiate dopaminergic differentiation

hMAST-TERT cells substantially enhanced TH$^+$DAT$^+$ (dopamine transporter$^+$)–defined dopaminergic differentiation from HES cells (Fig. 2c–h). When H9 cultures were exposed to FGF2 + FGF8 + SHH in stage 4, then cocultured with inserts bearing confluent hMAST-TERT midbrain astrocytes, the proportion of TH$^+$ neurons increased from 11.8 ± 4.0% to 39.6 ± 4.6% ($P < 0.05$ by ANOVA with post hoc Bonferroni t-tests; F = 15.15 [4, 44 d.f.]; for each culture condition tested, a minimum of 300 cells were scored from each of triplicate wells, and each experiment was repeated at least three times) (Fig. 2i). More notably, when FGF2 + FGF8 + SHH–exposed HES cells were cocultured continuously with hMAST-TERT cells from induction through differentiation, the proportion of TH$^+$ neurons increased to 67.4 ± 12.1%. This was a significantly higher proportion of TH$^+$ neurons than was noted in cultures raised with hMAST-TERT cells only in stage 5 ($P < 0.05$) or in cultures exposed only to FGF2 + FGF8 + SHH ($P < 0.01$) (Fig. 2j).

H1 cultures yielded results analogous to those obtained with H9. When H1-derived neural progenitors were raised in FGF2 + FGF8 + SHH at stage 4 and differentiated in hMAST-TERT coculture at stage 5, 27.7 ± 3.6% of βIII-tubulin$^+$ neurons expressed TH, significantly more than in cultures exposed only to FGF2 ($P < 0.01$ by ANOVA with post hoc t-tests; F = 12.15 [4, 10 d.f.]). When hMAST-TERT cocultures were included at both stages, the proportion of TH$^+$ neurons increased to 46.7 ± 16.3% of all βIII-tubulin$^+$ neurons ($P < 0.01$ compared with FGF2 + FGF8 + SHH alone) (Supplementary Fig. 1). In addition, the fraction of βIII-tubulin$^+$ neurons in the overall population was significantly higher among HES cells cocultured with hMAST-TERT cells than in controls maintained in FGF2 or FGF2 + FGF8 + SHH alone during stage 4. However, HES cells exposed only to hMAST-TERT cells, without benefit of

FGF2 + FGF8 + SHH, exhibited no more TH$^+$ neurons than did cultures maintained only in FGF2 at stage 4—despite manifesting a higher overall proportion of βIII-tubulin$^+$ neurons. Together, these data suggest that besides supporting neuronal survival[12], midbrain astrocytes specifically potentiated dopaminergic induction and maintenance.

We also assessed the incidence of serotonergic and GABAergic neurons in these cultures, given the developmental cogeneration of these phenotypes in the ventral mesencephalon (**Supplementary** Fig. 2 online). Serotonergic cells, defined as those that were 5-hydroxytryptamine–immunoreactive (5HT$^+$), respectively constituted 0.7 ± 0.4% and 1.6 ± 0.7% of all βIII-tubulin$^+$ neurons in FGF2 + FGF8 + SHH + hMAST–exposed H9 and H1 cultures (500 cells scored per experiment, n = 3). Similarly, GABA$^+$ neurons comprised 2.6 ± 1.0% and 4.1 ± 1.7% of all neurons in FGF2 + FGF8 + SHH + hMAST–exposed H9 and H1 cultures, respectively.

Glia-mediated dopaminergic differentiation is region specific

Regional heterogeneity among astrocytes has been demonstrated in regard to their expression profiles, factor responsiveness and cytoskeletal composition, among other features[16–21]. To determine if midbrain astrocytes are specifically competent to induce dopaminergic neurons from neural progenitors, we compared the relative efficiencies of mesencephalic and cortical astrocytes in potentiating dopaminergic neurogenesis. To this end, HES cells were cocultured with either the midbrain or cortical astrocyte lines described earlier. No significant difference was found in the effect of midbrain or cortical astrocytes with respect to the proportion of neurons generated by HES cells (Fig. 2k,l): when the cultures were exposed to astrocyte inserts during both stages 4 and 5, the proportion of βIII-tubulin$^+$ neurons rose to 24.9 ± 2.2% for cultures raised with midbrain astrocytes and 30.1 ± 2.8% for those exposed to cortical astrocytes (Fig. 2k). In contrast, a significant difference was noted in the proportion of TH$^+$ neurons generated in the presence of forebrain and midbrain astrocytes.

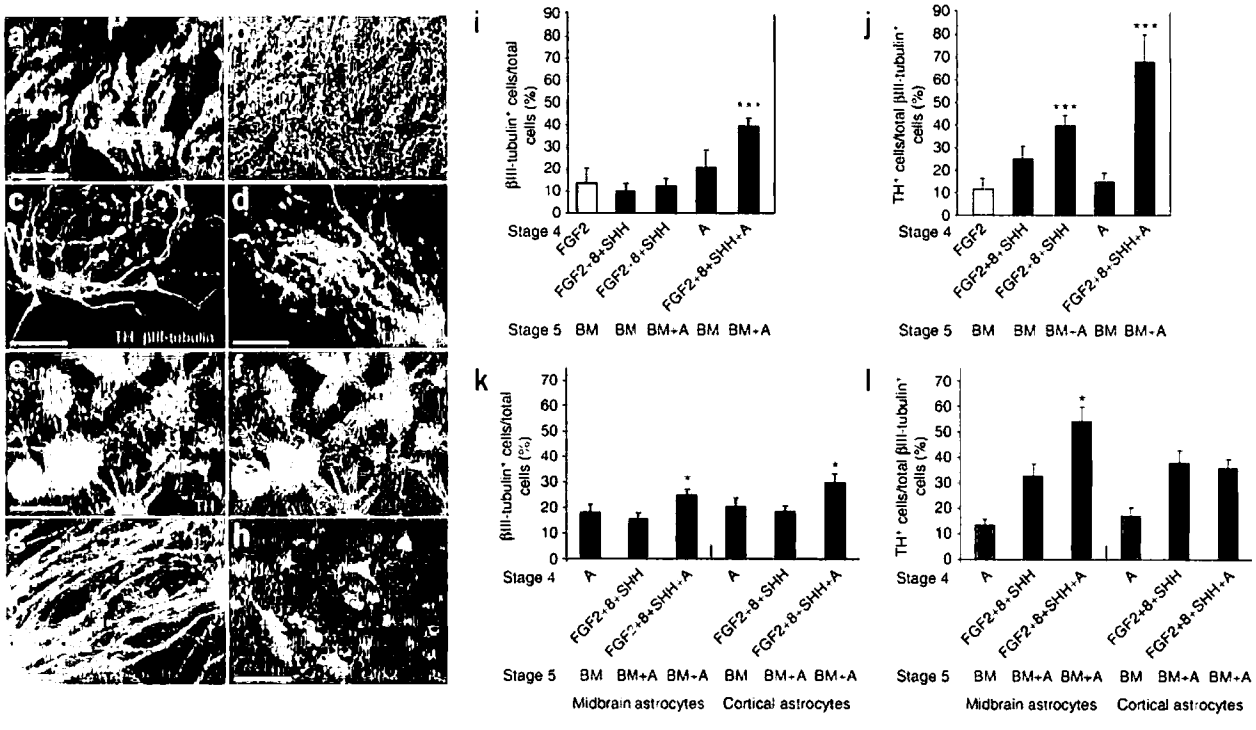

Figure 2 hTERT-immortalized human midbrain glia potentiate dopaminergic induction by FGF8 + SHH. (a,b) Human fetal mesencephalic astrocytes, derived from a 22-week-gestational-age fetus, were immortalized using a retroviral vector encoding human telomerase reverse transcriptase (hTERT). After puromycin antibiotic selection, the line (hMAST) was propagated through serial passage. At approximately 56 population doublings (b) its cells homogeneously expressed the astrocytic marker glial fibrillary acidic protein (a, green). (c) Human fetal astrocytic coculture substantially potentiated the SHH + FGF8–mediated induction of dopaminergic neurons from HES cells, as indicated by the expression of TH (green) by most βIII-tubulin$^+$ neurons (red) within 3 weeks of induction. (d) TH expression in stage 5 cultures typically colocalized with that of the dopamine transporter (DAT, red; double-labeled cells orange). (e–g) Low- (e,f) and high- (g) power images of βIII-tubulin$^+$ neurons (green) expressing TH (red), following serial induction and differentiation in hMAST coculture. Virtually all βIII-tubulin$^+$ neurons in these cultures expressed TH by 4 weeks after differentiation (stage 5). (h) Most TH$^+$ cells (green) expressed Girk2 (red; double-labeled cells yellow), which is preferentially expressed by A9 nigrostriatal neurons. The astrocytic potentiation of dopaminergic neurogenesis was specific to midbrain glia. (i,j) The percentage of βIII-tubulin$^+$ neurons among all cells (i), and the percentage of TH$^+$ cells among all βIII-tubulin$^+$ neurons (j). Each bar represents a different set of induction and differentiation conditions during stages 4 and 5. In i, $^*P < 0.01$ when compared with FGF2 only, and $^{**}P < 0.01$ compared with factor exposure alone, or factor exposure with hMAST-TERT coculture in stage 5. In j, $^*P < 0.05$ compared with hMAST-TERT coculture in stage 5 only, $^{**}P < 0.01$ compared with FGF2 + FGF8 + SHH exposure and $^{***}P < 0.01$ compared with FGF2 only. (k,l) Comparison of the influence of midbrain and cortical astrocytes on the proportion of βIII-tubulin$^+$ neurons (k), and on the percentage of TH$^+$ cells among those βIII-tubulin$^+$ neurons (l). In k, $^*P < 0.01$ compared with coculture with hMAST-TERT in stage 5 only. In l, $P < 0.05$ compared with coculture with cortical hMAST-TERT through stage 4 and 5. The data in i,j were derived from passage 31–35 cells, whereas those in k,l were obtained from cells at passages 44–48. As the fraction of neurogenic embryoid bodies in H9 cultures declined with passage, the proportion of dopaminergic neurons, relative to the total population, was lower in k than l. A, immortalized astrocytes; BM, basal medium; 8, FGF8. Scale bars: a–d and g–h, 50 μm; e,f, 200 μm.

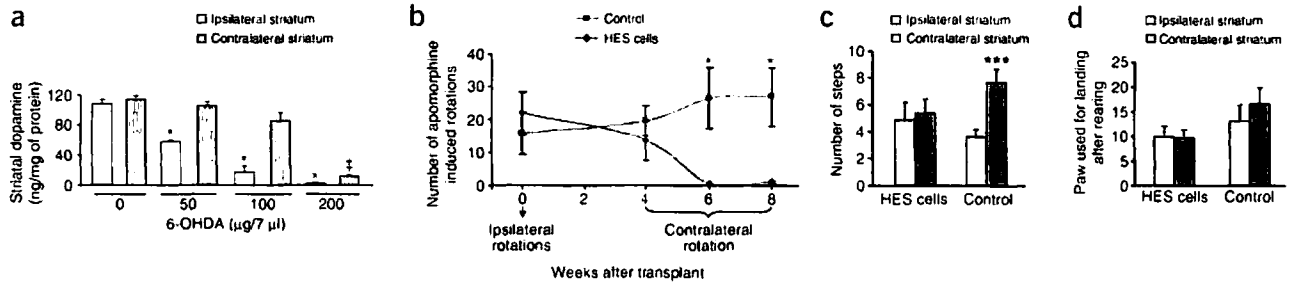

Figure 3 6-OHDA–lesioned rats given dopaminergic grafts exhibited functional benefit. (a) Inverse correlation between the 6-OHDA concentration used and the level of dopamine in the striata of lesioned rats. (b) Apomorphine-induced rotations in 6-OHDA–lesioned rats transplanted with HES cells ($n = 6$), compared with their lesioned but untreated controls (vehicle-only; $n = 5$). The implanted rats showed a decrease in apomorphine-induced rotations with time ($P < 0.01$). (c) Adjusting-step test results for 6-OHDA–lesioned rats treated with either dopaminergic grafts or vehicle control. The graph plots for each forelimb the number of adjusting steps taken during 5 s while being moved 0.9 m. The transplanted rats performed equally with either paw, whereas the untransplanted rats used the contralateral paw more than the ipsilateral one (***$P < 0.001$). (d) Data from the cylinder test, in which the number of times each forelimb was used for landing after rearing for 10 min was scored. Both groups used either paw with equal frequency.

Coculture with hMAST-TERT midbrain astrocytes throughout stage 4 and 5 yielded cultures containing 53.7 ± 5.5% TH^+ neurons, a significantly higher incidence of TH^+ cells than was noted in preparations cocultured either with hMAST-TERT cells at stage 4 only, or with cortical hFAST-TERT astrocytes at stages 4 and 5 ($P < 0.01$ for each comparison, by ANOVA with post hoc Bonferroni comparisons ($F = 16.48$ [5, 30]) (Fig. 2l). These data indicate that whereas both midbrain and cortical astrocytes enhanced neuronal maturation and survival, only midbrain astrocytes specifically potentiated dopaminergic phenotype.

Most dopaminergic neurons are of A9 nigrostriatal phenotype

We next assessed the specific types of dopaminergic neurons generated from hMAST-TERT exposed HES cells. A9 neurons of the substantia nigra pars compacta (SNpc) and A10 neurons of the ventral tegmental area (VTA) are the two major subtypes of midbrain dopaminergic neurons; only the A9 phenotype is lost in Parkinson disease. The G protein–gated inwardly rectifying K^+ channel Girk2, which within the midbrain is expressed only by TH^+ A9 neurons[22,23], was used to identify A9 neurons, and calbindin-D 28K (CD28k), which is expressed by dopaminergic neurons of the tegmentum but not the SNpc (refs. 22–24), was used in tandem with TH to identify A10 neurons.

In both H9- and H1-derived cultures raised in hMAST-TERT coculture, most TH^+ neurons expressed Girk2 (Supplementary Fig. 3 online). These apparent A9 nigral neurons comprised 71.2 ± 14.6% and 83 ± 7.5% of TH^+ neurons in H9 and H1 cultures, respectively ($n = 3$; 300 scored cells per experiment). In contrast, the A10 marker CD28k was expressed by only 4.9 ± 2.7% and 6.1 ± 2.9% of TH^+ neurons in H9 and H1-derived cultures, respectively.

HES cell derived TH^+ neurons were functional *in vitro*

Both H9 and H1-derived dopaminergic neurons achieved functional maturation in culture. This was first evident from the expression of dopamine transporter (DAT) by all scored TH^+ neurons ($n = 300$) after 1 week at stage 5, after generation in FGF2 + FGF8 + SHH + hMAST-TERT (Fig. 2d and Supplementary Fig. 1). HPLC revealed high levels of basal dopamine release from both H9- and H1-derived dopaminergic neurons, after 7 weeks in stage 5: H9- and H1-derived cultures contained 10.2 ± 0.2 ng/ml and 7.7 ± 1.5 ng/ml dopamine, respectively, 12 h after medium change (mean ± s.e.m., $n = 3$ experiments). The HES cell–derived neurons also demonstrated dopamine release in response to KCl depolarization (Supplementary Fig. 3): H9 cells released 5.9 ± 1.4 ng/ml dopamine in response to KCl, compared with 0.6 ± 0.1 ng/ml in no-KCl controls ($n = 3$ experiments; $P < 0.01$ by Student's t-test). Similarly, H1-derived dopaminergic cultures released 2.6 ± 0.2 ng/ml of dopamine in response to KCl, significantly more than the 0.3 ± 0.02 ng/ml in cultures not exposed to KCl ($n = 3$; $P < 0.05$, Student's t-test).

6-OHDA yields a dose-dependent reduction in striatal dopamine

We next assessed the ability of these highly enriched dopaminergic progenitor preparations to ameliorate the behavioral deficits of experimental Parkinson disease. To this end, we generated adult rats with chemical lesions of the nigrostriatal pathway, using a single intraventricular injection of 6-OHDA hydrobromide (100 μg/7 μl; $n = 6$). Before assessing the effects of dopaminergic engraftment in these rats, we verified that 6-OHDA induced a dose-dependent reduction in neostriatal dopamine dopamine in the ipsilateral striatum (one-way ANOVA, $P < 0.001$): intrastriatal injection of 50, 100 or 200 μg/7 μl of 6-OHDA reduced the levels of dopamine in the ipsilateral striatum by 48%, 85% and 99%, respectively ($P < 0.05$). Only at 200 μg/7 μl of 6-OHDA was a significant ($P < 0.05$) depletion (90%) observed in the contralateral striatum. A dose of 100 μg/7 μl was thus chosen, as it induced dopaminergic depletion ipsilaterally without significantly altering contralateral dopamine levels (Fig. 3a).

Extrapyramidal dysfunction normalizes after transplantation

Having validated this model of striatal dopaminergic depletion, we transplanted 6-OHDA–lesioned rats with 500,000 H9-derived, FGF2 + FGF8 + SHH + hMAST-TERT–induced dopaminergic neurons ($n = 6$), or with a cell-free, PBS control ($n = 5$). In addition, four rats were implanted with 500,000 naive H9 HES cells, with no antecedent induction of dopaminergic phenotype. The rats were then challenged with apomorphine (2.5 mg per kg body weight, intraperitoneal (i.p.)), which induces rotations contralateral to the lesioned side in rats with unilateral striatal loss; these rotations reflect unbalanced output from the unlesioned striatum, and may be scored as such[25]. Importantly, apomorphine-induced rotations correlate to the underlying degree of nigrostriatal loss and dopaminergic depletion, and may reflect the neurochemical anatomy more than alternative testing agents such as amphetamine[26,27].

We found that the untreated 6-OHDA–lesioned rats developed apomorphine-induced rotations within a month of lesion, and continued to exhibit sustained rotations in response to apomorphine for the entire 10 weeks of assessment. In contrast, by 6 weeks after transplantation, rats given H9-derived dopaminergic grafts exhibited significantly fewer apomorphine rotations than their unimplanted controls ($P < 0.05$ by one-way ANOVA; $F = 9.77$ [1, 9 d.f.]), and this difference was sustained at 8 weeks ($P < 0.05$; $F = 10.64$ [1, 9 d.f.]) (Fig. 3b). Notably, rats transplanted with H1-derived dopaminergic cells likewise exhibited substantial improvement in the rotation challenges, manifesting a significant decrease in the number of apomorphine-induced rotations compared with their unimplanted controls, at both 6 ($P < 0.01$, $F = 31.53$ [8 d.f.] and 8 weeks ($P < 0.05$, $F = 5.92$ [8 d.f.]) after transplant (Supplementary Fig. 4 online). Thus, axial function improved in 6-OHDA–lesioned rats after intrastriatal transplantation, and this effect was noted using both H9 and H1-derived dopaminergic grafts.

Appendicular function also improved in the implanted rats relative to their controls. In the adjusting step test[28,29], rats transplanted with H9-derived dopaminergic grafts performed equally with either paw, whereas their unimplanted but lesioned controls strongly preferred using the contralateral paw ($P < 0.001$ by one-way ANOVA; $F = 14.56$ [1, 28]). The total number of steps taken with both paws did not differ between the two groups, indicating similar levels of motor activity (Fig. 3c). In the cylinder test[30,31], a measure of forelimb preference during vertical exploration, the transplanted rats used either paw with equal frequency for landing after rearing, not exhibiting the asymmetry in this test manifested by their lesioned but unimplanted controls (Fig. 3d).

HES-derived dopaminergic cells engraft as TH$^+$ neurons

Ten weeks after engraftment, the rats were killed and their brains analyzed, to assess the incidence and maintenance of dopaminergic phenotype in the grafts. To correlate the behavioral performance of each lesioned rat to its treatment and dopaminergic engraftment, sagittal sections were taken and scored for (i) the mediolateral spread of the xenografted cells, as identified by their expression of human nuclear antigen (HNA); (ii) the number of cells engrafted; and (iii) the number of HNA$^+$ donor cells expressing TH. In this context, we noted extensive engraftment of the donor-derived HNA$^+$ cells in all six H9

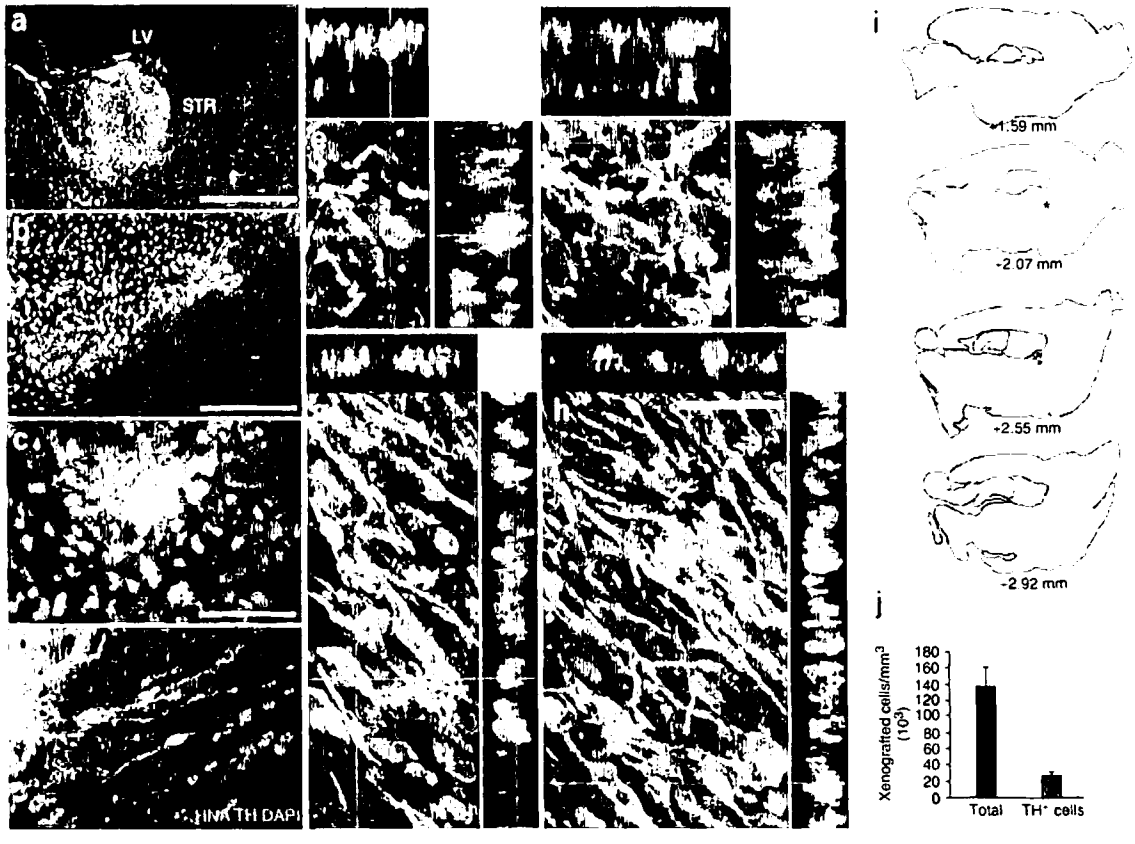

Figure 4 HES cell–derived progenitors dispersed and differentiated as TH$^+$ neurons in lesioned striatum. (a) Dopaminergic differentiation could be seen as early as 4 weeks after transplant. Transplanted cells engrafted extensively in the striatum and on analysis of serial sections were observed to have spread 1.59 ± 0.57 mm across the mediolateral axis. Shown here is a low-power sagittal image of a xenograft localized with antibody to human nuclear antigen (HNA, red). Most of the TH$^+$ neurons (green) are observed at the graft edge. LV, lateral ventricle. STR, striatum; Xeno, xenograft. (b,c) High-power images of HNA$^+$ (red) TH$^+$ (green) neurons at the xenograft edge corresponding to the areas denoted by an asterisk in a and i. (d) Some TH$^+$ neurons (arrow) migrated away from the xenograft core. (e–h) Confocal optical sections of HES cell–derived TH$^+$ neurons (HNA, red; TH, green) confirming that TH$^+$ neurons were donor derived. Grafts in e,f are derived from H9 cells, those in g,h from H1. (i) Distribution of transplanted cells in sagittal rat brain sections at different points along the mediolateral axis. In this brain, cell engraftment spanned at least 2.5 mm. Asterisk corresponds to the graft area in a–d. (j) Average density of both total engrafted cells and TH$^+$ engrafted cells in six rat brains. The density of TH$^+$ neurons exceeded 20,000/mm^3 within the transplant bed. Scale: a, 450 μm; b, 180 μm; c,d, 60 μm; e–h, 30 μm.

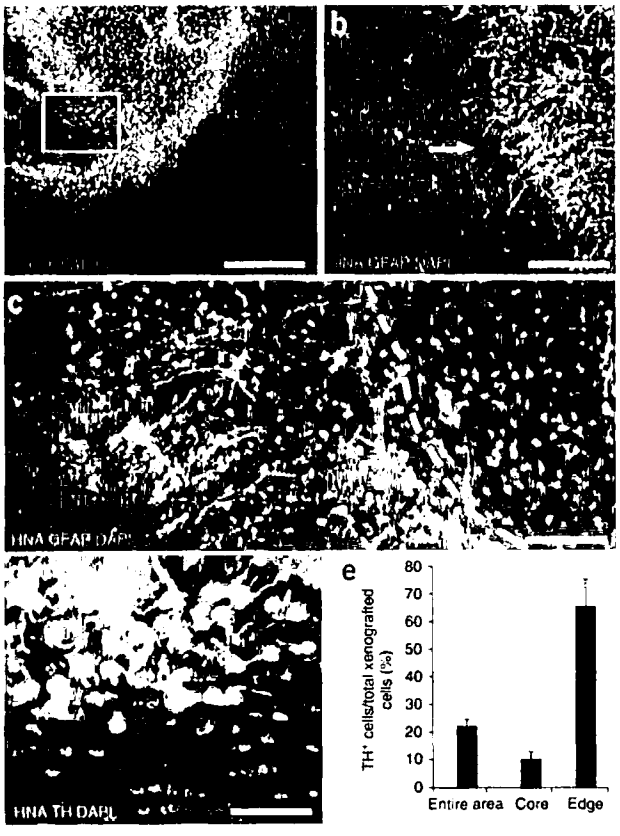

Figure 5 Dopaminergic differentiation by donor cells is associated with host astroglia. Pronounced colocalization was observed between regions of host glial response and sustained dopaminergic differentiation. (a,b) Low-power image of the entire xenograft (HNA, red). A dense population of reactive host astrocytes (GFAP, green) can be seen localized in and around the edges of the xenograft. Note the low density and low morphological complexity of the GFAP-expressing host astrocytes in areas away from the xenograft (arrow). (c) A high-power image of host astrocytes (green) interspersed with nuclei (HNA, red) of xenografted cells (white boxed area in a). (d) An adjacent section showing the presence of TH^+ neurons (green) overlapping with areas rich in reactive host astrocytes (green boxed area in a). (e) Percentage of cells expressing TH in different areas of the xenograft. A significantly higher relative proportion of TH^+ neurons, 65.0 ± 10.0%, was observed within the graft periphery, in proximity to reactive host astrocytes. Scale bars: a, 300 μm; b, 120 μm; c, 60 μm; d, 30 μm.

HES cell–transplanted striata analyzed (Fig. 4). The donor cells were dispersed over an average radius of 1.6 ± 0.6 mm, and the mean number of HNA^+ nuclei/mm^3 within each was 136,726 ± 23,515 (Fig. 4i,j). Efficient generation of TH^+ neurons was observed in all rats, which harbored 27,185 ± 4,226 TH^+ cells/mm^3 (range: 14,904–43,234 cells/mm^3) (Fig. 4j). However, the donor-derived TH^+ cells preferentially localized to the donor-host interface in every graft evaluated (Fig. 4a,b). Analogous assessment of three brains transplanted with H1 HES cell–derived cells revealed efficient engraftment of TH^+ cells in all three brains, and invariably remained within the recipient striata; these similarly localized to the graft-recipient interface (Supplementary Fig. 4). Confocal imaging confirmed that somal TH expression in both H1 and H9-derived grafts was donor-derived, in that TH^+ cell bodies were uniformly HNA^+ (Fig. 4e–h).

Dopaminergic phenotype is maintained in gliotic border zones

Histological analysis revealed that each xenograft, including both the H9- and H1-derived implants, was surrounded by host-derived reactive astrocytes (Fig. 5a–c and Supplementary Fig. 4). These glia directly abutted the TH^+ neurons in the graft, typically within each graft's periphery. To better describe the relative distribution of TH^+ neurons, we scored the incidence of TH^+ neurons in each transplant core, relative to its periphery. We noted a strong correlation between the local proportion of HES cells differentiating as TH^+ neurons and their proximity to $GFAP^+$ host astrocytes (Fig. 5d). Thus, whereas the proportion of TH^+ neurons among all donor cells was 21.5 ± 3.0% at 10 weeks, the distribution of TH^+ cells within each graft was nonuniform: 65.0 ± 10.0% of cells within the peripheral 0.2 mm of the grafts expressed TH, but only 9.8 ± 2.9% of cells within the transplant cores did so ($P < 0.01$, $F = 31.69$ [1, 16 d.f.]; $n = 9$ scored sections from three rats per group; Fig. 5e). Notably, rats with fewer engrafted cells had higher proportions of TH^+ neurons, possibly because a greater fraction of their donor cells lay in proximity to host astrocytes. This observation likely contributed to the lack of correlation between the number of engrafted cells and the behavioral outcomes of individual rats, at least as assessed by apomorphine rotations.

Central loss of TH^+ cells and undifferentiated expansion occurs

We next sought to define the cellular phenotypes within the non-dopaminergic central cores of these xenografts. Though gliosis in association with foamy macrophages and some local necrosis were observed, no evidence of teratoma or overt anaplasia was seen in any sections sampled from the six H9 and three H1 engrafted brains, each of which was sampled 70 d after transplantation (Fig. 6a). However, some mitotic figures were noted, prompting us to analyze mitosis among the engrafted population, using histone-3 and PCNA immunolabeling as well as 5-bromodeoxyuridine (BrdU) incorporation *in vivo*. To this end, we injected three transplanted rats with BrdU 68 d after implantation (every 12 h, three times beginning 48 h before death). Among all donor cells in the transplant beds of these H9-implanted rats, 6.6 ± 1.6% showed BrdU incorporation (Fig. 6c,d), suggesting a daily mitotic incidence of roughly 4%. Fewer cells, <1%, expressed histone-3, a marker of M phase, whereas 1.48 ± 0.7% of the counted cells expressed PCNA, a broader marker of active division (Fig. 6c,d). The H1 transplanted brains showed a similar incidence of both $PCNA^+$ and BrdU-incorporating cells (Fig. 6f,g), indicating that the persistence of donor cell division was not a function of cell line.

To establish whether the dividing cells within these grafts included remnant pluripotent HES cells, we immunostained for a panel of undifferentiated HES-cell markers that included nanog, SSEA-4 and Oct-4. These immunostains revealed no evidence of persistent pluripotent HES cells in brains transplanted with either H9- or H1-derived dopaminergic grafts (data not shown). However, a large fraction of cells, largely localized at center of each graft in both H9- and H1-transplanted brains, expressed the immature neural proteins nestin and musashi, suggesting the immature neuroepithelial lineage of these cells (Fig. 6b,e). Thus, a cohort of actively dividing HES cell–derived neuroepithelial cells appeared to persist within the transplants, and were likely responsible for their sustained undifferentiated expansion.

To compare the behavior of transplanted SHH + FGF8 + hMASH-TERT–generated dopaminergic neurons with naive HES cells, we then implanted four 6-OHDA–lesioned rats with stage 1, undifferentiated 1 HES cells, of both H1 and H9 origin. Clinical deterioration of all four of these rats precluded their behavioral analysis; all were killed instead

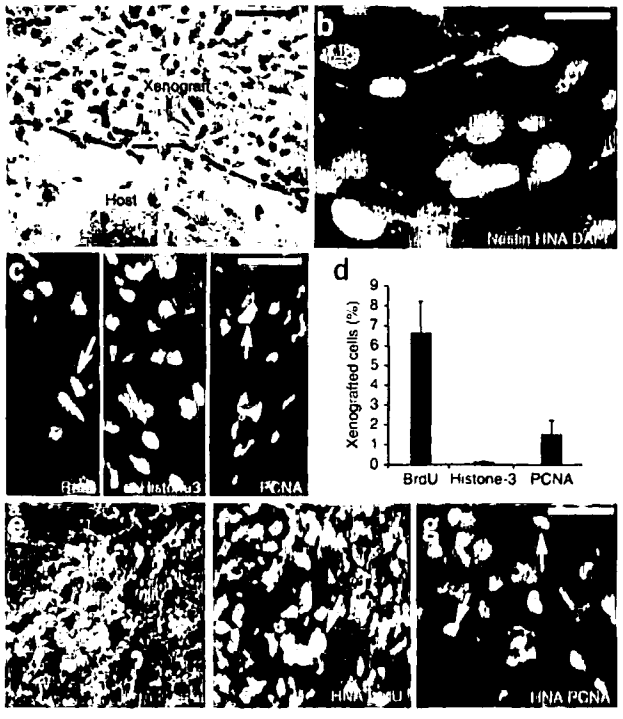

Figure 6 HES cell–derived dopaminergic grafts exhibit persistent undifferentiated expansion. (a) Hematoxylin and eosin–stained view of graft border in rats transplanted with H9 HES cell–derived dopaminergic progenitors. (b) These grafts of induced dopaminergic cells exhibited no teratoma, but rather manifested an expanding core of nestin-expressing cells (b, red) among the xenografted cells (HNA, green). (c,d) Of the engrafted cells (HNA, red), 6.6 ± 1.6% incorporated BrdU (c, left panel, green), and 1.5 ± 0.7% expressed PCNA (c, right panel, green), whereas <1% expressed histone-3, an M-G2–restricted marker (c, middle panel, green). (e) Nestin$^+$ (green) donor cells were also abundant in the grafts of rats transplanted with H1-derived dopaminergic progenitors. (f,g) Proliferating cells, as indicated by BrdU incorporation (f, green arrow) and PCNA immunostaining (g, green, arrow) were observed in rats transplanted with H1-derived dopaminergic cells. Scale bars: a, 60 μm; b, 20 μm; c, 30 μm; e–g, 50 μm.

at 4 weeks. Histology revealed overtly neoplastic tumor masses in each rat; all four exhibited high rates of antemortem BrdU uptake, as well as both histone-3 and PCNA expression, of >10% each (Supplementary Fig. 5 online). Antigenically, these tumors were primitive and relatively homogeneous; most cells coexpressed the prototypic ES markers SSEA-4 and Oct-4 as well as abundant nestin expressing cells. As such, these undifferentiated HES cell–derived tumors were antigenically and anatomically distinct from the nestin$^+$ graft cores observed after implantation of SHH + FGF8 + hMAST-induced dopaminergic progenitor cells. Whereas the former appeared to comprise highly neoplastic tumors of primitive, still-pluripotent HES cells, the latter appeared to arise from the slower expansion of a non-anaplastic neuroepithelial lineage. Nonetheless, these neuralized cells appeared to sustain undifferentiated expansion until the time point of death and histologic observation, 10 weeks after transplant.

DISCUSSION

These results indicate that mesencephalic astroglial coculture may be useful in driving dopaminergic neurogenesis from HES cells, and they demonstrate the ability of these cells to mediate functional improvement in an experimental model of Parkinson disease. Yet these findings also suggest the need for caution in this approach, given the phenotypic instability and potential for undifferentiated donor cell expansion that we observed, often in many of the same rats that exhibited neurological improvement after dopaminergic engraftment.

In the first phase of this study, we addressed the need to achieve higher efficiency enrichment of dopaminergic neurons from HES cells, by attempting to better replicate the *in vivo* environment of the fetal mesencephalon during SHH + FGF8–mediated dopaminergic induction. To this end, we generated a telomerase-immortalized line of human ventral midbrain astrocytes that strongly potentiated dopaminergic neuronal differentiation from HES cells of both the H9 and H1 cell lines: when embryoid bodies were generated in mesencephalic glial coculture with concurrent FGF8 + SHH induction, TH$^+$ neurons were by the far the most common neuronal phenotype produced, comprising over 60% of all neurons by 4 weeks. Of note, by propagating cells in conditioned media under feeder-free conditions, and then coculturing with human mesencephalic hMAST-TERT astrocytes in stage 4 and beyond, we were able to generate human dopaminergic neurons under largely humanized conditions, with minimal exposure to animal cells.

On the basis of these results, we then assessed the utility of enriched dopaminergic cells as therapeutic vectors, by transplanting HES cell–derived dopaminergic progenitors to 6-OHDA–lesioned rat striata. We observed excellent graft acceptance and sustained survival with cyclosporine immunosuppression, which was associated with substantial functional benefit. Indeed, among those lesioned rats that received H9-derived dopaminergic grafts, all exhibited robust engraftment by TH$^+$ donor-derived neurons when assessed 10 weeks after transplantation. Histologically, 27,185 ± 4,226 TH$^+$ cells/mm^3 were scored in the recipient striata, among the 136,726 ± 23,515/mm^3 donor-derived cells in these grafts. These numbers compare very favorably with past studies that have noted functional improvement after dopaminergic transplantation. For instance, when monkey ES cell-derived dopaminergic neurons were allografted into MPTP-lesioned adult cynomolgus monkeys, treatment-associated behavioral improvement was similarly noted within 10 weeks[32]. These monkeys had received enriched dopaminergic grafts, the result of *in vitro* differentiation in media supplemented with FGF-20 and conditioned by a permissive stromal cell line. Nonetheless, only 2,130 dopaminergic neurons were reported to survive among the 300,000–600,000 injected per striatum, indicating that <1% of the injected cells survived the 14 weeks until death as dopaminergic neurons. The net dopaminergic engraftment of our transplanted rats was thus almost tenfold that which sufficed to yield a behavioral improvement in the lesioned monkey. The differences between these species and models notwithstanding, our relatively efficient dopaminergic engraftment was clearly associated with strong functional results. Behaviorally, we observed a significant, substantial and functionally meaningful improvement in the motor performance of engrafted 6-OHDA–lesioned rats relative to their lesioned but untreated controls. These data indicated that coculture of HES cells with telomerase-immortalized human mesencephalic astrocytes strongly potentiated dopaminergic neurogenesis, that these cells could efficiently engraft as dopaminergic neurons, and that they were competent to ameliorate the behavioral deficits of striatal dopaminergic denervation.

These promising results were unfortunately accompanied by several potentially disturbing outcomes. First, we noted that the incidence of

neurons manifesting dopaminergic antigenicity fell sharply over a month *in vivo*; this was especially remarkable in light of the highly enriched nature of these cells at the time of implantation, and raised the possibility that the maintenance of the dopaminergic phenotype could not be assumed even after successful enrichment and engraftment. Second, the diminution in proportion of TH^+ neurons as a function of time suggested the possibility of a dilution of surviving dopaminergic neurons by the selective expansion of an undifferentiated, mitotically active cohort within the implanted pool. This appears to have been the case, in that undifferentiated expansion of ES cells was reproducibly noted within otherwise successfully integrated grafts. Although we noted no evidence of either histological anaplasia or persistent antigenically defined undifferentiated ES cells in these grafts, and even though their mitotic indices appeared relatively low as defined both by histone-H3 and BrdU immunolabeling, their persistent, uncontrolled and grossly homogeneous expansion over a 10-week span before the animals were killed nonetheless suggested graft-associated tumorigenesis. The cellular composition of these grafts reflected an abundance of primitive neuroepithelial cells that were immunoreactive for the early neuroepithelial transcript nestin, but largely immunonegative for astrocytic GFAP, which was instead localized to the graft borders and appeared to be largely of host origin. The lack of GFAP immunoreactivity argued also against the possibility that hMAST-TERT cells, which are strongly $GFAP^+$, had somehow escaped the confines of their culture inserts to contaminate the HES cell–derived grafts. Furthermore, the dopaminergic-enriched grafts contained no cells immunoreactive for SSEA4, Tra-1, Oct-3 or nanog, implying that ongoing undifferentiated expansion within these HES cell–derived grafts was due not to persistent pluripotent cells, but rather to already neuralized cells that failed to complete terminal neuronal or glial differentiation before transplant.

The expansion of undifferentiated neural precursors after host engraftment, despite otherwise compelling therapeutic benefit, poses a strong cautionary note for the use of unpurified neural derivatives in clinical transplantation. At present, we have no data to indicate whether those undifferentiated cells persisting beyond our 10-week survival point would eventually differentiate and exit the cell cycle, or whether they would instead continue to divide either autonomously or with minimal restraint, ultimately leading to tumor formation. Given this uncertainty, our results suggest the need for isolating terminally differentiated phenotypes, or at least their fate-restricted progenitors, as a prerequisite to transplanting HES cell–derived neural cells into the adult central nervous system. In particular, these late complications of otherwise successful HES cell–derived dopaminergic grafts suggest the wisdom of establishing strategies not only for high-efficiency dopaminergic neurogenesis, but also methods for ridding the resultant preparations of any remaining undifferentiated cells[33]. Furthermore, the progressive restriction of TH activity to the graft periphery indicates the need to actively sustain the mature phenotype of those dopaminergic neurons that do engraft, and suggest the likely wealth of information to be gleaned from studying the host-graft interaction at its interface.

METHODS

HES cell culture. HES cells of the H9 and H1 lines were provided by Geron and WiCell, respectively. H9 cells were cultured on Matrigel (Becton-Dickinson, USA), and fed daily with FGF2 (4 ng/ml; Invitrogen)-supplemented conditioned medium obtained from irradiated mouse embryonic feeder cells (MEFs). The HES cells were passaged every 7–14 d, or when 80% confluent. At each passage, the cells were treated with collagenase type IV (200 U/ml; Invitrogen) for 10 m, gently scraped from the culture dish, then split 1:3–1:4 onto Matrigel-coated six well plates. The cells were fed every 24 h with KO-DMEM (Invitrogen) supplemented with 20% KO-Serum replacement (KO-medium), and FGF2 (4 ng/ml; Invitrogen). In contrast, H1 cells (WiCell) were grown on irradiated MEFs (see Supplementary Methods online) and maintained in KO-medium supplemented with 4 ng/ml FGF2.

Induction and differentiation of dopaminergic neurons. Dopaminergic neurons were induced from HES cells using a modification of a previously published protocol[6,7] (Fig. 1a). Briefly, at 80% confluency, HES cell cultures were dissociated to form embryoid bodies. These bodies were generated by scraping collagenase-treated HES cells and suspending them in Ultralow cluster six-well plates (Corning) in KO-medium without FGF2 for 4 d. Embryoid bodies thus obtained were mechanically triturated and plated on tissue culture dishes in serum-free medium supplemented with insulin, transferrin, selenite and fibronectin (ITSF medium)[34]. The cultures were maintained in this medium for 10 d, with medium changes every 3 d.

For induction of dopaminergic progenitors, cells were collected by mechanical trituration following 0.05% trypsin (Invitrogen) + EDTA dissociation. The cells were transferred to polyornithine + 1 μg/ml laminin (BD)-coated plates in DMEM-F12 supplemented with N2 (Invitrogen), laminin (1 μg/ml) and FGF2 (10 ng/ml). Some cultures were also exposed to the N-terminal active fragment of human SHH (200 ng/ml; provided by Curis, Inc.) and FGF8 (100 ng/ml; R&D), cultured in the presence or absence of immortalized hTERT-overexpressing human midbrain astrocytes (hMAST-TERT cells; see below). Medium with fresh supplements was partially replaced every 3 d. Dopaminergic differentiation was induced after 6–8 d, by withdrawing SHH and the FGFs, and replacing with DMEM-F12 + N2 supplemented with GDNF (20 ng/ml), BDNF (20 ng/ml) and 0.5% FBS (basal medium, BM). Fresh inserts of hMAST-TERT cells were added to some wells at this point. For transplantation, cells were harvested after 2 d in differentiation conditions, whereas for assessing dopaminergic differentiation, plates were fixed after 7–14 d.

Generation of immortalized hTERT overexpressing astrocyte lines. Human fetal tissue was obtained under a protocol approved by the institutional review board of the Weill Medical College of Cornell University, and informed consent for its research use was obtained from donating women. Midbrain or cortical tissues were dissected out from human 21–22 week gestational brains in Ca^{2+}- and Mg^{2+}-free Hanks balanced salt solution (HBSS), then minced and dissociated into single cell suspension culture, as described (see Supplementary Methods). The cells were then plated in DMEM-F12 + N1 (Sigma) supplemented with 10% FBS, and distributed into six-well tissue culture dishes at 10^6 per well. For telomerase immortalization, the cells were then infected with VSVg-pseudotyped retrovirus encoding hTERT in pBABE-puro under CMV control (courtesy of M. Carpenter, Geron Corp.)[15]. Fresh viral supernatant was added every 8 h for 1 d with 8 μg/ml polybrene. The cells were then split to lower densities to decrease the number of transfectants per culture dish. 1–2 weeks later, transduced cells were selected in 1 μg/ml puromycin (Sigma) for 2 weeks. Successful selectants were isolated using sterile cloning rings and propagated in DMEM-F12 + N1 + 10% FBS. Once lines were propagated in sufficient numbers, their astrocytic identity was confirmed by immunocytochemistry for GFAP, A2B5 and S100β.

HES cell + hMAST-TERT coculture. hMAST-TERT astrocytes were cultured on 0.4 μm filter inserts (Corning) for 3 d in DMEM-F12 + N1 + 10% FBS, or until 70–80% confluent. For use, the hMAST-bearing inserts were rinsed with DMEM-F12 and placed in wells so as to overlay each HES cell–derived culture. After every 7 d, the inserts were replaced with freshly prepared inserts. The total amount of medium used was 1.8 ml per well for 12-well plates (0.4 ml in insert, and 1.4 in well) and 0.9 ml per well for 24-well plates (0.2 ml in insert, 0.7 ml in well). These volumes immersed each insert membrane, without allowing any medium from that transwell to contact medium in its parental well. Using the same medium volumes, hMAST-TERT–bearing inserts were also placed into cell-free control wells that were verified by phase microscopy as having no contaminating hMAST-TERT cells after a week. All media were changed every 3 d.

6-Hydroxydopamine lesions. Adult male Sprague-Dawley rats (8 weeks old, 250 g, Taconic) were used for cell transplantation following 6-OHDA lesion, following protocols approved by the institutional animal care

and use committee of the Weill Medical College of Cornell University. To determine the optimum dose of 6-OHDA needed to elicit maximum ipsilateral striatal dopamine loss without contralateral extension or lethality, we first titrated 6-OHDA dose against striatal dopamine level and mortality. In this set of experiments, rats were anesthetized with 100 mg/kg ketamine + 10 mg/kg xylazine i.p. before injection with 6-OHDA HBr (Sigma) into the right ventricle (AP: −1; ML: −1.5; DV: −3.2, relative to Bregma). The 6-OHDA HBr was dissolved in 0.9% NaCl with 0.05% ascorbic acid, at 50, 100 or 200 μg in 7 μl. Either 1 or 3 months later, the rats were killed for histology. Dopamine levels of their dissected striata were determined by HPLC, as noted (see Supplementary Methods). 100 μg/7 μl 6-OHDA was determined to achieve ipsilateral dopamine depletion without significant lethality (Fig. 3a).

Determination of dopamine level by HPLC. Measurement of dopamine secreted *in vitro* was performed by HPLC. Conditioned medium was collected after overnight exposure to cells in the seventh week of stage 5. For depolarization-induced dopamine release, the cultures were washed once with HBSS and then treated to 56 mM KCl in HBSS for 30 m; control cultures were exposed only to HBSS. HPLC was performed as previously described[35] (see Supplementary Methods).

Cell transplantation and immunosuppression. Rats were lesioned with one injection of 100 μg /7 μl of 6-OHDA HBr delivered into the right ventricle (n = 6). Four weeks later, each rat was monitored for 20 m to measure apomorphine (2.5 mg/kg, i.p.)-induced rotations. From the results obtained, rats were divided into two equally distributed groups. One week later, rats from one group were transplanted with cells (500,000 in 3 μl HBSS) and another group with saline in the striatum ipsilateral to the lesion (AP: 0, ML: −2.8) at three different heights (DV: −6, −5, −4). Rats were immunosuppressed 2 d before implantation, and daily until 3 d after, with i.p. injections of cyclosporine A (20 mg/kg; Sandimmune; Novartis). Thereafter, the rats received cyclosporine A daily (15 mg/kg, i.p.).

Behavioral testing. Apomorphine-induced rotations were assessed at 4, 6 and 8 weeks after lesion, so as to evaluate the effects of transplantation on motor symmetry, as described[25]. Nine weeks after grafting, rats were also evaluated by the adjusting step test[28]. Briefly, each rat was held by the experimenter with one hand fixing the hindlimbs and slightly raising the hind part off the surface, while the other hand fixed the forelimb not to be monitored. The rat was moved sideways (0.9 m in 5 s) by the experimenter, with its free paw touching the table. The number of adjusting steps for each forelimb was measured three times per session with two sessions per day, for 3 d. During the ninth week we also measured each rat's performance in the cylinder test, which assesses the symmetry or lack thereof of limb use[30]. Specifically, it measures the level of preference for using the unimpaired forelimb for weight shifting movements during spontaneous vertical exploration. To this end, the rat was put in a transparent cylinder (30 cm height, 20 cm diameter) for 10 min, and the number of times each forelimb was used for landing after rearing for 10 min was scored.

Immunocytochemistry. Cultures were fixed with 4% paraformaldehyde for 5 min. Rats were perfusion fixed with 4% paraformaldehyde and their brains collected and postfixed for 4 h in the cold, then cryoprotected in 30% sucrose and sectioned at 15 μm by cryostat. Both cells and tissue were permeabilized with 0.1% saponin + 1% normal goat serum (NGS) for 15 min at 25 °C and blocked with 0.05% saponin + 5% NGS for 15 m. Incubation with primary antibody was for 72 h at 4 °C. Incubation with fluorescently tagged secondary antibodies was for 2 h at 25 °C. All antibodies, sources, dilutions and relevant staining protocols used are listed in Supplementary Methods.

Statistical analysis. Statistical analysis was done for each dataset as noted in the text describing each experiment. For detailed sample descriptions, sampling methods and statistical tests employed, see the Supplementary Methods.

Note: Supplementary information is available on the Nature Medicine website.

ACKNOWLEDGMENTS

We thank B. Germin, J. Powers and M. Edgar for their neuropathological evaluations and H.M. Keyoung for advice. We are grateful to the late W.K. Rashbaum for his obstetric assistance in providing fetal tissue samples for this research. We are also grateful to Melissa Carpenter and Geron Corp. for providing the H9 cell line and retroviral hTERT used in this study, Curis for sonic hedgehog protein, and G. Corte (National Institute of Cancer Research, Genova, Italy) for the antibody to Otx2. Work in the Goldman laboratory was supported by NINDS and the Michael J. Fox Foundation, and work in the Beal laboratory was supported by the US Department of Defense and the Michael J. Fox Foundation.

AUTHOR CONTRIBUTIONS

N.S.R. generated the hMAST-TERT line with S.A.G., conducted the *in vivo* experiments done in S.A.G.'s laboratory and performed or supervised the *in vitro* and histological data analysis. C.C. conducted the transplantation and behavior studies with the H9 line, done in M.F.B.'s laboratory. S.K.S. conducted the transplant and behavior studies with the H1 line, done in S.A.G.'s laboratory. L.Y. conducted dopamine analysis by HPLC. M.F.B. supervised C.C. and L.Y. in their *in vivo* experiments. S.A.G. supervised the overall project, developed the experimental designs, performed the final data analysis and wrote the paper with N.S.R.

COMPETING INTERESTS STATEMENT

The authors declare that they have no competing financial interests.

Published online at http://www.nature.com/naturemedicine
Reprints and permissions information is available online at http://npg.nature.com/reprintsandpermissions/

1. Thomson, J.A. *et al.* Embryonic stem cell lines derived from human blastocysts. *Science* 282, 1145–1147 (1998).
2. Shamblott, M.J. *et al.* Derivation of pluripotent stem cells from cultured human primordial germ cells. *Proc. Natl. Acad. Sci. USA* 95, 13726–13731 (1998).
3. Reubinoff, B.E., Pera, M.F., Fong, C.Y., Trounson, A. & Bongso, A. Embryonic stem cell lines from human blastocysts: somatic differentiation *in vitro*. *Nat. Biotechnol.* 18, 399–404 (2000).
4. Reubinoff, B.E. *et al.* Neural progenitors from human embryonic stem cells. *Nat. Biotechnol.* 19, 1134–1140 (2001).
5. Zhang, S.C., Wernig, M., Duncan, I.D., Brustle, O. & Thomson, J.A. *In vitro* differentiation of transplantable neural precursors from human embryonic stem cells. *Nat. Biotechnol.* 19, 1129–1133 (2001).
6. Lee, S.-H., Lumelsky, N., Studer, L., Auerbach, J. & McKay, R. Efficient generation of midbrain and hindbrain neurons from mouse embryonic stem cells. *Nat. Biotechnol.* 18, 675–679 (2000).
7. Perrier, A.L. *et al.* Derivation of midbrain dopamine neurons from human embryonic stem cells. *Proc. Natl. Acad. Sci. USA* 101, 12543–12548 (2004).
8. Ye, W., Shimamura, K., Rubenstein, J.L., Hynes, M.A. & Rosenthal, A. FGF and Shh signals control dopaminergic and serotonergic cell fate in the anterior neural plate. *Cell* 93, 755–766 (1998).
9. Yan, Y. *et al.* Directed differentiation of dopaminergic neuronal subtypes from human embryonic stem cells. *Stem Cells* 23, 781–790 (2005).
10. Kawasaki, H. *et al.* Induction of midbrain dopaminergic neurons from ES cells by stromal cell-derived inducing activity. *Neuron* 28, 31–40 (2000).
11. Buytaert-Hoefen, K., Alvarez, E. & Freed, C.R. Generation of tyrosine hydroxylase positive neurons from human embryonic stem cells after coculture with cellular substrates and exposure to GDNF. *Stem Cells* 22, 669–674 (2004).
12. Takeshima, T., Johnston, J. & Commissiong, J. Mesencephalic type 1 astrocytes rescue dopaminergic neurons from death induced by serum deprivation. *J. Neurosci.* 14, 4769–4779 (1994).
13. Wagner, J. *et al.* Induction of a midbrain dopaminergic phenotype in Nurr1-overexpressing neural stem cells by type 1 astrocytes. *Nat. Biotechnol.* [see comments] 17, 653–659 (1999).
14. Bjorklund, L. *et al.* Embryonic stem cells develop into functional dopaminergic neurons after transplantation in a Parkinson rat model. *Proc. Natl. Acad. Sci. USA* 99, 2344–2349 (2002).
15. Roy, N. *et al.* Telomerase-immortalization of neuronally restricted progenitor cells derived from the human fetal spinal cord. *Nat. Biotechnol.* 22, 297–305 (2004).
16. Lafon-Cazal, M. *et al.* Proteomic analysis of astrocytic secretion in the mouse. Comparison with the cerebrospinal fluid proteome. *J. Biol. Chem.* 278, 24438–24448 (2003).
17. Egnaczyk, G.F. *et al.* Proteomic analysis of the reactive phenotype of astrocytes following endothelin-1 exposure. *Proteomics* 3, 689–698 (2003).
18. Morga, E., Faber, C. & Heuschling, P. Cultured astrocytes express regional heterogeneity of the immunoreactive phenotype under basal conditions and after γ-IFN induction. *J. Neuroimmunol.* 87, 179–184 (1998).
19. Onofre, G.R. *et al.* Astroglial cells derived from lateral and medial midbrain sectors differ in their synthesis and secretion of sulfated glycosaminoglycans. *Braz. J. Med. Biol. Res.* 34, 251–258 (2001).
20. Reuss, B., Leung, D.S., Ohlemeyer, C., Kettenmann, H. & Unsicker, K. Regionally distinct regulation of astroglial neurotransmitter receptors by fibroblast growth factor-2. *Mol. Cell. Neurosci.* 16, 42–58 (2000).

21. Yoshida, M. Intermediate filament proteins define different glial subpopulations. *J. Neurosci. Res.* 63, 284–289 (2001).
22. Mendez, I. *et al.* Cell type analysis of functional fetal dopamine cell suspension transplants in the striatum and substantia nigra of patients with Parkinson's disease. *Brain* 128, 1498–1510 (2005).
23. Thompson, L., Barraud, P., Andersson, E., Kirik, D. & Bjorklund, A. Identification of dopaminergic neurons of nigral and ventral tegmental area subtypes in grafts of fetal ventral mesencephalon based on cell morphology, protein expression and efferent projections. *J. Neurosci.* 25, 6467–6477 (2005).
24. McRitchie, D., Hardman, C. & Halliday, G. Cytoarchitectural distribution of calcium binding proteins in midbrain dopaminergic regions of rats and humans. *J. Comp. Neurol.* 364, 121–150 (1996).
25. Schwarting, R. & Huston, J. The unilateral 6-hydroxydopamine lesion model in behavioral brain research. Analysis of functional deficits, recovery and treatments. *Prog. Neurobiol.* 50, 275–331 (1996).
26. Carman, L., Gage, F. & Shults, C. Partial lesions of the substantia nigra: relation between extent of lesion and rotational behavior. *Brain Res.* 553, 275–283 (1991).
27. Hudson, J. *et al.* Correlation of apomorphine and amphetamine-inducing turning with nigrostriatal dopamine content in unilateral 6-hydroxydopamine lesioned rats. *Brain Res.* 626, 167–174 (1993).
28. Olsson, M., Nikkhah, G., Bentlage, C. & Bjorklund, A. Forelimb akinesia in the rat Parkinson model: differential aspects of dopamine agonists and nigral transplants as assessed by a new stepping test. *J. Neurosci.* 15, 3863–3875 (1995).
29. Chang, J., Wachtel, S., Young, D. & Kang, U. Biochemical and anatomical characterization of forepaw adjusting steps in rat models of Parkinson's disease: studies on medial forebrain bundle and striatal lesions. *Neuroscience* 88, 617–628 (1999).
30. Schallert, T., Fleming, S., Leasure, J., Tillerson, J. & Bland, S. CNS plasticity and assessment of forelimb sensorimotor outcome in unilateral rat models of stroke, cortical ablation, parkinsonism and spinal cord injury. *Neuropharmacology* 39, 777–787 (2000).
31. Iancu, R., Mohapel, P., Brundin, P. & Paul, G. Behavioral characterization of a unilateral 6-OHDA-lesion model of Parkinson's disease in mice. *Behav. Brain Res.* 162, 1–10 (2005).
32. Takagi, Y. *et al.* Dopaminergic neurons generated from monkey embryonic stem cells function in a Parkinson primate model. *J. Clin. Invest.* 115, 102–108 (2005).
33. Chung, S. *et al.* Genetic selection of sox1GFP-expressing neural precursors removes residual tumorigenic pluripotent stem cells and attenuates tumor formation after transplantation. *J. Neurochem.* 97, 1467–1480 (2006).
34. Okabe, S., Forsberg-Nilsson, K., Spiro, A.C., Segal, M. & McKay, R.D. Development of neuronal precursor cells and functional postmitotic neurons from embryonic stem cells *in vitro*. *Mech. Dev.* 59, 89–102 (1996).
35. Yang, L. *et al.* A novel systemically active caspase inhibitor attenuates the toxicities of MPTP, malonate and 3NP *in vivo*. *Neurobiol. Dis.* 17, 250–259 (2004).

Erratum: A brief history of T_H17, the first major revision in the T_H1/T_H2 hypothesis of T cell–mediated tissue damage

Lawrence Steinman

Nature Med. 13, 139–145 (2007); published online 6 February 2007; corrected after print 21 February 2007

In the version of this article initially published, the labeling in Figure 1 is incorrect. Tregs should be shown as producing TGF-β, not IL-17. The error has been corrected in the HTML and PDF versions of the article.

Corrigendum: Functional engraftment of human ES cell–derived dopaminergic neurons enriched by coculture with telomerase-immortalized midbrain astrocytes

Neeta S Roy, Carine Cleren, Shashi K Singh, Lichuan Yang, M Flint Beal & Steven A Goldman

Nature Medicine 12, 1259–1268 (2006); published online 22 October 2006.

In page 1264 of this article, it is stated that "The donor cells were dispersed over an average radius of 1.6 ± 0.6 mm, and the mean number of HNA^+ nuclei/mm^3 within each was 136,726 ± 23,515". The authors wish to clarify that they used the word "radius" in the non-geometric sense, as in this definition of the American Heritage Dictionary: "A bounded range of effective activity or influence". At the same time, they want to remark that the numbers, figures and scale bars shown in the paper are correct.

Mitochondrial dysfunction and oxidative stress in neurodegenerative diseases

Michael T. Lin[1] & M. Flint Beal[1]

Many lines of evidence suggest that mitochondria have a central role in ageing-related neurodegenerative diseases. Mitochondria are critical regulators of cell death, a key feature of neurodegeneration. Mutations in mitochondrial DNA and oxidative stress both contribute to ageing, which is the greatest risk factor for neurodegenerative diseases. In all major examples of these diseases there is strong evidence that mitochondrial dysfunction occurs early and acts causally in disease pathogenesis. Moreover, an impressive number of disease-specific proteins interact with mitochondria. Thus, therapies targeting basic mitochondrial processes, such as energy metabolism or free-radical generation, or specific interactions of disease-related proteins with mitochondria, hold great promise.

Neurodegenerative diseases are a heterogeneous group of disorders characterized by gradually progressive, selective loss of anatomically or physiologically related neuronal systems. Prototypical examples include Alzheimer's disease (AD), Parkinson's disease (PD), amyotrophic lateral sclerosis (ALS) and Huntington's disease (HD). Despite this heterogeneity, we argue that mitochondrial involvement is likely to be an important common theme in these diseases. Mitochondria are key regulators of cell survival and death (Fig. 1; for a review see ref. 1), have a central role in ageing, and have recently been found to interact with many of the specific proteins implicated in genetic forms of neurodegenerative diseases (Table 1).

Mitochondria and ageing

By far the greatest risk factor for neurodegenerative diseases such as AD, PD and ALS is ageing, and mitochondria have been thought to contribute to ageing through the accumulation of mitochondrial DNA (mtDNA) mutations and net production of reactive oxygen species (ROS).

Although most mitochondrial proteins are encoded by the nuclear genome, mitochondria contain many copies of their own DNA. Human mtDNA is a circular molecule of 16,569 base pairs that encodes 13 polypeptide components of the respiratory chain, as well as the rRNAs and tRNAs necessary to support intramitochondrial protein synthesis using its own genetic code. Inherited mutations in mtDNA are known to cause a variety of diseases, most of which affect the brain and muscles — tissues with high energy requirements. One hypothesis has been that somatic mtDNA mutations acquired during ageing contribute to the physiological decline that occurs with ageing and ageing-related neurodegeneration.

It is well established that mtDNA accumulates mutations with ageing, especially large-scale deletions[2] and point mutations. In the mtDNA control region, point mutations at specific sites can accumulate to high levels in certain tissues: T414G in cultured fibroblasts, A189G and T408A in muscle, and C150T in white blood cells[3]. However, these control-region 'hot spots' have not been observed in the brain[4]. Point mutations at individual nucleotides seem to occur at low levels in the brain[5], although the overall level may be high. Using a polymerase chain reaction (PCR)-cloning-sequencing strategy, we found that the average level of point mutations in two protein-coding regions of brain mtDNA from elderly subjects was ~2 mutations per 10 kb[6]. Noncoding regions, which may be under less selection pressure, potentially accumulate between twice and four times as many[7].

The accumulation of these deletions and point mutations with ageing correlates with decline in mitochondrial function. For example, a negative correlation has been found between brain cytochrome oxidase

Table 1 | Proteins that have a function in major neurodegenerative diseases with mitochondrial involvement

Disease	Genetic causes	Function
Alzheimer's disease	APP	Gives rise to Aβ, the primary component of senile plaques
	PS1 and PS2	A component of γ-secretase, which cleaves APP to yield Aβ
Parkinson's disease	α-Synuclein	The primary component of Lewy bodies
	Parkin	A ubiquitin E3 ligase
	DJ-1	Protects the cell against oxidant-induced cell death
	PINK1	A kinase localized to mitochondria. Function unknown. Seems to protect against cell death
	LRRK2	A kinase. Function unknown
	HTRA2	A serine protease in the mitochondrial intermembrane space. Degrades denatured proteins within mitochondria. Degrades inhibitor of apoptosis proteins and promotes apoptosis if released into the cytosol
Amyotrophic lateral sclerosis	SOD1	Converts superoxide to hydrogen peroxide. Disease-causing mutations seem to confer a toxic gain of function
Huntington's disease	Huntingtin	Function unknown. Disease-associated mutations produce expanded polyglutamine repeats

[1]Department of Neurology and Neuroscience, Weill Medical College of Cornell University, Room F-610, 525 East 68th Street, New York 10021, USA.

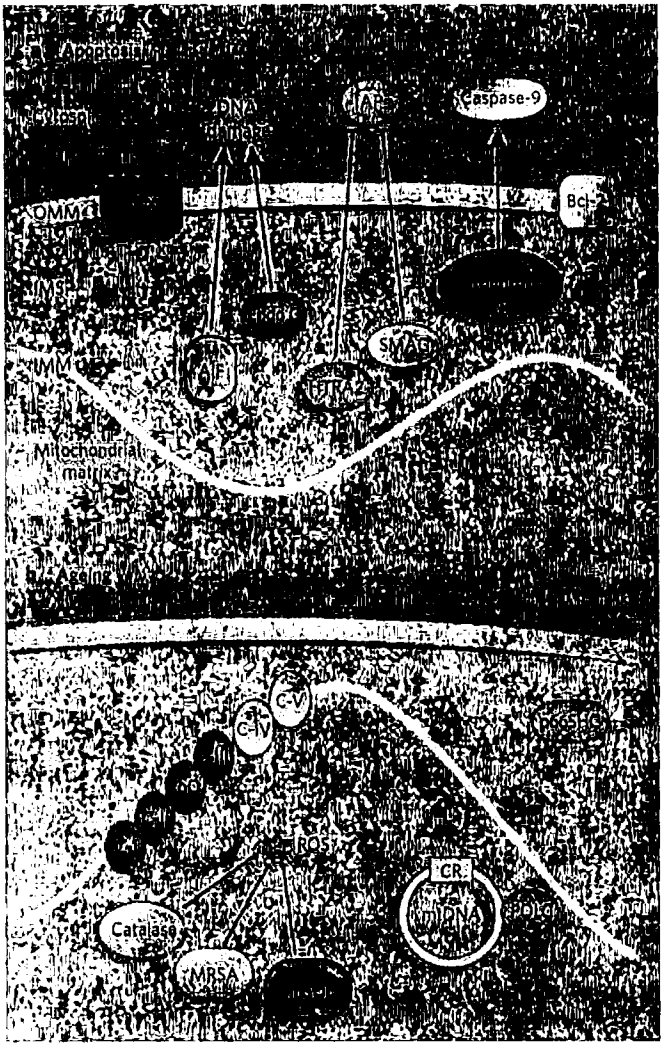

Figure 1 | Role of mitochondria in apoptosis and ageing. **a**, Several intermembrane space (IMS) proteins are pro-apoptotic if released into the cytosol. Cytochrome *c* (C) activates caspase-9. SMAC (second mitochondrial activator of caspases) and HTRA2 inhibit cytosolic inhibitor of apoptosis proteins (IAPs). HTRA2 is a serine protease that might function to remove denatured proteins within mitochondria, but degrades IAPs when released from mitochondria. Inhibiting HTRA2's normal quality control function or enhancing its IAP-degrading activity could both promote cell death. Apoptosis inhibitor factor (AIF) and endonuclease G (endo G) translocate to the nucleus and induce chromatin condensation and DNA fragmentation. Release of these proteins into the cell is modulated by recruitment of BAX (which is proapoptotic) or Bcl-2 (anti-apoptotic) to the outer mitochondrial membrane (OMM). Numerous extracellular and intracellular signals converge to regulate mitochondrial apoptosis (reviewed in ref. 1; see also page 796). **b**, Mitochondrial DNA (mtDNA) mutations and oxidative stress may contribute to ageing. Somatic mutations accumulate in mtDNA with age. Inducing mtDNA mutations by disabling the proofreading activity of mtDNA POLG accelerates ageing-related pathology in transgenic mice. Certain mtDNA polymorphisms are associated with increased longevity, possibly by reducing membrane potential and decreasing the generation of reactive oxygen species (ROS, white stars). Overexpression of ROS-scavenging enzymes manganese superoxide dismutase (MnSOD), methionine sulphoxide reductase A (MSRA) or catalase within mitochondria prolongs lifespan. Knockout of p66SHC, a protein that promotes ROS generation and mitochondrial apoptosis, also prolongs lifespan. Complex IV (C-IV) and complex V activities decline with ageing, and knockdown of complex V activity causes oxidative damage to nuclear DNA, which probably results in decreased gene expression with ageing. IMM, inner mitochondrial membrane.

activity and increased point-mutation levels in a cytochrome oxidase gene (*CO1*)[6]. Moreover, somatic deletions can be clonally expanded in individual neurons, and high levels of such deletions correlate with cytochrome oxidase deficiency on a cell-by-cell basis in the substantia nigra, perhaps contributing to the age dependence of PD[8,9]. However, although the cell-by-cell correlation provides strong circumstantial evidence, correlations do not prove that somatic mtDNA mutations cause age-related pathology.

Recently, several groups have addressed the issue of causation using a clever approach to generate mtDNA mutations experimentally (for a review see ref. 10). MtDNA replication is carried out by mtDNA polymerase-γ (POLG), which has 3′-to-5′ exonuclease (proofreading) activity in addition to its 5′-to-3′ polymerase activity. If the proofreading activity of POLG is eliminated and the polymerase activity preserved, mtDNA mutations accumulate because of uncorrected errors during replication. In mice with such proofreading-deficient POLG (mtDNA-mutator mice), mtDNA mutations accumulate to high levels in all tissues. By 8 weeks of age, homozygous *Polg*$^{-/-}$ animals had 9 point mutations per 10 kb in cytochrome *b*. By contrast, normal mice had less than 1 mutation per 10 kb. This marked increase in mtDNA mutations resulted in decreased respiratory enzyme activity and ATP production. To begin with, the mice appeared normal, but by 25 weeks of age began to exhibit pathology frequently seen in human (although not necessarily murine) ageing, including weight loss, alopecia, osteoporosis, kyphosis, cardiomyopathy, anaemia, gonadal atrophy and sarcopaenia. The median lifespan of such mice was 48 weeks (none lived beyond 61 weeks of age) — much shorter than the typical murine lifespan of 2 years.

A second, independent mtDNA-mutator mouse showed a similar marked increase in mtDNA mutations, progeric features and early mortality. Notably, neuropathology was not reported in either mouse model, although detailed examination was not carried out. Humans with *POLG* mutations exhibit parkinsonism, ophthalmoplegia and myopathy (see below), and the reasons for the differences between mice and humans with such mutations are not yet known.

In both mtDNA-mutator mouse models, markers of apoptosis such as activated caspase 3 were increased at times coinciding with tissue degeneration, suggesting that apoptosis mediates deleterious effects of somatic mtDNA mutations. Interestingly, tissues from the mtDNA-mutator mice did not show increased levels of lipid, protein or DNA oxidation, hydrogen peroxide production, or sensitivity to oxidative stress. Thus, the effects of mtDNA mutations in these mice do not seem to be mediated through ROS production.

Net production of ROS is another important mechanism by which mitochondria are thought to contribute to ageing. Mitochondria contain multiple electron carriers capable of producing ROS, as well as an extensive network of antioxidant defences (Fig. 2). Mitochondrial insults, including oxidative damage itself, can cause an imbalance between ROS production and removal, resulting in net ROS production[11]. The importance to ageing of net mitochondrial ROS production is supported by observations that enhancing mitochondrial antioxidant defences can increase longevity. In *Drosophila*, overexpression of the mitochondrial antioxidant enzymes manganese superoxide dismutase (MnSOD)[12] and methionine sulphoxide reductase[13] prolongs lifespan. This strategy is most successful in short-lived strains of *Drosophila*, and has no effect in already long-lived strains. However, it has recently been shown that overexpression of catalase experimentally targeted to mitochondria increased lifespan in an already long-lived mouse strain[14]. The authors of this work generated transgenic mice overexpressing catalase targeted to peroxisomes, nuclei or mitochondria. The mitochondrially targeted construct provided the maximal benefit, increasing median and maximal lifespan by 20%. Hydrogen peroxide production and oxidative inactivation of aconitase were reduced in isolated cardiac mitochondria, DNA oxidation and levels of mitochondrial deletions were reduced in skeletal muscle, and cardiac pathology, arteriosclerosis and cataract development were delayed.

In humans, a recent study of gene expression in the brain suggests that oxidative damage has a major role in the cognitive decline that

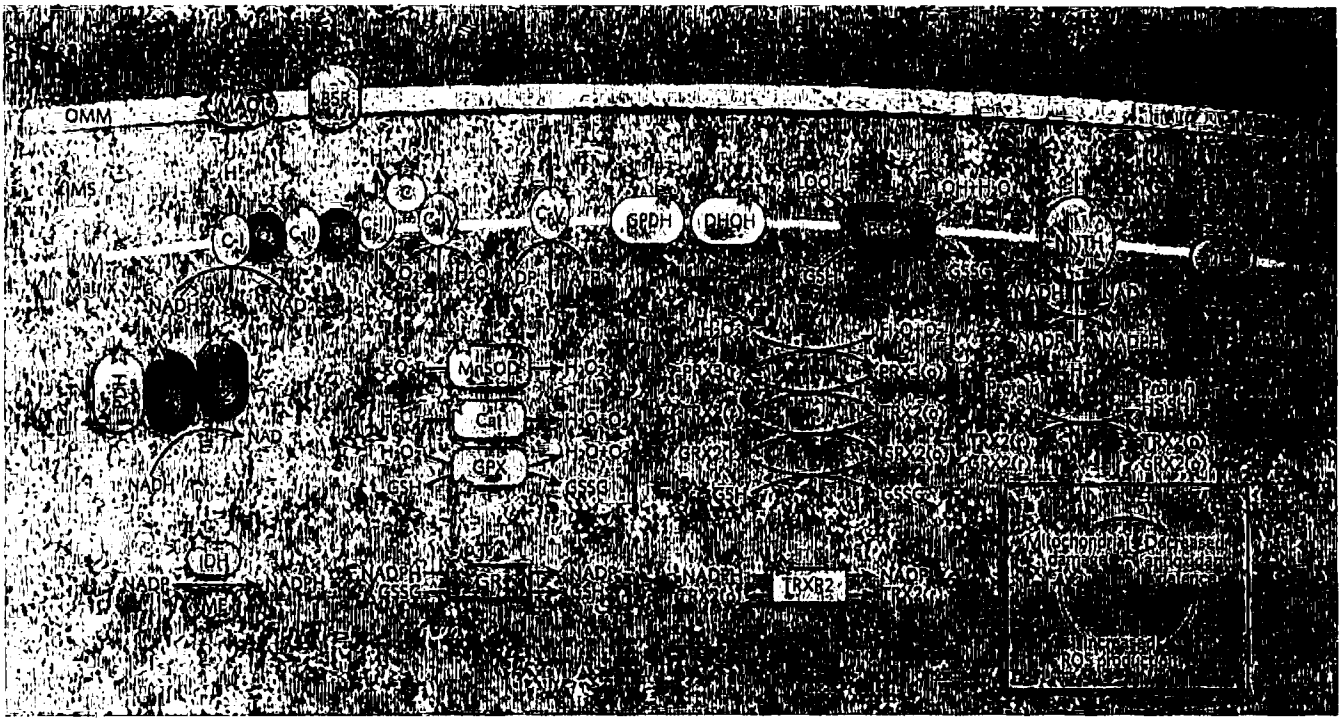

Figure 2 | Role of mitochondria in reactive oxygen species metabolism. The processes and components involved in ROS generation (white stars) and antioxidant defence (red stars). Mitochondria are the primary cellular consumers of oxygen and contain numerous redox enzymes capable of transferring single electrons to oxygen, generating the ROS superoxide ($O_2^{\cdot-}$). Mitochondrial enzymes so far known to generate ROS include the tricarboxylic acid (TCA) cycle enzymes aconitase (ACO) and α-ketoglutarate dehydrogenase (KGDH); the electron-transport chain (ETC) complexes I, II and III; pyruvate dehydrogenase (PDH) and glycerol-3-phosphate dehydrogenase (GPDH); dihydroorotate dehydrogenase (DHOH); the monoamine oxidases (MAO) A and B; and cytochrome b_5 reductase (B5R). The transfer of electrons to oxygen, generating superoxide, is more likely when these redox carriers are abundantly charged with electrons and the potential energy for transfer is high, as reflected by a high mitochondrial membrane potential. ROS generation is decreased when available electrons are few and potential energy for the transfer is low. Mitochondria also contain an extensive antioxidant defence system to detoxify the ROS generated by the reactions described above. Both the membrane-enclosed and soluble compartments are protected. Nonenzymatic components of the system include α-tocopherol (aTCP), coenzyme Q10 (Q), cytochrome *c* (C) and glutathione (GSH). Enzymatic components include manganese superoxide dismutase (MnSOD), catalase (Cat), glutathione peroxidase (GPX), phospholipid hydroperoxide glutathione peroxidase (PGPX), glutathione reductase (GR); peroxiredoxins (PRX3/5), glutaredoxin (GRX2), thioredoxin (TRX2) and thioredoxin reductase (TRXR2). The regeneration of GSH (through GR) and reduced TRX2 (through TRXR2) depends on NADPH, which is derived from substrates (through isocitrate dehydrogenase, IDH, or malic enzyme, ME) or the membrane potential (through nicotinamide nucleotide transhydrogenase, NNTH). So, like ROS generation, antioxidant defences are also tied to the redox and energetic state of mitochondria. GSSG, glutathione disulphide; LOH, lipid hydroxide; LOOH, lipid hydroperoxide; o, oxidized state; r, reduced state. In structurally and functionally intact mitochondria, a large antioxidant defence capacity balances ROS generation, and there is little net ROS production. Mitochondrial damage with decrease of antioxidant defence capacity is a prerequisite for net ROS production. Once this occurs, a vicious cycle (inset) can ensue whereby ROS can further damage mitochondria, causing more free-radical generation and loss or consumption of antioxidant capacity. For example, the Fe–S cluster in aconitase is easily inactivated by superoxide, the iron is released, and this induces hydroxyl radical production. (For a review of the role of mitochondria in ROS metabolism, see ref. 11.)

accompanies ageing[15]. Transcriptional profiling of postmortem frontal cortex samples from individuals aged from 26 to 106 revealed that after the age of 40 there was a decrease in the expression of genes involved in synaptic plasticity, vesicular transport and mitochondrial function, followed by increased expression of stress-response, antioxidant and DNA-repair genes. In the brain, the age-downregulated genes suffered markedly increased oxidative DNA damage compared with the age-stable or age-upregulated genes. Promoter regions were particularly affected, perhaps because they contain G/C-rich sequences that are sensitive to oxidation, or do not undergo transcription-coupled repair. In SH-SY5Y cells, promoters of the same age-downregulated genes were both more sensitive to hydrogen-peroxide-induced damage and less able to undergo base excision repair of such damage than promoters of age-stable or age-upregulated genes.

To investigate whether impaired mitochondrial function could predispose these age-downregulated genes to DNA damage, small interfering RNA (siRNA) was used to reduce the expression of mitochondrial F_1-ATPase 2.5-fold in SH-SY5Y cells, approximating the reduction seen in the aged human cortex. This resulted in significantly increased promoter DNA damage in age-downregulated genes, which was partly reversed by the antioxidant vitamin E. These findings support the idea that mitochondrial dysfunction contributes to the damage of vulnerable genes in the ageing brain. The vulnerable-gene promoters are both more sensitive to oxidative stress and deficient in repair, and mitochondrial dysfunction could potentially exacerbate both by increasing ROS or decreasing the availability of ATP, which is necessary for repair.

Mitochondria and Alzheimer's disease

AD is characterized clinically by progressive cognitive decline, and pathologically by the presence of senile plaques composed primarily of amyloid-β peptide (Aβ) and neurofibrillary tangles made up mainly of hyperphosphorylated tau. About 5–10% of cases are familial, occurring in an early-onset, autosomal-dominant manner. Three proteins are known to be associated with such familial cases: amyloid precursor protein (APP) — which is cleaved sequentially by β- and γ-secretases to produce Aβ — and presenilins 1 and 2 (PS1 and PS2), one or other of which is a component of each γ-secretase complex.

There is extensive literature supporting a role for mitochondrial dysfunction and oxidative damage in the pathogenesis of AD. Oxidative damage occurs early in the AD brain, before the onset of significant

plaque pathology[16]. Oxidative damage also precedes Aβ deposition in transgenic APP mice[17], with upregulation of genes relating to mitochondrial metabolism and apoptosis occurring even earlier and co-localizing with the neurons undergoing oxidative damage[18].

Moreover, such oxidative damage and mitochondrial dysfunction probably contribute causally to AD-related pathology. In fetal guinea pig neurons, hydrogen peroxide treatment increased intracellular Aβ levels[19]. Treatment with the mitochondrial uncoupler CCCP (carbonyl cyanide m-chlorophenylhydrazone) caused cultured astrocytes to mimic the amyloidogenic APP processing and intracellular Aβ accumulation that is seen in Down syndrome astrocytes[20]. In a transgenic APP-mutant mouse, hemizygous deficiency of the mitochondrial antioxidant enzyme MnSOD markedly increased brain Aβ levels and plaque deposition[21]. In another transgenic APP-mutant mouse, energy metabolism inhibitors (insulin, 2-deoxyglucose, 3-nitropropionic acid and kainic acid) elevated β-secretase levels and activity and Aβ levels[22].

Several pathways connecting oxidative stress and AD pathology have recently been uncovered. Oxidative stress may activate signalling pathways that alter APP or tau processing. For example, oxidative stress increases the expression of β-secretase through activation of c-Jun amino-terminal kinase and p38 mitogen-activated protein kinase (MAPK)[23], and increases aberrant tau phosphorylation by activation of glycogen synthase kinase 3 (ref. 24). Oxidant-induced inactivation of critical molecules may also be important. In a proteomic study, the prolyl isomerase PIN1 was found to be particularly sensitive to oxidative damage[25]. PIN1 catalyses protein conformational changes that affect both APP and tau processing. Knockout of *Pin1* increases amyloidogenic APP processing and intracellular Aβ levels in mice[26]. *Pin1*-knockout mice also exhibit tau hyperphosphorylation, motor and behavioural deficits, and neuronal degeneration[27].

There is some evidence that mtDNA may be involved in the mitochondrial dysfunction seen in AD. When patient mtDNA is transferred into mtDNA-deficient cell lines, the resulting 'cybrids' reproduce the respiratory enzyme deficiency seen in the brain and other tissues in AD, suggesting that the defect is carried at least in part by mtDNA abnormalities[28]. However, identifying AD-specific mtDNA mutations has been a challenge. Complete sequencing of mtDNA from 145 AD patients and 128 controls did not reveal any significant association with mitochondrial haplogroup or with inherited mtDNA mutations[29]. There was also no association with acquired mtDNA mutations when a coding region (for CO1) was examined[6]. However, in the same way that promoters appeared more sensitive to damage than coding regions in nuclear genes[15], the mtDNA control region showed an increase in acquired mutations in AD[30]. AD brains had on average a 63% increase in heteroplasmic mtDNA control-region mutations, and in individuals older than 80 years there was a 130% increase in mutations. These mutations preferentially altered known mtDNA regulatory elements and suppressed mitochondrial transcription and replication.

Finally, several recent reports suggest that many of the proteins implicated in AD pathogenesis have direct physical involvement with mitochondria or mitochondrial proteins (Fig. 3). APP has been found to have a dual endoplasmic reticulum/mitochondrial-targeting sequence, and in transfected cells and transgenic mice overexpressing APP it clogged the mitochondrial protein importation machinery, causing mitochondrial dysfunction and impaired energy metabolism[31]. Aβ binds to a mitochondrial-matrix protein termed Aβ-binding alcohol dehydrogenase (ABAD)[32]. Blocking the interaction of Aβ and ABAD with a 'decoy peptide' suppressed Aβ-induced apoptosis and free-radical generation in neurons. Conversely, overexpression of ABAD in transgenic APP-mutant mice exaggerated neuronal oxidative stress and impaired memory. Two other groups have also reported that Aβ interacts with mitochondria, inhibiting cytochrome oxidase activity and increasing free-radical generation[33,34]. Aβ also inhibits α-ketoglutarate dehydrogenase activity in isolated mitochondria[35], and deficiency of α-ketoglutarate dehydrogenase[36] and cytochrome oxidase activities[37] has previously been observed in the brain and other tissues in AD. Aβ also interacts with the serine protease HTRA2 (also known as OMI)[38]. Presenilin and all the other components of the γ-secretase complex have also been localized to mitochondria, where they form an active γ-secretase complex[39].

Mitochondria and Parkinson's disease

PD is characterized clinically by progressive rigidity, bradykinesia and tremor, and pathologically by loss of pigmented neurons in the substantia nigra and the presence of Lewy bodies — distinctive cytoplasmic inclusions that immunostain for α-synuclein and ubiquitin.

Mitochondria were first implicated in PD because MPTP (1-methyl 4-phenyl-1,2,3,6-tetrahydropyridine), whose metabolite MPP+ inhibits complex I of the mitochondrial electron-transport chain, caused parkinsonism in designer-drug abusers. This model has since been refined in laboratory animals, in which chronic infusion of rotenone[40] — another complex-I inhibitor — or MPTP[41] results clinically in a parkinsonian phenotype and pathologically in nigral degeneration with cytoplasmic inclusions immunoreactive for α-synuclein and ubiquitin. The mechanism of toxicity in these complex-I inhibition models probably involves oxidative stress[42]. Complex-I inhibition and oxidative stress were shown to be relevant to naturally occurring PD when complex-I deficiency and glutathione depletion were found in the substantia nigra of patients with idiopathic PD and in patients with pre-symptomatic PD[43].

Many of the genes associated with PD also implicate mitochondria in disease pathogenesis. So far, mutations or polymorphisms in mtDNA and at least nine named nuclear genes have been identified as causing PD or affecting PD risk: α-synuclein, parkin, ubiquitin carboxy-terminal hydrolase L1, *DJ-1*, phosphatase and tensin homologue (PTEN)-induced kinase 1 (*PINK1*), leucine-rich-repeat kinase 2 (*LRRK2*), the nuclear receptor *NURR1*, *HTRA2* and tau. Of the nuclear genes, α-synuclein, parkin, *DJ-1*, *PINK1*, *LRRK2* and *HTRA2* directly or indirectly involve mitochondria.

In a small number of cases, inherited mtDNA mutations result in parkinsonism, typically as one feature of a larger syndrome. In one family, we found that the Leber's optic atrophy G11778A mutation was associated with L-DOPA-responsive parkinsonism, variably co-occurring with dementia, dystonia, ophthalmoplegia and ataxia[44]. Notably, this mutation is in a subunit of complex I. Mutations in the nuclear-encoded mtDNA polymerase-γ (*POLG*) gene impair mtDNA replication and result in multiple mtDNA deletions, typically causing chronic progressive external ophthalmoplegia and myopathy. In such families, *POLG* mutations also cosegregate with parkinsonism[45].

There is less evidence for mtDNA involvement in non-syndromic PD. Nigral neurons from PD patients contain increased levels of clonally expanded somatic mtDNA deletions compared with those from age-matched controls, although high levels are also seen in normal ageing[8,9]. We found no difference between PD and control subjects in inherited or acquired complex-I or tRNA point mutations[46,47]. Interestingly, however, several groups have found that certain continent-specific clusters of polymorphisms, termed mtDNA haplogroups, may decrease the risk of developing PD. Among Europeans, the haplogroup cluster UJKT is associated with a decreased risk for PD compared with haplogroup H (ref. 48). It is of note that haplogroups underrepresented in PD patients are overrepresented in healthy centenarians[49]. Protective mtDNA lineages seem to have arisen from areas requiring cold-adaptation, including relative uncoupling of mitochondria to increase heat generation at the expense of ATP production. It has been proposed that this partial uncoupling increases longevity and decreases risk of neurodegeneration by decreasing free-radical generation[50].

Mutations in α-synuclein are associated with autosomal dominant familial PD. α-Synuclein is a major component of Lewy bodies, and the primary effect of α-synuclein mutations is likely to be an increased formation of oligomeric or fibrillar aggregates. However, there seem to be close interrelationships between abnormal protein accumulation or degradation, oxidative stress and mitochondrial dysfunction. In transgenic mice, overexpression of α-synuclein impairs mitochondrial function, increases oxidative stress and enhances nigral pathology induced by MPTP[51]. Moreover, in a recent study of mice overexpressing

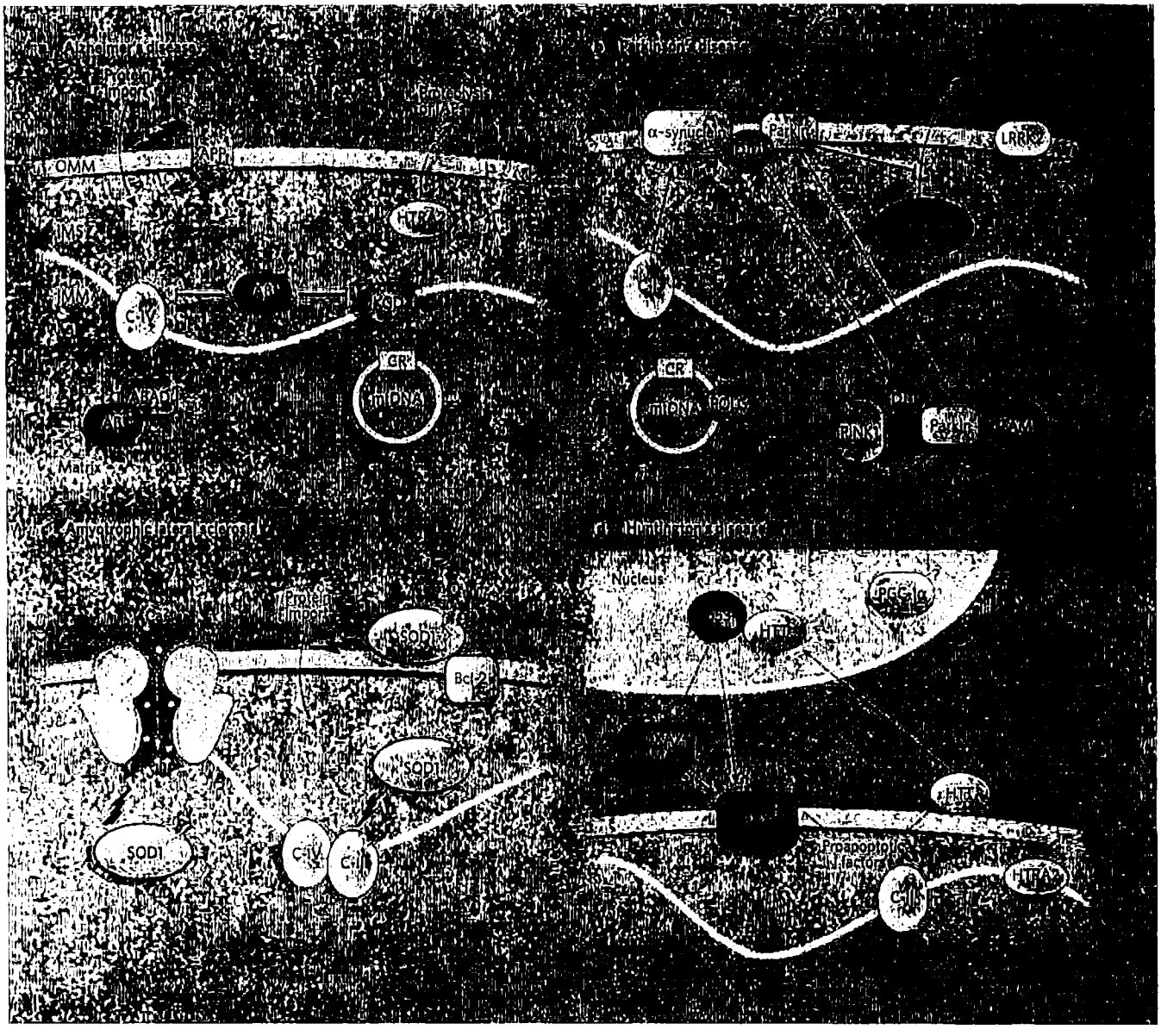

Figure 3 | The role of mitochondria in ageing-related neurodegenerative diseases. **a**, In AD, mitochondrial ROS generation and inhibition of energy metabolism increase Aβ levels in cells and transgenic mice, and Aβ can interact with mitochondria and cause mitochondrial dysfunction. Aβ inhibits complex IV and α-ketoglutarate dehydrogenase (KGD), and binds Aβ-binding alcohol dehydrogenase (ABAD). Both KGD and ABAD produce ROS (white stars). Amyloid precursor protein (APP) may be targeted to the OMM and interfere with protein import. Mitochondria have also been reported to contain active γ-secretase complexes, which are involved in cleaving APP to form Aβ and contain presenilin 1, which increases the proteolytic activity of HTRA2 towards IAPs. AD patients have on average more somatic mutations in the mtDNA control region than control subjects. **b**, Complex I activity is decreased in PD, and inhibition of complex I by MPTP or rotenone causes parkinsonism. Mutations in mtDNA-encoded complex I subunits, 12SrRNA, and POLG also cause parkinsonism. Many genes associated with PD also implicate mitochondria in disease pathogenesis. α-Synuclein immunostaining is seen in degenerating mitochondria from mice overexpressing A53T α-synuclein. α-Synuclein overexpression impairs mitochondrial function and enhances the toxicity of MPTP. Parkin associates with the OMM and protects against cytochrome *c* release. It may also associate with mitochondrial-transcription-factor A (TFAM) and enhance mitochondrial biogenesis. When oxidized, DJ-1 translocates to mitochondria (IMS and matrix), downregulates the PTEN-tumour suppressor (not shown), and protects the cell from oxidative-stress-induced cell death. The mitochondrial kinase PINK1 protects against apoptosis, an effect that is reduced by PD-related mutations or kinase inactivation. Physical associations have been reported between DJ-1 and α-synuclein, DJ-1 and parkin, and DJ-1 and PINK1, and there is genetic evidence that DJ-1, PINK1 and parkin function sequentially in the same pathway. About 10% of the kinase LRRK2 is localized to mitochondria, and PD-related mutations augment its kinase activity. A mutation in HTRA2 was found in ~1% of sporadic PD patients. Overexpression of the mutant impaired normal HTRA2 protease activity, and HTRA2 knockout results in striatal degeneration and parkinsonism. **c**, Overexpression of mutant SOD1 in ALS impairs electron-transport-chain activities and decreases mitochondrial calcium-loading capacity. SOD1 has been localized to the OMM, IMS and matrix, and targeting of mutant SOD1 to mitochondria causes cytochrome *c* release and apoptosis. Mutant SOD1 promotes aberrant mitochondrial ROS production and forms aggregates that may clog the OMM protein importation machinery or bind and sequester the antiapoptotic protein Bcl-2. **d**, Complex II activity is decreased in the HD brain, and the complex-II inhibitor 3-nitropropionic acid induces striatal degeneration and movement disorder in rodents and primates. Overexpression of complex-II subunits reduces cell death in striatal neurons expressing mutant HTT. Mutant HTT associates with the OMM and increases sensitivity to calcium-induced cytochrome *c* release. Mutant HTT also translocates to the nucleus, where it binds and increases the level and transcriptional activity of p53. p53 activates the pro-apoptotic protein BAX, either directly or by increasing expression of BH3-only Bcl-2 family members NOXA and PUMA. In mice, knockout of *Pgc-1α* or a missense mutation in *Htra2* causes involuntary movements and striatal degeneration.

A53T mutant α-synuclein, degenerating mitochondria were immunostained for α-synuclein, raising the possibility that mutant α-synuclein might damage mitochondria directly[52]. Whereas overexpression of α-synuclein increases sensitivity to MPTP, α-synuclein-null mice are resistant to MPTP[41] and other mitochondrial toxins such as malonate and 3-nitropropionic acid[53]. Thus, α-synuclein seems to mediate the toxic effects of MPTP.

Mutations in parkin are associated with autosomal recessive juvenile PD. Parkin encodes a ubiquitin E3 ligase, and the primary abnormality, therefore, is in the ubiquitin–proteasome system. However, as above, there seem to be close interrelationships between the ubiquitin–proteasome system, oxidative stress and mitochondrial dysfunction. On one hand, parkin deficiency or mutations lead to oxidative stress and mitochondrial dysfunction. *Parkin*-null *Drosophila*[54] and mouse[55] strains exhibit mitochondrial impairment and increased oxidative stress, and leukocytes from individuals with parkin mutations have a selective impairment in complex-I activity[56]. Parkin can associate with the outer mitochondrial membrane and prevent mitochondrial swelling, cytochrome *c* release and caspase activation, and this protective effect is abrogated by proteasome inhibitors and parkin mutations[57]. Parkin has also been localized to mitochondria in proliferating cells, where it has been shown to associate with mitochondrial transcription factor A and to enhance mitochondrial biogenesis[58]. On the other hand, mitochondrial dysfunction and oxidative stress can affect parkin function and exacerbate parkin mutations. S-nitrosylation of parkin, an oxidative modification, impairs its ubiquitin-ligase activity and compromises its protective function[59]. Conversely, overexpression of glutathione *S*-transferase, which has a role in detoxifying products of oxidative damage, suppresses neurodegeneration in *Drosophila parkin* mutants[60].

Mutations in *DJ-1* are also associated with autosomal recessive juvenile PD[61]. DJ-1 has been reported to interact with α-synuclein[62], parkin[63] and PINK1 (ref. 64). The overall function of DJ-1 seems to be to protect against cell death, especially that induced by oxidative stress. It can act as a redox sensor: oxidative stress causes a critical cysteine residue (C106) to be acidified, which leads to its relocalization to mitochondria. C106 mutations prevent this mitochondrial relocalization and impair the cell's response to oxidative stress and mitochondrial damage[65]. DJ-1 is a negative regulator of the PTEN tumour-suppressor protein, which promotes apoptosis by dephosphorylating phosphatidylinositol-3,4,5-trisphosphate, which is necessary for phosphatidylinositol 3OH-kinase-mediated activation of the cell-survival kinase Akt. *Dj-1* knockdown results in decreased phosphorylation of Akt[66], whereas *Dj-1* overexpression leads to Akt hyperphosphorylation and increased cell survival[67]. DJ-1-deficient mice are hypersensitive to MPTP and oxidative stress[68]. Moreover, in flies, DJ-1 undergoes progressive oxidative inactivation with ageing, which, in turn, increases sensitivity to oxidative stress, and could provide one potential explanation for the age dependence of sporadic PD[69].

Mutations in *PINK1* represent a third form of autosomal recessive juvenile PD[70]. PINK1 is a kinase localized to mitochondria[71], and, like DJ-1, seems to protect against cell death. Overexpression of wild-type PINK1 prevents apoptosis under basal and staurosporine-induced conditions by decreasing cytochrome *c* release and caspase activation, and this effect is abrogated by PD-related mutations and a kinase-inactive mutation[72]. In *Drosophila*, PINK1 deficiency causes mitochondrial pathology, increased sensitivity to paraquat and rotenone, and degeneration of flight muscles and dopaminergic neurons. This pathology resembles that of *parkin*-mutant flies, and can be rescued by overexpression of parkin, but not DJ-1 (ref. 73). Thus, PINK1 probably functions in the same pathway as parkin, with parkin downstream.

Mutations in *LRRK2* are the most common known cause of familial late-onset PD, and also account for 1–2% of sporadic late-onset PD cases. On the basis of its sequence, LRRK2 is predicted to have a ROC–COR GTPase domain, a MAPK kinase kinase domain and WD40 domains. Recently, West and colleagues showed that LRRK2 is a kinase, that two disease-associated mutations, including the most common G2019S mutation, augment the kinase activity, and that ~10% of LRRK2 is associated with mitochondria[74].

The gene most recently associated with PD is *HTRA2* (also known as *OMI*)[75]. A G399S mutation was found in 4 of 414 individuals with sporadic PD and none of 313 controls. An additional polymorphism, A141S, was found in a heterozygous state in 3% of controls and 6.2% of PD subjects (P=0.039, odds ratio=2.15). As noted above (Fig. 1), HTRA2 may be a protein quality control agent within mitochondria, and a pro-apoptotic factor when released into the cytosol from the mitochondrial intermembrane space through a mechanism mediated by the pro-apoptotic proteins BAX and BAK. Consistent with a role for HTRA2 in maintaining mitochondrial function, homozygous *Htra2*-knockout mice develop striatal degeneration and parkinsonism[76]. Expression in cultured cells of the G399S and A141S mutations found in people with PD impairs normal HTRA2 protease activity, causes mitochondrial swelling, decreases mitochondrial membrane potential and increases staurosporine-induced cell death[75].

Mitochondria and amyotrophic lateral sclerosis

ALS is characterized clinically by progressive weakness, atrophy and spasticity of muscle tissue, reflecting the degeneration of upper and lower motor neurons in the cortex, brainstem and spinal cord. Approximately 90% of cases are sporadic (SALS) and 10% are familial (FALS). About 20% of familial cases are caused by mutations in Cu/Zn-superoxide dismutase (*SOD1*).

In both SALS and FALS, postmortem and biopsy samples from the spinal cord, nerves and muscles show abnormalities in mitochondrial structure, number and localization. Defects in activities of respiratory-chain complexes have also been detected in muscle and spinal cord. However, it is difficult to know from single snapshots of already symptomatic individuals whether mitochondria contribute to pathogenesis or are innocent bystanders. Thus, research on mitochondrial involvement in ALS has focused on expression of mutant SOD1 in animal and cellular models of the disease.

Overexpressing the G93A *Sod1* mutation in transgenic mice causes impaired mitochondrial energy metabolism in the brain and spinal cord at disease onset[77]. However, long before disease onset there is a decrease in the calcium-loading capacity in mitochondria from the brain and spinal cord, but not the liver, of mice overexpressing G93A or G85R mutant *Sod1* (ref. 78). In G93A *Sod1* mice there is a transient explosive increase in vacuolar mitochondrial degeneration just preceding motor-neuron death[79], suggesting that mitochondrial abnormalities trigger the onset of ALS.

Interestingly, SOD1 immunoreactivity is concentrated inside vacuolated mitochondria[80]. SOD1 has traditionally been thought to be a cytoplasmic protein, but localization of a fraction of cellular SOD1 to the mitochondrial outer membrane, intermembrane space and matrix has now been demonstrated[81,82]. The localization of SOD1 to mitochondria has been reported to occur only in affected tissues and to occur preferentially for mutant SOD1 (ref. 83).

Interaction between SOD1 and mitochondria suggests a number of mechanisms by which mitochondrial function and cell survival may be adversely affected. Mitochondrial targeting of mutant SOD1 caused cytochrome *c* release and apoptosis, whereas targeting to the endoplasmic reticulum or nucleus did not cause cell death[84]. Cleveland and colleagues suggest that mutant SOD1 accumulates and aggregates in the outer mitochondrial membrane and clogs the protein importation machinery, eventually resulting in mitochondrial dysfunction[83]. Mutant SOD1 has been proposed to promote aberrant ROS production, and we found oxidative damage to mitochondrial lipids and proteins, accompanied by impaired respiration and ATP synthesis, in mice expressing mutant human SOD1 (ref. 77). Mutant, but not wild-type, SOD1 species bind to and aggregate with cytosolic heat-shock proteins[85] and mitochondrial Bcl-2 (ref. 86), rendering them unavailable for anti-apoptotic functions.

Mitochondria and Huntington's disease

HD is characterized clinically by chorea, psychiatric disturbances and dementia, and pathologically by loss of long projection neurons in the cortex and striatum. HD is inherited in an autosomal dominant

Table 2 | Mitochondrial involvement in less common neurodegenerative diseases

Disease	Clinical features	Protein	Function
Friedreich's ataxia	Ataxia and neuropathy due to degeneration of spinocerebellar tracts and dorsal-root ganglia; diabetes; cardiomyopathy Autosomal recessive	Frataxin	A mitochondrial iron chaperone that promotes the biogenesis of enzymes with Fe–S clusters and detoxifies excess iron. Frataxin deficiency causes iron accumulation and impairs the activity of Fe–S cluster-containing enzymes (complexes I and II, and aconitase). It may also perturb manganese balance and impair MnSOD activity
Hereditary spastic paraplegia (HSP)	Slowly progressive weakness and spasticity of the legs Autosomal recessive	SPG7*	An inner mitochondrial membrane m-AAA metalloprotease. It functions as a chaperone and is involved in the assembly of respiratory-chain complexes. SPG7 deficiency causes recessive HSP with mitochondrial myopathy
	Autosomal dominant	SPG13†	A mitochondrial protein chaperone
Neurodegeneration with brain iron accumulation (NBIA)	Progressive dementia, rigidity, involuntary movements, spasticity and retinal degeneration accompanied by iron deposition in globus pallidus and substantia nigra Autosomal recessive, paediatric onset	PANK2	PANK2 is localized to mitochondria and catalyses the first step in coenzyme A synthesis. PANK2 deficiency is the most common cause of NBIA, accounting for ~50% of cases
Optic atrophy type 1	Autosomal dominant optic neuropathy causing progressive visual loss	OPA1	OPA1 is a dynamin-related GTPase localized to mitochondria. It organizes the mitochondrial inner membrane and is necessary for maintaining cristae integrity. SiRNA knockdown of OPA1 causes fragmentation of the mitochondrial network, loss of mitochondrial membrane potential, disorganization of cristae, release of cytochrome c and activation of caspases

*Also known as paraplegin. †Also known as heat-shock protein 60. m-AAA, mitochondrial ATPases associated with diverse cellular activities; PANK2, pantothenate kinase 2; SPG, spastic paraplegia gene.

manner, and is due to expansion of a CAG trinucleotide repeat in the huntingtin (*HTT*) gene, which gives rise to an expanded polyglutamine stretch in the corresponding protein. The normal number of CAG (Q) repeats is less than 36; repeat numbers greater than 40 are associated with human disease.

Various lines of evidence demonstrate the involvement of mitochondrial dysfunction in HD. Nuclear magnetic resonance spectroscopy reveals increased lactate in the cortex and basal ganglia[87]. Biochemical studies show decreased activities of complexes II and III of the electron-transport chain in the human HD brain[88]. In striatal cells from mutant *Htt*-knock-in mouse embryos, mitochondrial respiration and ATP production are significantly impaired[89].

The mitochondrial dysfunction observed above is likely to be pathogenically important, because 3-nitropropionic acid and malonate — mitochondrial toxins that selectively inhibit succinate dehydrogenase and complex II — induce a clinical and pathological phenotype that closely resembles HD[90]. Moreover, in striatal neurons expressing the first 171 amino acids of HTT with an insertion of 82 glutamines, overexpression of complex-II subunits restored complex-II activity and blocked mitochondrial dysfunction and cell death[91].

There are several mechanisms by which the mutation could result in mitochondrial dysfunction. First, HTT may interact directly with mitochondria. In one study[92], lymphoblast mitochondria from HD patients and brain mitochondria from YAC transgenic mice expressing HTT with 72 repeats were found to have lower membrane potentials and to depolarize at lower calcium loads than control mitochondria. Amino-terminal mutant HTT was identified on neuronal mitochondrial membranes with immunoelectron microscopy, and the incubation of normal mitochondria with mutant HTT reproduced the calcium-handling defect seen in HD patients and transgenic mice. In another study[93], subfractionation of mitochondria from a knock-in HD-mouse model showed HTT in association with the outer mitochondrial membrane. Mitochondria from the knock-in HD mouse were more sensitive to calcium-induced mitochondrial permeabilization and cytochrome *c* release, an effect that was mimicked by incubating normal mitochondria with mutant, but not wild-type, HTT.

Another mechanism through which mutant HTT could affect mitochondrial function is by altering transcription[94]. HTT interacts with a number of transcription factors, including p53, CREB-binding protein and SP1 (for a review see ref. 95). p53 is a tumour suppressor known to regulate genes involved in mitochondrial function and oxidative stress. In response to genotoxic injury, p53 activates mitochondrial pathway apoptosis by increasing transcription of the pro-apoptotic BH3-only Bcl-2 family members such as PUMA[96]. p53 can also translocate to mitochondria and directly activate BAX[97]. In a recent study[98], mutant HTT bound p53 and increased p53 levels and transcriptional activity, leading to upregulation of downstream targets BAX and PUMA, and mitochondrial membrane depolarization. Pharmacological suppression or genetic deletion of *p53* prevented HTT-induced mitochondrial depolarization, cytochrome oxidase deficiency and cytotoxicity. Moreover, expression of mutant HTT in a p53-null background diminished retinal degeneration in *Drosophila* and reversed behavioural abnormalities in mice.

Although they have not yet been directly related to human HD, two mitochondria-related proteins are associated with HD-like phenotypes in transgenic mice. PGC-1α is a transcriptional coactivator that regulates mitochondrial biogenesis and metabolic pathways. *Pgc-1α*-knockout mice exhibit impaired mitochondrial function, a hyperkinetic movement disorder and striatal degeneration — features that are all also observed in HD[99]. HTRA2 is a serine protease that resides in the mitochondrial intermembrane space. In mice, a missense mutation in HTRA2 that reduces protease activity results in the Mnd2 (motor-neuron degeneration 2) phenotype, which shares many features of HD, including involuntary movements, abnormal postures and massive loss of striatal neurons[100].

Mitochondrial involvement in other, less common, neurodegenerative diseases is reviewed in Table 2.

Summary and future directions

Recent findings have greatly expanded our understanding of the role of mitochondria in the pathogenesis of neurodegenerative diseases. Mitochondrial-DNA mutations and oxidative stress contribute to ageing, the greatest risk factor for neurodegenerative diseases. Mitochondrial dysfunction and oxidative stress occur early in all major neurodegenerative diseases, and there is strong evidence that this dysfunction has a causal role in disease pathogenesis. Most impressively, specific interactions of disease-related proteins with mitochondria have recently been uncovered: APP, Aβ, presenilin, α-synuclein, parkin, DJ-1, PINK1, LRRK2, HTRA2, SOD1 and huntingtin have all been found within mitochondria, as discussed above. This explosion of findings raises further questions.

First, what is the basis for cell-type specificity in neurodegenerative disorders? For example, why does systemic overexpression of mutant SOD1 affect calcium handling in brain but not liver mitochondria[78]? The propensity of mitochondrial disorders to affect the brain and muscles has thus far been explained by the different tissue requirements for mitochondrial function — brain and muscle tissues have high energy requirements. However, we speculate that mitochondrial differences between different cell types might be at least as important in this selectivity,

if not more so. Most mitochondrial proteins are encoded by nuclear genes, and it is to be expected that the distinct nuclear programmes required to produce different cell types should also produce different mitochondria. However, knowledge of mitochondrial biology in different cell types is extremely rudimentary. Further investigation will probably provide a more fundamental understanding of neurodegenerative diseases, because cell selectivity is a fundamental characteristic of these disorders.

Second, the complexity of mitochondrial ROS metabolism suggests that interventions such as the administration of one or a few antioxidants may be too simplistic. Indeed, such interventions have generally been, at best, modestly successful in clinical trials, despite abundant evidence for oxidative stress in disease pathogenesis. A more complete approach to antioxidant therapy would be to decrease ROS generation (for example, by expressing uncoupling proteins) and to upregulate the multilayered endogenous mitochondrial and intracellular antioxidant defence network. However, this will require a considerably better understanding of ROS biology than we have at present. It will also require the global 'ROS bad, antioxidants good' impression to be replaced with knowledge of the specific targets of ROS (such as PIN1 in AD).

Finally, the interaction of mitochondria with specific disease-related proteins opens exciting new possibilities for therapeutic targets. For example, in HD, reducing p53 protects against mutant huntingtin. However, in the case of AD, PD and ALS, genetic forms of disease account for only a small percentage of cases, and the relevance of mitochondrial interactions with these proteins must be determined for sporadic cases.

Knowledge of neurodegenerative diseases has advanced rapidly in the last few years, and the field holds great promise for furthering our understanding and the eventual treatment of these devastating illnesses. ■

1. Danial, N. N. & Korsmeyer, S. J. Cell death: critical control points. *Cell* **116**, 205-219 (2004).
2. Corral-Debrinski, M. *et al.* Mitochondrial DNA deletions in human brain: regional variability and increase with advanced age. *Nature Genet.* **2**, 324-329 (1992).
3. Zhang, J. *et al.* Strikingly higher frequency in centenarians and twins of mtDNA mutation causing remodeling of replication origin in leukocytes. *Proc. Natl Acad. Sci. USA* **100**, 1116-1121 (2003).
4. Chinnery, P. F. *et al.* Point mutations of the mtDNA control region in normal and neurodegenerative human brains. *Am. J. Hum. Genet.* **68**, 529-532 (2001).
5. Simon, D. K. *et al.* Low mutational burden of individual acquired mitochondrial DNA mutations in brain. *Genomics* **73**, 113-116 (2001).
6. Lin, M. T., Simon, D. K., Ahn, C. H., Kim, L. M. & Beal, M. F. High aggregate burden of somatic mtDNA point mutations in aging and Alzheimer's disease brain. *Hum. Mol. Genet.* **11**, 133-145 (2002).
7. Jazin, E. E., Cavelier, L., Eriksson, I., Oreland, L. & Gyllensten, U. Human brain contains high levels of heteroplasmy in the noncoding regions of mitochondrial DNA. *Proc. Natl Acad. Sci. USA* **93**, 12382-12387 (1996).
8. Bender, A. *et al.* High levels of mitochondrial DNA deletions in substantia nigra neurons in aging and Parkinson disease. *Nature Genet.* **38**, 515-517 (2006).
9. Kraytsberg, Y. *et al.* Mitochondrial DNA deletions are abundant and cause functional impairment in aged human substantia nigra neurons. *Nature Genet.* **38**, 518-520 (2006).
10. Trifunovic, A. Mitochondrial DNA and ageing. *Biochim. Biophys. Acta* **1757**, 611-617 (2006).
11. Andreyev, A. Y., Kushnareva, Y. E. & Starkov, A. A. Mitochondrial metabolism of reactive oxygen species. *Biochemistry (Mosc.)* **70**, 200-214 (2005).
12. Sun, J., Folk, D., Bradley, T. J. & Tower, J. Induced overexpression of mitochondrial Mn-superoxide dismutase extends the life span of adult *Drosophila melanogaster*. *Genetics* **161**, 661-672 (2002).
13. Ruan, H. *et al.* High-quality life extension by the enzyme peptide methionine sulfoxide reductase. *Proc. Natl Acad. Sci. USA* **99**, 2748-2753 (2002).
14. Schriner, S. E. *et al.* Extension of murine life span by overexpression of catalase targeted to mitochondria. *Science* **308**, 1909-1911 (2005).
15. Lu, T. *et al.* Gene regulation and DNA damage in the ageing human brain. *Nature* **429**, 883-891 (2004).
16. Nunomura, A. *et al.* Oxidative damage is the earliest event in Alzheimer disease. *J. Neuropathol. Exp. Neurol.* **60**, 759-767 (2001).
17. Pratico, D., Uryu, K., Leight, S., Trojanoswki, J. Q. & Lee, V. M. Increased lipid peroxidation precedes amyloid plaque formation in an animal model of Alzheimer amyloidosis. *J. Neurosci.* **21**, 4183-4187 (2001).
18. Reddy, P. H. *et al.* Gene expression profiles of transcripts in amyloid precursor protein transgenic mice: up-regulation of mitochondrial metabolism and apoptotic genes is an early cellular change in Alzheimer's disease. *Hum. Mol. Genet.* **13**, 1225-1240 (2004).
19. Ohyagi, Y. *et al.* Selective increase in cellular A β 42 is related to apoptosis but not necrosis. *Neuroreport* **11**, 167-171 (2000).
20. Busciglio, J. *et al.* Altered metabolism of the amyloid β precursor protein is associated with mitochondrial dysfunction in Down's syndrome. *Neuron* **33**, 677-688 (2002).
21. Li, F. *et al.* Increased plaque burden in brains of APP mutant MnSOD heterozygous knockout mice. *J. Neurochem.* **89**, 1308-1312 (2004).
22. Velliquette, R. A., O'Connor, T. & Vassar, R. Energy inhibition elevates β-secretase levels and activity and is potentially amyloidogenic in APP transgenic mice: possible early events in Alzheimer's disease pathogenesis. *J. Neurosci.* **25**, 10874-10883 (2005).
23. Tamagno, E. *et al.* β-Site APP cleaving enzyme up-regulation induced by 4-hydroxynonenal is mediated by stress-activated protein kinases pathways. *J. Neurochem.* **92**, 628-636 (2005).
24. Lovell, M. A., Xiong, S., Xie, C., Davies, P. & Markesbery, W. R. Induction of hyperphosphorylated tau in primary rat cortical neuron cultures mediated by oxidative stress and glycogen synthase kinase-3. *J. Alzheimers Dis.* **6**, 659-671 (2004).
25. Sultana, R. *et al.* Oxidative modification and down-regulation of Pin1 in Alzheimer's disease hippocampus: a redox proteomics analysis. *Neurobiol. Aging* **27**, 918-925 (2006).
26. Pastorino, L. *et al.* The prolyl isomerase Pin1 regulates amyloid precursor protein processing and amyloid-β production. *Nature* **440**, 528-534 (2006).
27. Liou, Y. C. *et al.* Role of the prolyl isomerase Pin1 in protecting against age-dependent neurodegeneration. *Nature* **424**, 556-561 (2003).
28. Swerdlow, R. H. *et al.* Cybrids in Alzheimer's disease: a cellular model of the disease? *Neurology* **49**, 918-925 (1997).
29. Elson, J. L. *et al.* Does the mitochondrial genome play a role in the etiology of Alzheimer's disease? *Hum. Genet.* **119**, 241-254 (2006).
30. Coskun, P. E., Beal, M. F. & Wallace, D. C. Alzheimer's brains harbor somatic mtDNA control-region mutations that suppress mitochondrial transcription and replication. *Proc. Natl Acad. Sci. USA* **101**, 10726-10731 (2004).
31. Anandatheerthavarada, H. K., Biswas, G., Robin, M. A. & Avadhani, N. G. Mitochondrial targeting and a novel transmembrane arrest of Alzheimer's amyloid precursor protein impairs mitochondrial function in neuronal cells. *J. Cell Biol.* **161**, 41-54 (2003).
32. Lustbader, J. W. *et al.* ABAD directly links Aβ to mitochondrial toxicity in Alzheimer's disease. *Science* **304**, 448-452 (2004).
33. Crouch, P. J. *et al.* Copper-dependent inhibition of human cytochrome c oxidase by a dimeric conformer of amyloid-β_{1-42}. *J. Neurosci.* **25**, 672-679 (2005).
34. Manczak, M. *et al.* Mitochondria are a direct site of Aβ accumulation in Alzheimer's disease neurons: implications for free radical generation and oxidative damage in disease progression. *Hum. Mol. Genet.* **15**, 1437-1449 (2006).
35. Casley, C. S., Canevari, L., Land, J. M., Clark, J. B. & Sharpe, M. A. β-amyloid inhibits integrated mitochondrial respiration and key enzyme activities. *J. Neurochem.* **80**, 91-100 (2002).
36. Gibson, G. E. *et al.* Reduced activities of thiamine-dependent enzymes in the brains and peripheral tissues of patients with Alzheimer's disease. *Arch. Neurol.* **45**, 836-840 (1988).
37. Parker, W. D., Filley, C. M. & Parks, J. K. Cytochrome oxidase deficiency in Alzheimer's disease. *Neurology* **40**, 1302-1303 (1990).
38. Park, H. J., Seong, Y. M., Choi, J. Y., Kang, S. & Rhim, H. Alzheimer's disease-associated amyloid β interacts with the human serine protease HtrA2/Omi. *Neurosci. Lett.* **357**, 63-67 (2004).
39. Hansson, C. A. *et al.* Nicastrin, presenilin, APH-1, and PEN-2 form active γ-secretase complexes in mitochondria. *J. Biol. Chem.* **279**, 51654-51660 (2004).
40. Betarbet, R. *et al.* Chronic systemic pesticide exposure reproduces features of Parkinson's disease. *Nature Neurosci.* **3**, 1301-1306 (2000).
41. Fornai, F. *et al.* Parkinson-like syndrome induced by continuous MPTP infusion: convergent roles of the ubiquitin-proteasome system and α-synuclein. *Proc. Natl Acad. Sci. USA* **102**, 3413-3418 (2005).
42. Sherer, T. B. *et al.* Mechanism of toxicity in rotenone models of Parkinson's disease. *J. Neurosci.* **23**, 10756-10764 (2003).
43. Schapira, A. H. *et al.* Mitochondrial complex I deficiency in Parkinson's disease. *Lancet* i, 1269 (1989).
44. Simon, D. K. *et al.* Familial multisystem degeneration with parkinsonism associated with the 11778 mitochondrial DNA mutation. *Neurology* **53**, 1787-1793 (1999).
45. Luoma, P. *et al.* Parkinsonism, premature menopause, and mitochondrial DNA polymerase gamma mutations: clinical and molecular genetic study. *Lancet* **364**, 875-882 (2004).
46. Vives-Bauza, C. *et al.* Sequence analysis of the entire mitochondrial genome in Parkinson's disease. *Biochem. Biophys. Res. Commun.* **290**, 1593-1601 (2002).
47. Simon, D. K. *et al.* Somatic mitochondrial DNA mutations in cortex and substantia nigra in aging and Parkinson's disease. *Neurobiol. Aging* **25**, 71-81 (2004).
48. Pyle, A. *et al.* Mitochondrial DNA haplogroup cluster UKJT reduces the risk of PD. *Ann. Neurol.* **57**, 564-567 (2005).
49. Tanaka, M. Mitochondrial genotypes and cytochrome b variants associated with longevity or Parkinson's disease. *J. Neurol.* **249** (Suppl. 2), II11-II18 (2002).
50. Wallace, D. C. A mitochondrial paradigm of metabolic and degenerative diseases, aging, and cancer: a dawn for evolutionary medicine. *Annu. Rev. Genet.* **39**, 359-407 (2005).
51. Song, D. D., Shults, C. W., Sisk, A., Rockenstein, E. & Masliah, E. Enhanced substantia nigra mitochondrial pathology in human α-synuclein transgenic mice after treatment with MPTP. *Exp. Neurol.* **186**, 158-172 (2004).
52. Martin, L. J. *et al.* Parkinson's disease α-synuclein transgenic mice develop neuronal mitochondrial degeneration and cell death. *J. Neurosci.* **26**, 41-50 (2006).
53. Klivenyi, P. *et al.* Mice lacking α-synuclein are resistant to mitochondrial toxins. *Neurobiol. Dis.* **21**, 541-548 (2006).
54. Pesah, Y. *et al. Drosophila* parkin mutants have decreased mass and cell size and increased sensitivity to oxygen radical stress. *Development* **131**, 2183-2194 (2004).
55. Palacino, J. J. *et al.* Mitochondrial dysfunction and oxidative damage in *parkin*-deficient mice. *J. Biol. Chem.* **279**, 18614-18622 (2004).
56. Muftuoglu, M. *et al.* Mitochondrial complex I and IV activities in leukocytes from patients with parkin mutations. *Mov. Disord.* **19**, 544-548 (2004).
57. Darios, F. *et al.* Parkin prevents mitochondrial swelling and cytochrome c release in mitochondria-dependent cell death. *Hum. Mol. Genet.* **12**, 517-526 (2003).
58. Kuroda, Y. *et al.* Parkin enhances mitochondrial biogenesis in proliferating cells. *Hum. Mol. Genet.* **15**, 883-895 (2006).
59. Chung, K. K. *et al.* S-nitrosylation of parkin regulates ubiquitination and compromises parkin's protective function. *Science* **304**, 1328-1331 (2004).

60. Whitworth, A. J. *et al.* Increased glutathione S-transferase activity rescues dopaminergic neuron loss in a *Drosophila* model of Parkinson's disease. *Proc. Natl Acad. Sci. USA* **102**, 8024-8029 (2005).
61. Bonifati, V. *et al.* Mutations in the *DJ-1* gene associated with autosomal recessive early-onset parkinsonism. *Science* **299**, 256-259 (2003).
62. Meulener, M. C. *et al.* DJ-1 is present in a large molecular complex in human brain tissue and interacts with α-synuclein. *J. Neurochem.* **93**, 1524-1532 (2005).
63. Moore, D. J. *et al.* Association of DJ-1 and parkin mediated by pathogenic DJ-1 mutations and oxidative stress. *Hum. Mol. Genet.* **14**, 71-84 (2005).
64. Tang, B. *et al.* Association of PINK1 and DJ-1 confers digenic inheritance of early-onset Parkinson's disease. *Hum. Mol. Genet.* **15**, 1816-1825 (2006).
65. Canet-Aviles, R. M. *et al.* The Parkinson's disease protein DJ-1 is neuroprotective due to cysteine-sulfinic acid-driven mitochondrial localization. *Proc. Natl Acad. Sci. USA* **101**, 9103-9108 (2004).
66. Yang, Y. *et al.* Inactivation of *Drosophila* DJ-1 leads to impairments of oxidative stress response and phosphatidylinositol 3-kinase/Akt signaling. *Proc. Natl Acad. Sci. USA* **102**, 13670-13675 (2005).
67. Kim, R. H. *et al.* DJ-1, a novel regulator of the tumor suppressor PTEN. *Cancer Cell* **7**, 263-273 (2005).
68. Kim, R. H. *et al.* Hypersensitivity of DJ-1-deficient mice to 1-methyl-4-phenyl-1,2,3,6-tetrahydropyrindine (MPTP) and oxidative stress. *Proc. Natl Acad. Sci. USA* **102**, 5215-5220 (2005).
69. Meulener, M. C., Xu, K., Thompson, L., Ischiropoulos, H. & Bonini, N. M. Mutational analysis of DJ-1 in *Drosophila* implicates functional inactivation by oxidative damage and aging. *Proc. Natl Acad. Sci. USA* **103**, 12517-12522 (2006).
70. Valente, E. M. *et al.* Hereditary early-onset Parkinson's disease caused by mutations in *PINK1*. *Science* **304**, 1158-1160 (2004).
71. Silvestri, L. *et al.* Mitochondrial import and enzymatic activity of PINK1 mutants associated to recessive parkinsonism. *Hum. Mol. Genet.* **14**, 3477-3492 (2005).
72. Petit, A. *et al.* Wild-type PINK1 prevents basal and induced neuronal apoptosis, a protective effect abrogated by Parkinson disease-related mutations. *J. Biol. Chem.* **280**, 34025-34032 (2005).
73. Yang, Y. *et al.* Mitochondrial pathology and muscle and dopaminergic neuron degeneration caused by inactivation of *Drosophila* Pink1 is rescued by Parkin. *Proc. Natl Acad. Sci. USA* **103**, 10793-10798 (2006).
74. West, A. B. *et al.* Parkinson's disease-associated mutations in leucine-rich repeat kinase 2 augment kinase activity. *Proc. Natl Acad. Sci. USA* **102**, 16842-16847 (2005).
75. Strauss, K. M. *et al.* Loss of function mutations in the gene encoding Omi/HtrA2 in Parkinson's disease. *Hum. Mol. Genet.* **14**, 2099-2111 (2005).
76. Martins, L. M. *et al.* Neuroprotective role of the Reaper-related serine protease HtrA2/Omi revealed by targeted deletion in mice. *Mol. Cell. Biol.* **24**, 9848-9862 (2004).
77. Mattiazzi, M. *et al.* Mutated human SOD1 causes dysfunction of oxidative phosphorylation in mitochondria of transgenic mice. *J. Biol. Chem.* **277**, 29626-29633 (2002).
78. Damiano, M. *et al.* Neural mitochondrial Ca^{2+} capacity impairment precedes the onset of motor symptoms in G93A Cu/Zn-superoxide dismutase mutant mice. *J. Neurochem.* **96**, 1349-1361 (2006).
79. Kong, J. & Xu, Z. Massive mitochondrial degeneration in motor neurons triggers the onset of amyotrophic lateral sclerosis in mice expressing a mutant SOD1. *J. Neurosci.* **18**, 3241-3250 (1998).
80. Jaarsma, D. *et al.* CuZn superoxide dismutase (SOD1) accumulates in vacuolated mitochondria in transgenic mice expressing amyotrophic lateral sclerosis-linked SOD1 mutations. *Acta Neuropathol. (Berl.)* **102**, 293-305 (2001).
81. Higgins, C. M., Jung, C. & Xu, Z. ALS-associated mutant SOD1G93A causes mitochondrial vacuolation by expansion of the intermembrane space and by involvement of SOD1 aggregation and peroxisomes. *BMC Neurosci.* **4**, 16 (2003).
82. Vijayvergiya, C., Beal, M. F., Buck, J. & Manfredi, G. Mutant superoxide dismutase 1 forms aggregates in the brain mitochondrial matrix of amyotrophic lateral sclerosis mice. *J. Neurosci.* **25**, 2463-2470 (2005).
83. Liu, J. *et al.* Toxicity of familial ALS-linked SOD1 mutants from selective recruitment to spinal mitochondria. *Neuron* **43**, 5-17 (2004).
84. Takeuchi, H., Kobayashi, Y., Ishigaki, S., Doyu, M. & Sobue, G. Mitochondrial localization of mutant superoxide dismutase 1 triggers caspase-dependent cell death in a cellular model of familial amyotrophic lateral sclerosis. *J. Biol. Chem.* **277**, 50966-50972 (2002).
85. Okado-Matsumoto, A. & Fridovich, I. Amyotrophic lateral sclerosis: a proposed mechanism. *Proc. Natl Acad. Sci. USA* **99**, 9010-9014 (2002).
86. Pasinelli, P. *et al.* Amyotrophic lateral sclerosis-associated SOD1 mutant proteins bind and aggregate with Bcl-2 in spinal cord mitochondria. *Neuron* **43**, 19-30 (2004).
87. Jenkins, B. G., Koroshetz, W. J., Beal, M. F. & Rosen, B. R. Evidence for impairment of energy metabolism *in vivo* in Huntington's disease using localized 1H NMR spectroscopy. *Neurology* **43**, 2689-2695 (1993).
88. Gu, M. *et al.* Mitochondrial defect in Huntington's disease caudate nucleus. *Ann. Neurol.* **39**, 385-389 (1996).
89. Milakovic, T. & Johnson, G. V. Mitochondrial respiration and ATP production are significantly impaired in striatal cells expressing mutant huntingtin. *J. Biol. Chem.* **280**, 30773-30782 (2005).
90. Brouillet, E. *et al.* Chronic mitochondrial energy impairment produces selective striatal degeneration and abnormal choreiform movements in primates. *Proc. Natl Acad. Sci. USA* **92**, 7105-7109 (1995).
91. Benchoua, A. *et al.* Involvement of mitochondrial complex II defects in neuronal death produced by N-terminus fragment of mutated huntingtin. *Mol. Biol. Cell* **17**, 1652-1663 (2006).
92. Panov, A. V. *et al.* Early mitochondrial calcium defects in Huntington's disease are a direct effect of polyglutamines. *Nature Neurosci.* **5**, 731-736 (2002).
93. Choo, Y. S., Johnson, G. V., MacDonald, M., Detloff, P. J. & Lesort, M. Mutant huntingtin directly increases susceptibility of mitochondria to the calcium-induced permeability transition and cytochrome c release. *Hum. Mol. Genet.* **13**, 1407-1420 (2004).
94. Luthi-Carter, R. & Cha, J.-H. J. Mechanisms of transcription dysregulation in Huntington's disease. *Clin. Neurosci. Res.* **3**, 165-177 (2003).
95. Sugars, K. L. & Rubinsztein, D. C. Transcriptional abnormalities in Huntington disease. *Trends Genet.* **19**, 233-238 (2003).
96. Yu, J., Zhang, L., Hwang, P. M., Kinzler, K. W. & Vogelstein, B. PUMA induces the rapid apoptosis of colorectal cancer cells. *Mol. Cell* **7**, 673-682 (2001).
97. Chipuk, J. E. *et al.* Direct activation of Bax by p53 mediates mitochondrial membrane permeabilization and apoptosis. *Science* **303**, 1010-1014 (2004).
98. Bae, B. I. *et al.* p53 mediates cellular dysfunction and behavioral abnormalities in Huntington's disease. *Neuron* **47**, 29-41 (2005).
99. Lin, J. *et al.* Defects in adaptive energy metabolism with CNS-linked hyperactivity in PGC-1α null mice. *Cell* **119**, 121-135 (2004).
100. Rathke-Hartlieb, S. *et al.* Progressive loss of striatal neurons causes motor dysfunction in MND2 mutant mice and is not prevented by Bcl-2. *Exp. Neurol.* **175**, 87-97 (2002).

Acknowledgments This work was supported by grants from the National Institutes of Health and the American Federation for Aging Research/Beeson Program. We apologize to our many colleagues whose work we were unable to cite due to space limitations.

Author Information Reprints and permissions information is available at npg.nature.com/reprintsandpermissions. The authors declare no competing financial interests. Correspondence should be addressed to M.F.B. (fbeal@med.cornell.edu).